Mathematical modelling of cartilage and bone defect healing after cell implantation

Kelly Campbell

Submitted in partial fulfilment of the requirements of the degree of

Doctor of Philosophy

July 2020

Keele University

School of Computing and Mathematics

Abstract

This thesis is concerned with mathematically modelling the regeneration of cartilage and cartilage-bone defects. Defects of the bone-cartilage unit, namely chondral and osteochondral defects, are a leading cause of osteoarthritis, the most common type of arthritis in the UK. These defects can occur through acute trauma, natural wear and tear of the joint, and underlying disease of the bone, and are typically found in the articular joints. Autologous Chondrocyte Implantation (ACI) is the most commonly used cell implantation therapy for treating chondral defects in joints and has good clinical outcomes in osteochondral defects. The procedure begins by inserting chondrocytes into the defect region. The chondrocytes initiate healing by proliferating and depositing extracellular matrix, which allows them to migrate into the defect until it is completely filled with new cartilage. Mesenchymal stem cells (MSCs) can be used instead of chondrocytes with similar long term results. The main differences between these implantation techniques is observable at early times, as MSCs must first differentiate into chondrocytes before cartilage is formed. For osteochondral defect regeneration, the mechanism behind healing is not fully understood. Though osteochondral defects can spontaneously repair, the tissue is usually fibrous, typically leading to subsequent degradation of the newly regenerated tissue. A recent study in ovine models show osteochondral defects heal by first filling with regenerative cartilage tissue which is subsequently remodelled into bone, replicating the endochondral ossification process.

We refine an existing model of cartilage defect regeneration using ACI to include important regulatory effects of growth factors, FGF-1 (fibroblast growth factor-1) and BMP-2 (bone morphogenetic protein-2). *In vitro* studies hypothesise these growth factors have a trophic effect on the chondral defect regeneration process. We then model the regeneration of a

bone-cartilage defect using ACI in the presence of growth factors to verify the circumstances behind osteochondral healing. To the best of our knowledge, this is the first time this has been modelled for ACI therapy. The mathematical models formulated in this thesis successfully demonstrate the above proposed healing and growth factor mechanisms in chondral and osteochondral defect regeneration. Our key findings indicate a novel cell therapy that combines the ACI and MSC-implantation strategies increases the cartilage tissue formation rate within the first year of healing in chondral defects, regardless of the cell implantation ratio. Additionally, we show that osteochondral defects follow expected regeneration patterns when endochondral ossification is the proposed healing mechanism, under the influence of regulatory growth factors PTHrP (Parathyroid hormone-related protein) and Ihh (Indian hedgehog).

The findings of these models enable us to better understand chondral and osteochondral defect regeneration by giving invaluable insight into the healing processes that are occurring, the impact growth factors have on these healing mechanisms, and highlighting the potential for advances of novel cell-based therapies.

Acknowledgements

Firstly, I would like to express my deepest gratitude to my supervisor, Dr. Shailesh Naire. Your knowledge, guidance, encouragement and never-wavering belief in me has been fundamental to the successful completion of this work. This PhD has been a life-changing endeavour that I feel very lucky to have experienced under your supervision. I would like to thank Dr. Jan Herman Kuiper for always providing new perspectives and invaluable insights that were critical to the direction and success of this work. I am extremely grateful for the support you've provided during this PhD.

I would like to thank my partner for being there when times were hard and always believing in me. You often kept me going. To my siblings, extended family, and friends, thanks for just being yourselves. PhD life can be quite daunting, and your company provided the escapism I needed.

I would like to thank my parents, Penny and Paul, for teaching me many life lessons that have shaped who I am today. I will never be able to express how thankful I am to have you as parents and life-long friends. I dedicate this work to you.

Finally, I would like to thank Keele University for funding this PhD and being my second home for the past 7 years.

Statement

Sections of this thesis have been taken verbatim from publications arising from the work undertaken in this PhD:

Campbell, K., Naire, S., and Kuiper, J. H. (2019). A mathematical model of cartilage regeneration after chondrocyte and stem cell implantation – I: the effects of growth factors. Journal of Tissue Engineering, 'The Role and Contributions of Mathematical Modelling in Tissue Engineering and Regenerative Medicine'. 10, p. 204173141982779. doi: 10.1177/2041731419827791.

Campbell, K., Naire, S., and Kuiper, J. H. (2019). A mathematical model of cartilage regeneration after chondrocyte and stem cell implantation – II: the effects of co-implantation. Journal of Tissue Engineering, 'The Role and Contributions of Mathematical Modelling in Tissue Engineering and Regenerative Medicine'. 10, p. 204173141982779. doi: 10.1177/2041731419827792.

Contents

List of Figures

List of Tables

Chapter 1

Introduction

Mathematical models have the ability to give information quickly and efficiently, and are a useful tool for alleviating the need for *in vitro* and *in vivo* models for therapies in regenerative medicine by giving insight into and simulating these complex physiological processes. As the thesis title suggests, our focus is to mathematically model the regeneration of defects of the bone-cartilage unit, more specifically chondral and osteochondral defects. The etymology of these terms helps to make sense of and give context to the work undertaken in this thesis. Derived from the Greek 'ostéon', osteo refers to bone, and serves as an indicative prefix for many bone-related terminologies such as osteoporosis, osteopathy, and osteoarthritis. In fact, osteon itself is defined to be the canal-like structures found in compact bone. The term 'chondral' is derived from the Greek 'khóndros', a word used to describe something of granular structure. Hyaline cartilage extracellular matrix is often categorised to be granular in composition and glassy in appearance, with cartilage cells embedded within. A defect of either cartilage or cartilage and bone is described to be an area of damage that results in weakness and structural changes within the affected tissue. In this thesis, the problem focuses on defects of both cartilage (chondral) and those that penetrate through cartilage to

underlying subchondral bone (osteochondral) within the bone-cartilage unit. Specifically, we focus on defects located in the knee joint, and aim to mathematically model the morphology of defect regeneration after cell implantation techniques.

Figure 1.1: Arthroscopic image of a cartilage defect in the knee.

Figure 1.2: Arthroscopic image of a cartilage defect 1 year after repair.

Developing and improving upon the treatment of defects of the bone-cartilage unit is a fundamental clinical problem. Articular cartilage damage occurs in several ways, from playing high contact sport to natural wear and tear, affecting a variety of different age groups and sexes, with many people experiencing symptoms such as locking and stiffness of the joint later in life [31, 47]. Articular cartilage is a type of hyaline cartilage that covers the end of

bones at the articular joint, i.e. the knee, in order to reduce friction, and as a result allows bones to glide smoothly over one another [11, 121, 164]. This type of cartilage can be found only in small volumes in the human body and as a result does not absorb shock well [191]. The ability of damaged cartilage to self-repair is limited due to its avascularity [164] and can often lead to osteoarthritis when left untreated through an osteochondral defect forming due to an exposure of the end of bones, causing them to rub against one another at a joint without cushioning and protection [121]. Almost 9 million people in the UK are affected by osteoarthritis, which carries a lifetime risk in the knee of approximately 45% [13, 5]. Osteochondral defects are defects of the articular cartilage that puncture the subchondral bone and can undergo spontaneous repair. The tissue that fills the defect is of subsidiary quality compared with natural articular cartilage due to its fibro-cartilaginous nature, and as a result degrades quickly. Finding appropriate treatments for these defects is an ongoing clinical issue with great importance due to the pain and discomfort a defect can cause, leaving many sufferers debilitated [2]. Though various treatment strategies are available, cell implantation results in the most promising outcomes for both chondral and osteochondral defects, and will be the treatment option focused on in this thesis [130].

The clinical translation of *in vitro* or animal research around treatments for chondral defects, whether they arise from trauma or diseases such as osteoarthritis, faces one common barrier: the long time needed for demonstrating clinical effectiveness of such treatments. For instance, up to a period of five years there is no evidence for a clinical difference between cell-based treatments of chondral defects and their non cell-based comparators [130]. Such long time periods are well beyond the reach of *in vitro* models or animal models. Even animal models that allow a relatively long-term follow-up of 1-2 years, such as equine models, may still be insufficient. An example is an equine model comparing between mesenchymal stem

cell implantation and fibrin implantation for chondral defects [128, 179]. At 1 month, this model suggested better cartilage formation with mesenchymal stem cells, but at 8 months no difference was visible. Although this has been used as an example of how short-term results in animal models can be misleading and that long-term results are needed [128], it is also important to realise that even 8 months of follow-up is still short when it comes to clinical translation. After all, the 8 month findings do not preclude that differences might appear after 5 years' follow-up. Mathematical models do not have this practical time limit and can be used to study long-term outcomes. Chapter 3 and 4 of this thesis contain examples of such use of mathematical models, where we investigate the longer term (2-year) implications for the repair of cartilage defects of short-term (1-month) *in vitro* experiments.

Autologous chondrocyte implantation is commonly regarded as a treatment for cartilage defects. For instance, the title of the NICE recommendation is "Autologous chondrocyte implantation for treating symptomatic articular cartilage defects of the knee" and the title of the first report on its clinical use, which appeared in 1994, was "Treatment of deep cartilage defects in the knee with autologous chondrocyte transplantation" [60, 17]. However, the German cartilage registry found that a majority of patients treated with ACI have an ICRS grade IV defect, which is a defect that also involves the underlying bone [142]. This reflects the clinical practice at The Robert Jones and Agnes Hunt Orthopaedic Hospital (RJAH), Oswestry, where 60% of patients treated with ACI had an ICRS grade IV defect (Personal communication, J.H. Kuiper, 2020 [104]). RJAH is a leading orthopaedic hospital specialising in the treatment of bone, joint and muscular conditions nationally. In order to be clinically relevant, mathematical models of cartilage repair must therefore be able to include the mechanism by which cartilage-bone (osteochondral) defects repair. Chapter 5 of this thesis contains a first step to mathematically model the repair of osteochondral defects.

Despite significant effort to better understand the circumstances behind chondral and osteochondral defect regeneration, the role growth factors play within this process is not fully understood. The mechanism behind osteochondral defect regeneration is elusive, with scant studies successfully pinpointing the underlying mechanism. Co-implantation as the chosen therapy to treat chondral defects has not been extensively explored, despite *in vitro* studies indicating the potential for earlier matrix deposition caused by a trophic healing scenario due to growth factor influence, a streamlined operative procedure, and earlier remobilisation [9, 184]. The works undertaken in this thesis aim to answer these key open questions within cartilage tissue engineering by formulating mathematical models to utilise the available data and observations to predict long-term outcomes, to better understand chondral defect regeneration under the influence of important growth factors (Wu *et al.* [184], *in vitro*), the benefits of co-implantation for chondral defects and if an optimal ratio of cells can be identified (Wu *et al.* [184], *in vitro*), and finally, the process by which osteochondral defects regenerate, hypothesised to be via endochondral ossification (Lydon *et al.* [120], *in vivo, ovine*).

Mathematical models of biological phenomena can give fundamental information to clinicians in order to determine treatment strategies that might otherwise be elusive [56, 110]. These models and computer simulations can also help to reduce the number of animal experiments conducted, with theoretical results replacing those of sometimes spurious animal experiments [156, 165]. With regard to chondral and osteochondral defect regeneration, mathematical models can be formulated to better understand how healing occurs and over what time frame a defect is fully healed. Previous work of Lutianov *et al.* [119] on cartilage regeneration after cell therapy simulated chondral defect healing after chondrocyte or mesenchymal stem

cell implantation. This work successfully captures some essential features of cartilage defect regeneration and resulted in some clinically useful information, such as the relatively small importance of the number of implanted cells. However, it does not address an important open question: do growth factors thought to have an important influence on the modelled healing mechanism impact overall healing time? This lack of inclusion could mean certain healing benchmarks and characteristics may not be captured. This model of cartilage regeneration will act as a basis for the works undertaken in this thesis, primarily by extending it to include the effects of important growth factors, such as FGFs (Fibroblast growth factors) and BMPs (Bone morphogenetic proteins), and to explore a potential new cell therapy, where a co-implantation of mesenchymal stem cells and chondrocytes are inserted into the defect to investigate the expected outcome of a trophic healing scenario, where an optimal ratio of MSCs and chondrocytes could be identified from the findings of the model to formulate a novel cell implantation. Additionally, using this refined mathematical model as a basis and synthesizing further advances within the literature from animal and clinical experiments of osteochondral defect regeneration, a model of osteochondral defect healing after cell implantation therapy will be formulated. This model will be used to verify the mechanisms behind osteochondral defect regeneration, whilst including the effects of key regulatory growth factors as hypothesised in the literature (Chapter 2).

The data that populates any mathematical model comes from some form of experimentation, whether *in vitro, in silico*, *in vivo* or human. These experiments are conducted to obtain information about potentially important mechanisms occurring over the course of the chosen experiment, whether that be, for example, to better understand the role of growth factors within chondral defect regeneration (*in vitro*, [184]), or to verify the mechanism driving osteochondral defect regeneration (*in vivo, ovine*, [120]). However, there are barriers involved

in translating experimental data to useful parameters that populate a mathematical model. For example, the data obtained from clinical experimentation could be qualitative and not quantitative, or could be represented as a raw dataset where data was recorded at specific time points, instead of converted to a rate. The data used from experimentation also has to performed in a realistic environment, such as the correct mechanical environment (as seen in bioreactor studies [145]), or with a realistic supply of nutrients over the time-scale the experiment is performed. Additionally, experimentation *in vitro* has its own weaknesses, such as cell de-differentiation [145]. It could also be the case that no data has been published to approximate a parameter that is required to mathematically model a specific scenario. To help alleviate this barrier, data can be converted into the required format, i.e. a rate, or an approximation of an unknown parameter can be made, which can then be used within a mathematical model. To verify data validity, a sensitivity analysis of parameters can be undertaken where parameters are varied (increased and decreased) to better understand their sensitivity to change. If parameters are deemed not sensitive to change it is likely their approximation or conversion from experimental data is representative of the model environment.

Thesis outline

Chapter 2 reviews the biology of chondral and osteochondral defects, first focusing on the physiology and pathophysiology of the bone-cartilage unit as a whole, specifically the structure and development of the bone-cartilage unit. Following on from this we discuss cartilage and bone injury, focusing on possible causes of cartilage only (chondral) and cartilage and bone (osteochondral) defects. We then discuss how these chondral and osteochondral defects heal, whether naturally or after a treatment strategy is undertaken, exploring the details and limitations of current treatment strategies, such as autologous chondrocyte implantation,

mosaicplasty and microfracture. Following on from this, we then review current mathematical models within tissue engineering, focusing on various different modelling types such as reaction-diffusion and multi-phase approaches. We discuss in-depth mathematical models relevant to the work undertaken in this thesis, such as Lutianov *et al.* [119], along with other potentially relevant models, such as those concerned with fracture healing and long bone growth [7, 64].

Chapter 3 extends the mathematical model formulated by Lutianov *et al.* concerned with chondral defect healing following Autologous Chondrocyte Implantation (ACI), a current cell therapy used to treat chondral defects [119]. Lutianov *et al.* [119] also explored the effects of implanting mesenchymal stem cells into a chondral defect, a cell therapy strategy that replicates the ACI procedure with the hope MSC differentiation into chondrocytes will then stimulate new cartilage production, referred to as Articular Stem cell Implantation (ASI). This work is discussed in detail in Chapter 2, with the equations formulated and modelling choices explained in Chapter 3. We extend this work to answer the open question: does including the effects of important growth factors identified in the literature, in particular FGF-1 (Fibroblast Growth Factor-1) and BMP-2 (Bone Morphogenetic Protein-2), which are thought to have trophic effects on cell-to-cell interaction between mesenchymal stem cells and chondrocytes, impact matrix deposition, cell evolution and overall healing time? This inclusion of FGF-1 and BMP-2 is relevant to the mesenchymal stem cell implantation procedure. When MSCs are inserted the defect will contain a population of un-differentiated MSCs and chondrocytes (from differentiated MSCs), meaning during this time we have two cell populations where important trophic effects on chondrogenesis and chondrocyte proliferation are taking place. The inclusion of these growth factors will result in a refined mathematical model of cartilage defect regeneration.

In Chapter 4, we continue with the model from Chapter 3 to simulate a co-implantation procedure of mesenchymal stem cells and chondrocytes, a treatment strategy currently in clinical trial that is thought to result in earlier healing due to a trophic effect caused by growth factors released by cell-to-cell interactions. We explore several cell-implantation ratios, ranging from 10:90 to 90:10 (MSC:chondrocyte), and compare matrix levels for these ratios with ACI and ASI as shown in Chapter 3 and Lutianov *et al.* [119], to answer the open question: can a novel cell implantation therapy be formulated to treat chondral defects that utilises both MSCs and chondrocytes to reduce healing time and streamline the cell implantation procedure? The implications of these findings could be indicative to clinicians about potential cell implantation strategies currently used in the treatment of chondral defects. We also demonstrate the differences in cell-evolution and nutrient utilisation following co-implantation when compared with single-cell implantation procedures.

In Chapter 5 we formulate a new mathematical model to describe osteochondral defect healing following autologous chondrocyte implantation. Details of osteochondral defect regeneration are relatively elusive, with literature indicating healing occurs via an endochondral ossification-like process in several animal models [120, 161], where a cartilage model is first formed within the defect, followed by cartilage calcification and eventual bone production occurring from the base continuing towards the top until bone formation ceases and a cartilage layer is left remaining along the top of the newly regenerated defect. Important growth factors such as parathyroid hormone-related protein (PTHrP) and Indian Hedgehog (Ihh) are thought to regulate chondrocyte hypertrophy and suppress endochondral ossification where necessary, with hypertrophic chondrocytes and bone cells such as osteoblasts and osteoclasts

driving bone formation [103]. The open question we primarily aim to answer with this model is: can the endochondral ossification pathway replicate clinical findings by reproducing cartilage and bone formation as described in the literature, whilst also including the effects of important regulatory factors? We endeavour to demonstrate the impact growth factors have on the system by conducting a thorough sensitivity analysis, which allows us to understand how growth factors such as PTHrP and Ihh regulate the remaining layer of cartilage in the regenerated defect, whilst also considering the sensitivity of important parameters within the model such as the rate of chondrocyte hypertrophy, the initial cartilage healing phase and cartilage calcification rate.

Finally, in Chapter 6 we summarise our findings, discuss the implications of this work and possible future work that arises from this thesis.

Chapter 2

Background

In this chapter we begin by summarising the biological and mathematical background underpinning the mathematical models formulated in the following chapters. We begin with describing the physiology and pathophysiology of the bone-cartilage unit in the joints of the body. This will be followed by the pathophysiology of chondral and osteochondral defects, how they occur, and repair. Relevant developmental biology will also be explored such as endochondral and intramembranous ossification. We then discuss current treatment strategies and clinical problems associated with these types of defects. Following on from this, we will look at various mathematical modelling techniques used within regenerative medicine, discussing relevant examples in more detail that demonstrate the modelling techniques we undertake in the work of this thesis.

2.1 Physiology and pathophysiology of the bone-cartilage unit

Bone and cartilage are connective tissues within the human body, with relatively few cells embedded in extracellular matrix. The bone-cartilage unit is comprised of articular cartilage, a calcified cartilage layer and the subchondral bone plate, which lies between the articular

cartilage and the subchondral trabecular bone [117, 124, 189] (Fig. 2.1). The bone-cartilage unit is found in articular joints such as the ankle and the knee, with the subchondral bone acting as a key structural component supporting the articular cartilage it lies beneath [124].

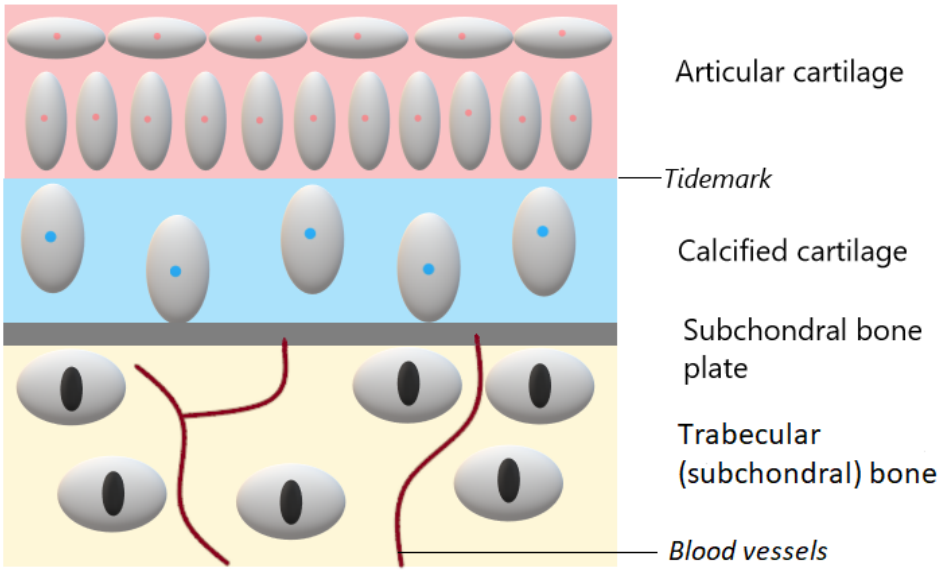

Figure 2.1: Schematic of a healthy bone-cartilage unit, comprised of articular cartilage (≈ 2-4mm thick [62, 135]), a tidemark, calcified cartilage (≈ 0.1-0.2mm thick [135]) and subchondral bone, with blood vessels indicated. Adapted from Lories *et al.* [117]. *NB: this schematic is not to scale.*

2.1.1 Structure and composition of the bone-cartilage unit

Articular cartilage is a type of hyaline cartilage that covers the end of bones that form a joint in order to reduce friction, and as a result allows bones to glide smoothly over one another. Being smooth and pearly-white in appearance, articular cartilage is described to have a firm texture [29, 133, 191]. Chondrocytes (cartilage cells) are embedded within cartilaginous extracellular matrix which is largely formed of water, various collagens, hyaluronic acid and proteoglycans and non-collagenous proteins [172]. There are at least 16 types of collagen in the body, and they are all highly abundant fibrous proteins. The main type of

collagen found in articular cartilage is type II, and its properties supply ECM with its durable properties [26, 51]. The calcified cartilage zone acts as a barrier between the hyaline cartilage and the hard subchondral bone plate, transferring mechanical stresses and biological stimulus between the two tissues [192]. The subchondral bone plate's primary function is to support the overlying articular cartilage within the bone-cartilage unit [124]. Subchondral bone is a highly vascular and neural material, filled with many hollow gaps that connect normal articular cartilage and subarticular spongiosa, an area of subchondral bone located below the subchondral plate. The health of the subchondral bone is highly important to the health of the entire bone-cartilage unit as it supplies the overlying cartilage with nourishment [111, 189].

Biomechanical and biochemical properties of the bone-cartilage unit

Articular cartilage is a multiphasic tissue that provides various biomechanical functions within the bone-cartilage unit, more specifically, load bearing, shock absorption and wear resistance [118]. When we refer to articular cartilage as multiphasic, we speak of 3 phases, namely a solid phase, a fluid phase and an ion phase. These three phases all contribute to articular cartilage's ability to withstand high compressive loads and compressive and shear stresses. The solid phase is comprised of collagen fibrillar network containing proteoglycans and glycoproteins. The fluid and ion phase is water comprised of dissolved electrolytes, with both positive and negative charges [63].

Trabecular bone, a constituent of subchondral bone that is located beneath calcified cartilage and the subchondral plate (Fig. 2.1), demonstrates anisotropic and viscoelastic properties and has a density ranging from 0.14 g/cm^3 to 1.10 g/cm^3, lower than that of cortical bone [112]. Bone undergoes constant remodelling via bone resorption through osteoclasts and bone

remodelling through osteoblasts. Osteoclastic and osteoblastic activity is regulated by multiple factors, including locally produced molecules that control cell signalling, released under the influence of mechanical stimulus [97]. Osteocytes are highly sensitive to mechanical influence, and are thought to detect physical stimuli, meaning they are essential in mediating osteoclastic bone resorption. They respond to fluid flows caused by loading within bone, meaning bone remodelling can be attributed to physiological loading [145].

Mechanotransduction is the result of mechanical forces (such as pressure, shear and elongation) causing tissue remodelling by triggering cell reaction through influence on cellular metabolism [166]. Cellular responses thought to be a result of mechanical influence include cell differentiation and proliferation, matrix synthesis, the release of growth and paracrine factors, and the down- or up-regulation of gene expression. Tissues are influenced by both internal and externally applied mechanical forces [145]. *In vivo* external mechanical forces include flow-mediated shear stress and macroscale forces due to muscle contraction around the tissue and movement. Internal forces include cell movement, cell adhesion to scaffolds and extracellular matrix, along with stresses caused by reparative tissue growth and remodelling [145]. Mechanical influence is highly important to the maintenance of tissues located within the bone-cartilage unit, and also the regeneration of chondral and osteochondral defects.

2.1.2 Development of the bone-cartilage unit

Bone formation begins in foetal development, where the skeleton is primarily cartilaginous, and finishes in adulthood. Bone can form via two routes: intramembranous and endochondral ossification. Mineralised bone is comprised of cancellous and compact bone. Compact bone behaves as a weight-bearing component for the skeleton and can be found underneath

the periosteum, and cancellous bone is flexible and highly vascular and is located at the end of long bones beneath cartilage [172]. Cells found in bone are osteoblasts, osteocytes and osteoclasts, and all of these cells have different roles within bone. During bone formation, osteoblasts function in groups as single cells cannot make bone. Osteoblasts are a main cellular component of bone with single nuclei that secrete bone material [57]. Osteocytes, the most abundant cell type in bone, are found in mature bone located inside lacunae and are derived from osteoblasts [37]. Osteoclasts are essential in the remodelling, maintenance and repair of tissue due to their ability to break down bone [55, 57]. They have multiple nuclei and cleverly form macrophages, a type of white blood cell.

Intramembranous and Endochondral ossification

Ossification occurs via two bone formation pathways. Intramembranous ossification is bone formation that occurs in and replaces connective tissue in the absence of cartilage. This type of ossification happens primarily in the cranial bones of the skull and the clavicles and forms flat bones [61]. Mesenchymal cells cluster, where they differentiate into osteoblasts, forming an ossification centre. Bone matrix is then secreted by the osteoblasts which undergoes mineralisation within a few days. The remaining trapped osteoblasts become osteocytes [61].

Endochondral ossification is the process of cartilage being replaced by bone tissue occurring in the stages of prenatal development and healing. This type of ossification is the mechanism behind long bone growth in the epiphyseal plate (growth plate), first occurring in the centre of long bones and spreading to the periphery. During this process, chondrocytes synthesise a cartilage model which then undergoes calcification and is ossified [121]. This method of bone formation starts similarly to intramembranous ossification, when clusters of mesenchymal cells, referred to as condensations, form within the body from the influence of cell

adhesion molecules (CAMs). CAMs are made up of proteins that promote the attraction of cells, known as molecular binding, to other cells or ECM. These clusters of cells differentiate into chondrocytes, with the cells at the edges of these clusters forming perichondrium. The chondrocytes secrete matrix components, amongst which are type II collagen. The cartilage formed by these chondrocytes grows due to chondrocyte proliferation and matrix production [182]. Proliferation ceases in the central (core) chondrocytes which then undergo hypertrophy, synthesise type X collagen, and secrete matrix vesicles containing alkaline phosphatase. These form a structure for upcoming calcification and eventual endochondral ossification [167]. The hypertrophic chondrocytes (HCs), due to their 5-fold increase in size, are the main driver of bone growth [182]. Hypertrophic chondrocytes attract blood vessels, ensure mineralization in the surrounding matrix and attract chondroclasts [103]. Chondroclasts are giant multinucleated cells which are linked with cartilage absorption. The hypertrophic chondrocytes help form a bone collar by regulating the perichondrial cells to differentiate into osteoblasts; these HCs then undergo apoptosis [103]. A calcified cartilage matrix scaffold is left behind for osteoblasts to secrete true bone with the invasion of blood cells. A strong relationship has been identified between bone growth and the volume increase of hypertrophic chondrocytes [3]. Osteoblasts encased in bone form osteocytes or differentiate into bone lining cells [37]. This process occurs in the entire skeleton, converting the cartilaginous skeletal tissue into mineralised bone that acts as an essential framework with several important roles within the body. Aside from movement and support the skeleton helps protect and produce blood cells, as well as storing ions such as calcium, and regulating the secretion of important macromolecules such as insulin and other hormones. Cartilage located in the joints does not undergo ossification and as a result remains permanently in the body. These areas of remaining cartilage are primarily located at the end of long bones, and together with the subchondral bone form the bone-cartilage unit.

Regulators of endochondral ossification

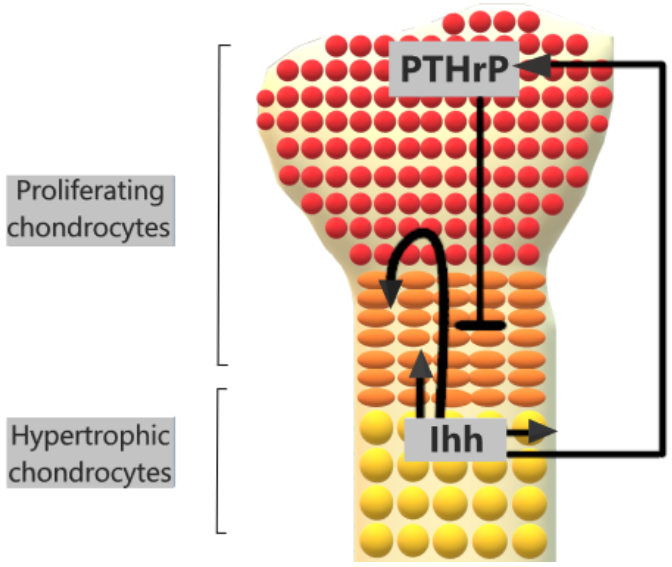

Figure 2.2: Schematic of the PTHrP-Ihh feedback loop that occurs during endochondral ossification. Adapted from Kronenberg *et al.* [103]

Growth factors such as PTHrP (Parathyroid hormone-related Protein) and Ihh (Indian Hedgehog) help regulate the process of endochondral ossification. Indian hedgehog (Ihh) is part of the Sonic hedgehog family of secreted proteins. Ihh is referred to as a master regulator of the development of bone and is needed during embryonic and post-natal growth for the proliferation of chondrocytes in addition to chondrocyte and osteoblast differentiation [103]. When chondrocytes are transitioning from a proliferative to a hypertrophic state Ihh is secreted; this stimulates the production of PTHrP by proliferative chondrocytes. Together they form a negative feedback loop due to PTHrP's role in keeping chondrocytes proliferating, which postpones the production of Ihh. Indian hedgehog is only produced when the source of PTHrP is 'distant enough' and its local concentration is low, which increases the rate of transition to a hypertrophic state and increases the production of PTHrP [173] (Fig. 2.2). Other growth factors such as fibroblast growth factors, C-type natriuretic peptide (CNP), epidermal

growth factors (EGF), insulin-like growth factors (IGFs), and transforming growth factor α (TGF-α) contribute to the maturation and hypertrophy of chondrocytes during endochondral ossification in the growth plate [100]. Fibroblast growth factor signalling, more specifically growth factors FGF-9 and FGF-18, are thought to influence chondrogenesis, acting in an antagonistic manner with CNP. C-type natriuretic peptide is secreted by pre-hypertrophic and proliferating chondrocytes and together with FGF-18 blocks chondrocyte hypertrophy. They are thought to act together as a sensor of sorts, to ensure appropriate levels of chondrocytes (proliferative and pre-hypertrophic) are present for hypertrophy to begin in cells that are distant enough from PTHrP [100].

2.1.3 Injury and repair of the bone-cartilage unit

The bone-cartilage unit acts in unison, with articular cartilage acting as a low-friction bearing component and the underlying subchondral plate absorbing shock and providing the required structural support. Once a component of the bone-cartilage unit is damaged, whether through disease of the joint or wear-and-tear of the tissue, the entire unit is affected and undergoes structural changes [117, 124]. A healthy bone-cartilage unit is essential to proper joint function, with changes in cartilage or bone mechanical properties attributed to increased OA (osteoarthritis) expression due to biochemical changes in cartilage and underlying subchondral bone.

Causes of chondral and osteochondral defects

Causes of articular cartilage damage are most commonly by injury or normal ‘wear and tear’, and less commonly by diseases of the subchondral bone, such as osteochondritis dissecans and

osteonecrosis [123, 129, 180]. Damaged articular cartilage can eventually cause long term degenerative arthritis due to an exposure of the end of bones, causing them to rub against one another at a joint junction without the cushioning and protection provided by articular cartilage [29, 191]. Symptoms of damaged articular cartilage can include joint swelling, stiffness and pain, with the ability to move being restricted.

Articular cartilage defects are usually categorised as either full-thickness defects or partial-thickness defects. Partial-thickness defects are defects of only articular cartilage, varying in size from small lesions to significant cartilage degradation, and typically have many suitable treatment options due to underlying subchondral bone being in-tact and lower risk of osteoarthritic characteristics. Full-thickness defects are articular cartilage defects that extend down to the underlying calcified cartilage zone, with the subchondral plate exposed but not damaged [123]. Osteochondral defects are classified as defects that puncture the underlying subchondral bone and vary greatly in dimension from patient to patient [177]. These defects can be caused by a number of factors including repetitive trauma, genetic and metabolic causes, and injuries that can cause cartilage to shear [76]. The 3 main areas of the body for chondral and osteochondral defects to occur are the knee, hip, and ankle, with injuries of the knee and ankle being very common sport injuries, resulting in a sizable proportion of young people being found to have partial and full-thickness defects [116]. The pathology of osteochondral defects can vary greatly, with some being classified as only a small lesion of the articular cartilage and subchondral bone, and with others being fractures of the articular cartilage and subchondral bone, with many other categorisations in-between [39]. A common example of an osteochondral defect resulting from injury would be a sprained ankle that gives painful symptoms long term, and therefore has not settled despite rehabilitation. Possible treatments of this type of defect would be through nonsurgical management or surgery such

as drilling of the subchondral bone, osteochondral grafting, and ACI [156]. It is commonly observed that adults with osteochondral defects will usually require surgery, with ankle lesions responding much better to surgical treatment than lesions of the knee [45, 101, 172].

Chondral and osteochondral defects are both a cause and result of osteoarthritis, a degenerative condition that causes the joints to become painful and stiff, primarily occurring in patients over 45 years old [52, 134]. Varying from patient to patient, the course of the disease can be unpredictable and in some cases can lead to complete degeneration of the joint leading to a permanent disability [89]. Osteoarthritis causes changes of all tissues in the joint affected [69]. Symptoms of osteoarthritis can be linked to a number of factors including age, sex, weight, genetics, previous joint injury, and other debilitating diseases [2]. Living with osteoarthritis can make normal day to day tasks much harder, often affecting the patient's ability to work, sleep, and exercise primarily. There is no cure for osteoarthritis meaning the disease can only be managed to make it easier to live with.

Natural repair of chondral and osteochondral defects

Lacking neural tissue and being avascular, articular cartilage's ability to self-heal is limited, partly due to an absence of supply of blood and oxygen [169]. Articular cartilage is composed of a sparsely distributed population of chondrocytes, and a much larger proportion of ECM, which acts as a structural component and supports the tissue [29, 191]. Chondrocytes are essential to producing and maintaining articular cartilage matrix and are the only type of cells found in healthy cartilage, besides a small number of chondro-progenitor cells in the surface zone. Autologous chondrocytes have been well documented for their reparative abilities of chondral defects, but as there is a very sparse population of chondrocytes in cartilage tissue,

it is hard to harvest them. Additionally, as chondrocytes are embedded in ECM their movement is limited [25], which is thought to also contribute to the cartilage's lack of capability to self-repair, as chondrocytes cannot migrate to the site of a wound [47]. Nevertheless, a proportion of the population has asymptomatic defects that seem to heal spontaneously [46]. It is not known how these defects heal, but perhaps the chondro-progenitor cells play a role.

Osteochondral defect healing is spontaneous with quality of the regenerated tissue unpredictable, and can often be primarily fibrous resulting in subsequent degradation. When an osteochondral defect forms, damaged blood vessels located within bone at the site of the defect produce blood which coagulates and forms a fibrous clot. Within this clot there are thought to be cartilage and bone precursors, such as mesenchymal stem cells, along with a fibrin net that acts as a scaffold for cells to travel along [123]. These MSCs are thought to move into the defect, differentiate into chondrocytes, fibroblasts and osteoblasts which synthesize new bone at the bottom of the defect. Growth factors such as Ihh and PTHrP help mediate the process of healing, which is hypothesised to occur via endochondral ossification, the process of cartilage being replaced by bone tissue occurring in the presence of chondrocytes [120]. Cartilage initially fills the osteochondral defect before endochondral ossification takes place, initially occurring at the base of the defect and continuing until bone tissue is restored and a layer of cartilage is left remaining at the top of the defect. The tissue resulting from natural healing of osteochondral defects is generally of poor quality overall; although the defect may fill it is typically with fibro-cartilaginous tissue which is not the hyaline-type needed to withstand the compressive forces exerted across the knee and other weight-bearing joints [74, 83]. Generally, this fibrocartilage tissue that fills the defect will degrade meaning the original symptoms of pain and discomfort return, occasionally with the patient developing osteoarthritis as a result, and as such is of inferior quality compared to natural articular

cartilage [177].

Natural repair in animal models

Various animal studies show osteochondral defects healing via an endochondral ossification-type process, with an initial cartilage template being formed with subsequent calcified cartilage and bone formation. Gotterbarm *et al.* [73] used the Gottingen mini-pig as a translational model to investigate healing of full-thickness chondral and osteochondral defects. Osteochondral defects of 5.4 - 6.3 mm x 8 - 10mm were created in the medial of the patello-femoral joint. These defects filled with fibrous tissue and fibrocartilage after 6 & 12 weeks, with endochondral ossification occurring first at the edges of the defect at 12 weeks. Bone restoration was reported to be 80% of maximum at 1 year. Despite these defects showing some reparative characteristics, overall these defects did not heal well, indicating they were of or above a critical size at which successful healing does not occur. Shapiro *et al.* [161] created 3 mm diameter osteochondral defects in New Zealand white rabbits. Their results showed that within a few weeks the defect had filled almost entirely with a cartilage matrix, with chondrocytes undergoing an endochondral type sequence in the deepest layers of the cartilage, with endochondral bone first formed here at 12-24 weeks post operation.

Lydon *et al.* [120] showed osteochondral defects located in the distal medial femoral condyle of an ovine model healed via endochondral ossification, with the purpose of the study being to uncover the underlying mechanism driving osteochondral defect healing after much hypothesis that defects exhibit endochondral ossification characteristics in rabbits and goats [83, 120, 161]. Defects of size 7mm x 6mm were created in 40 adult sheep, with no cells implanted so spontaneous repair could be observed. Their results showed blood clot and

fibrous tissue to fill the defect at 2 weeks, with new cartilage formation adjacent to the damaged articular cartilage layer between 4 and 8 weeks. It is thought the cartilage was first forming here due to chondrocytes at the edges of the damaged defect promoting healing, or chondrocytes derived from the fibrous tissue contributing to cartilage regeneration. By 8 weeks, chondrocytes lined the edges of the defect and cartilage formation had occurred, with new bone observed by 18 weeks at the edges and bottom of the defect. At 26 weeks healing was nearly complete, with cartilage and bone filling the entire defect but no proper tidemark formation. There was some remaining cartilage in the subchondral bone, which would likely undergo remodelling in the future. This study successfully showed the sequential process of osteochondral defect healing via endochondral ossification in ovine models.

2.1.4 Current treatment of chondral and osteochondral defects

Suitable treatment strategies for defects of the bone-cartilage unit are of high clinical importance due to cartilage's limited reparative capability and defects puncturing the subchondral plate typically resulting in fibrocartilage regenerative tissue, which is inferior to natural articular cartilage and subchondral bone. Symptomatic chondral and osteochondral defects that are left untreated can lead to gradually increasing cartilage loss and progressive degenerative osteoarthritis (OA). In humans, many details of tissue regeneration after surgical cell implantation are unknown. Some insight into cartilage healing can be obtained from animal models [1]. Characterising the success of the surgery is closely linked to the structural composition of the regenerated tissue [174].

Surgical strategies

Depending on various factors such as patient age, defect size, location and quality, surgical intervention is the appropriate treatment strategy for chondral and osteochondral defects that are not yet osteoarthritic. These treatment options include bone-marrow stimulus procedures such as microfracture and mosaicplasty, cell therapies such as ACI and ASI, and in some cases total knee arthroplasty [19].

Microfracture is a surgical keyhole procedure that involves creating a small incision into the knee in order to insert a camera and instruments to create small holes in the subchondral bone that stimulate cartilage healing [102, 131]. Creating these holes allows more vascular bone, such as cancellous and cortical bone, to be exposed near the joint along with a new blood supply [151]. The subchondral plate is avascular, meaning its capacity for healing is limited, whereas deeper bone contains marrow cells and can therefore promote cartilage growth [151]. This process however does have its limitations: the tissue thought to regenerate in the defect is of inferior quality to articular cartilage, and is expected to degenerate over time. Studies have shown that after a 5-year period the quality of tissue regenerated by microfracture surgery begins to deteriorate, with patients struggling with recurrence of pain due to their bone being re-exposed [98].

The procedure of mosaicplasty/OATs uses an autologous osteochondral graft, usually cylindrical, which is attached to the subchondral bone. This osteochondral graft is taken from a low weight-bearing area [155]. The procedure can be described as minimally invasive due to the small incisions required to obtain and insert grafts and the short healing time (2-4 weeks for weight-bearing activity) [29]. Mosaicplasty is only used on 'young' patients and

is not suitable for patients showing early signs of osteoarthritis, which makes this treatment unsuitable in many cases due to the reasonable proportion of chondral and osteochondral defects presenting with osteoarthritic attributes [10, 29, 155]. OATs performs well in large size osteochondral defects with regenerated tissue of hyaline quality, but drawbacks of this technique include donor site morbidity, lack of availability of healthy cartilage in the human body, and the difficulty to match grafts [80, 90, 125].

Total knee replacement arthroplasty first began in the 1970s and it has since been a challenge for researchers to find materials that can replicate the longevity and absorbability of articular cartilage [6, 162]. The materials currently used are metals, plastics (such as polyethylene), and ceramics [162, 168]. Patients sometimes find their movement is limited as soon as one year after knee replacement surgery and can also experience swelling of the joint along with pain and numbness around the scar left behind from the surgery. Knee replacements are usually recommended for patients over the age of 55 as artificial joints are not expected to function fully for much more than 15 years [132, 162]; the number of young patients receiving this surgery is very low because of this [39, 70]. There are several possible surgical complications that can occur during the procedure, with patients being at risk of a fracture in the femur, patella or tibia [169]. Blood vessels and nerves can also become damaged and deep-vein thrombosis can occur [72, 157]. Despite these complications and drawbacks, satisfaction levels for total knee arthroplasty are reported to be greater than 80% [88].

Autologous Chondrocyte Implantation (ACI) was first put into practice in the late 20th century and is usually performed on the knee, although it can also be carried out on defects in the ankle, shoulder, hip, and elbow, but this is less common [29]. ACI involves a keyhole

harvest procedure to obtain chondrocytes from healthy cartilage, a period of culturing and expanding the chondrocytes *in vitro*, and implantation of these cultured cells into the defect. Once the cells have been cultured to an amount in the region of 5-10 million there is thought to be a sufficient amount to implant into the defect [10]. The defect is debrided to healthy cartilage and sealed by either a periosteal patch obtained from the shin-bone or a collagen-membrane cover [71, 75, 123] (Fig. 2.3).

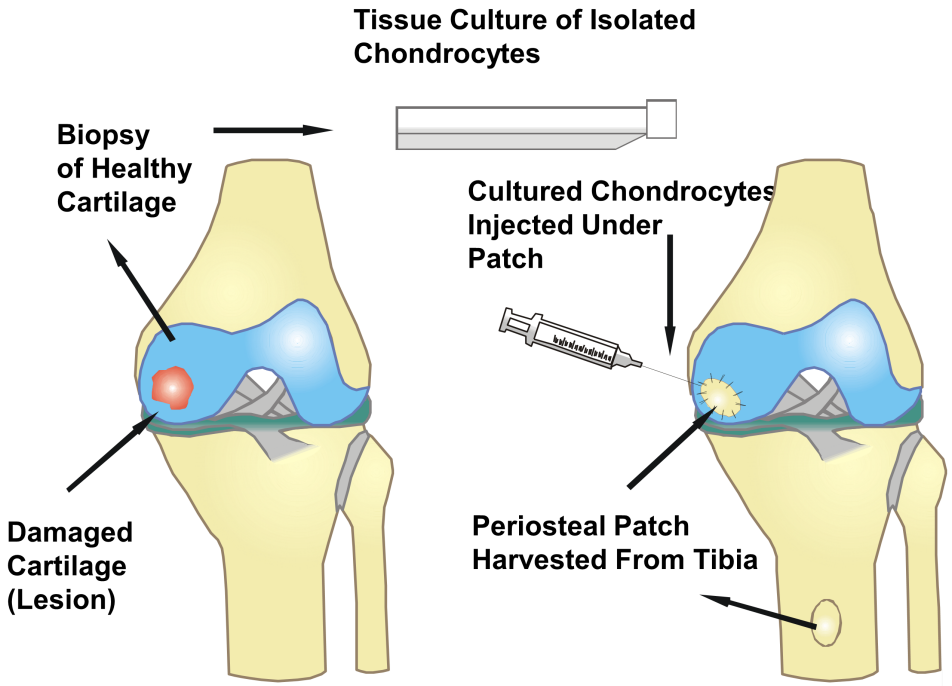

Figure 2.3: Schematic of an ACI procedure. The ACI scheme is courtesy of Andy Biggs (medical illustrator at the RJAH Orthopaedic Hospital, Oswestry).

Trials have suggested that ACI treated defects produce a better quality articular cartilage, surpassing that of most other available treatments [10]. Generally, ACI repair tissue is similar to that in appearance of natural articular cartilage, albeit a little softer in texture, as shown in animal models [35]. ACI is a treatment strategy widely used for chondral and osteochondral defects, with favourable outcomes in both small and large sized defects [43, 142]. In October 2017, the National Institute for Health and Care Excellence (NICE) decided this procedure

was cost-effective and approved its use in the NHS [60, 130].

A comparison study conducted by Bentley, Biant *et al.*, [10] suggests the quality of articular cartilage produced by the method of mosaicplasty is inferior to that of autologous chondrocyte implantation (ACI) in osteochondral defects. The results from this study showed that 88% of patients who had lesions treated with ACI had a 'good or excellent' quality of cartilage in the defect after 1 year, as opposed to mosaicplasty which only had 69% categorised in the same way. It is also noteworthy that of those treated with mosaicplasty, 17% had worse quality of cartilage in the defect than prior to the procedure; all ACI treated cartilage showed an improvement over the duration of the experiment [10]. Additionally, a review by Harris *et al.* [75] shows both ACI and microfracture treated articular cartilage defects showed improvement when tested on a sample of 60 patients; this was also reported by Basad *et al.* [8]. It was clear from the studies conducted that patients treated with ACI had a better outcome overall, with patients having a better quality of life and suffering less pain than that of microfracture treated patients [75]. The patients' ability to return to intensive activities such as sports after 2 years was equal between both treatments, whereas after 5 years microfracture treated defects had seen a deterioration in ability but ACI treated defects had not. This demonstrates that long term ACI is better able to restore functionality of damaged articular cartilage [75]. It is natural to conclude that ACI is the most promising treatment for articular cartilage damage due to lowest prevalence of complications, a generally better quality of cartilage reproduction, and longer durability. Studies by de Windt *et al.* [43] also suggest ACI is the preferred treatment strategy for defects varying in size from below 2.5cm^2 to larger than 4cm^2, located in both the femoral and patella compartment with the knee joint, whether chondral or osteochondral, with only chondral and osteochondral defects below 2.5cm^2 located in the femoral recommended for treating with a microfracture or OATs

procedure over ACI, respectively. This also demonstrates that in most cases of cartilage and subchondral bone damage, ACI is the gold standard treatment [43].

Novel cell therapies

An alternate cell-based therapy, which we refer to as Articular Stem Cell Implantation (ASI), replicates the ACI procedure except instead of chondrocytes, mesenchymal stem cells (MSCs) are used [141]. The capacity of stem cells to differentiate into different cell types along with their abundance within the body and the ease with which they can be harvested makes them advantageous to be used in cell-based therapies instead of chondrocytes. This larger volume of stem cell availability could mean the culturing period of cells required during ACI is not necessary. Despite these advantages, when using stem cells in place of chondrocytes in an implantation procedure there may be a delay period in which the stem cells must first differentiate into chondrocytes before the healing process can be initiated.

The co-implantation of mesenchymal stem cells and chondrocytes into chondral and osteochondral defects in an ACI-like procedure is hypothesised to result in enhanced chondrogenesis and extracellular matrix production, and is a new potential cell therapy for the treatment of defects of the bone-cartilage unit [35, 140, 194].

Wu *et al.* published a series of articles focused on the trophic effect mesenchymal stem cells have during cartilage regeneration [187, 188, 185, 186, 107]. Their work demonstrated co-cultures of human mesenchymal stem cells (hMSCs) and bovine mesenchymal stem cells (bMSCs) resulted in enhanced matrix formation when compared with matrix formation of

the individual cell populations. This was verified by histology and glycosaminoglycan levels in assay. Their work also demonstrated an increase in cartilage matrix production regardless of the source of MSCs, whilst also studying the effects of different culture media to show this enhanced effect occurred, regardless of culture conditions. They also set up experiments to identify the soluble factors they noted as responsible for this trophic effect on matrix formation when MSCs and chondrocytes are co-implanted. They identified candidate genes for the factors, validated by human qPCR. Immuno-fluorescent staining confirmed fibroblast growth factor-1 (FGF-1) was being expressed primarily by MSCs. BMP-2 is thought to be predominantly expressed by chondrocytes, and was also identified at higher levels in the co-culture pellets. Drawbacks of such *in vitro* studies include a short time-frame upon which the experiment is conducted, the lack of physiological mechanical loading, which would influence *in vivo* cell behaviour, and risk of de-differentiation of cells. Work by Bekkers *et al.* [9] also demonstrated the combination of chondrons (chondrocytes in their native matrix) with mesenchymal stromal cells resulted in increased cartilage formation in freshly created goat cartilage defects. Their study showed the combination of chondrons and MSCs performed favourably compared to microfracture.

The assumptions we made in this model do simplify the biological process occurring during osteochondral healing, potentially limiting conclusions we can draw from this work. Important factors we do not consider in our model include biochemical and biomechanical influences (as detailed in Chapter 2), which play a key role in cell differentiation, matrix synthesis and cell proliferation, among other important mechanisms within osteochondral defect regeneration [106]. Mechanical loading is also thought to influence the patterns of endochondral ossification, specifically in the formation of long bones [183]. We also excluded the effects of other local growth factors, with FGFs and BMPs thought to play an important role in the endochondral ossification process [103]. Additionally, we considered our critical cartilage density,

$m_{C_{crit}}$, as the local hypertrophy-initiating factor, following earlier work [24, 66]. However, a biologically more appropriate method of modelling the local factor might be through a locally produced growth factor. A specific candidate would be C-type natriuretic peptide (CNP), which is produced by chondrocytes and is thought to have a critical concentration above which hypertrophy is initiated [100]. Effectively, our model used cartilage density as a proxy for CNP concentration and although modelling CNP separately might affect the results, the change is most likely minor.

Stimulated repair in animal models

Schlichting *et al.*[160] created critical sized osteochondral defects in the femoral condyle in an ovine model, to explore the effects of scaffold implantation and stiffness in osteochondral healing. Critical sized defects are defined to be defects that fail to heal as they are too large in size, with classification differing between animal species. In ovine models this critical size is assumed to be approximately 20 mm^3 [1]. They observed in untreated defects endochondral ossification occurring as early as 3 months post defect creation, with their work concluding that the inclusion of a stiff scaffold supports the defect during repair and results in improved reparative tissue at early time. Soft scaffolds did not show good healing at 3 months, but by 6 months both groups with soft and stiff scaffold exhibited similar results, indicating stiff scaffolds have the most significant effect at early time, but do not change the overall outcome of defect healing. These findings indicate changes in mechanical properties in critical sized ovine osteochondral defects can impact healing success at early times.

Wakitani *et al.* [177] explored the implantation of osteochondral progenitor cells, such as mesenchymal stem cells, into osteochondral defects in the hope to promote tissue regenera-

tion, akin to an ASI procedure. They created defects sized 3×6mm in the medial femoral condyle of rabbits. They inserted collagen gels seeded with bone-marrow-derived or periosteal cells into half of the defects. Defects in the contralateral knee were used as the control, with some left empty and some with a cell-free collagen gel implanted. Their results showed the implantation of MSCs/periosteal cells resulted in very similar results, so there was no significant difference with the two cell sources. The implanted cells differentiated uniformly into chondrocytes, with cartilage formation first observed to fill the defect which was subsequently converted into bone at the base, with completely repaired subchondral bone by 24 weeks. The empty defects also healed, with mechanical testing showing the cell-implanted defects had stiffer repair tissue, but less stiff than natural articular cartilage.

2.2 Mathematical modelling

A simple mathematical model transforms a concept using mathematical notation in place of ordinary language to represent a complex scientific problem. Mathematical modelling in regenerative medicine has been developed and improved upon to give an understanding of the regrowth of bone and cartilage in joints, along with tumour angiogenesis, wound healing, fracture healing and many other important biological processes. These models simplify complicated processes while still capturing important components of real world problems and producing relevant and informative results.

Chondral and osteochondral defect regeneration is driven by cell behaviour and extracellular matrix deposition to form newly regenerated tissue; more specifically chondrocyte, mesenchymal stem cell and osteoblast motility, which can be modelled as a diffusive process, along with

cartilage and bone matrix production, cell proliferation, mesenchymal stem cell differentiation, chondrocyte hypertrophy, nutrient utilisation and apoptosis. The literature explored in this section will give examples of how these processes can be modelled, whether for cartilage and bone regeneration or more broadly within tissue engineering and regenerative medicine.

First, we will discuss the importance of and detail the principles that underpin mathematical modelling within regenerative medicine, including Fick's Law of diffusion, that can be used to describe cell motility, and Michaelis-Menten kinetics, that is used to model cell nutrient uptake and cell diffusion dependence on extracellular matrix. We will then discuss relevant literature that uses the reaction-diffusion modelling approach to describe cartilage and bone regeneration and the effects of growth factors on these healing mechanisms. Then, we will explore a multiphase modelling approach, followed by discussion of current mathematical models relevant to our problem of chondral and osteochondral defect regeneration. We will also discuss other relevant and important modelling examples, such as those of tumour growth and wound healing, to give a broader overview of the application of these modelling approaches. The modelling techniques undertaken in these works form a basis for the following chapters, where a continuum reaction-diffusion modelling approach is undertaken, independent of the influence of mechanics.

2.2.1 General modelling principles & regenerative medicine

Regenerative medicine underpins highly complex mechanisms which can be difficult to predict without knowledge of the processes governing tissue growth and cell to cell, matrix to cell and phase interactions. Although having various limitations such as unknown parameters, potentially unrealistic predictions and over-simplifications, mathematical models have

the ability to be refined and can allow us to better understand problems that would be otherwise unpredictable. Many cases can be explored using mathematical models that have not yet been predicted using clinical trials. Within mathematical modelling of regenerative medicine, either a continuum or discrete modelling approach is undertaken. The continuum approach considers a cell population as a whole that completely occupies its space, and is the approach typically undertaken when cell numbers are very large. Discrete models consider cells individually, referred to typically as agent-based models, and is applied to problems studying phenomena on a small scale, where cell properties differ spatially [20, 139]. In many scenarios of mathematical modelling within tissue engineering and regenerative medicine cell numbers exceed the levels appropriate to undertake a discrete modelling approach, and understanding the fate of each individual cell is not informative, and as such we focus on the continuum modelling technique in the remainder of this chapter and is the chosen approach for the following models formulated in this thesis [20].

Reaction-Diffusion modelling Reaction-diffusion systems are systems of equations where spatial variance, x, is of importance within the specific problem [176]. Reaction-diffusion modelling is an approach widely used in many biological scenarios, such as population dynamics, predator-prey systems, competition, symbiosis, and chemical reactions [105], and is formulated to predict how concentration changes over time by diffusion. Reaction terms within these systems of equations can describe cell behaviour, with cell motility described by Fick's first and second laws. These laws were refined by Alan Turing in 1952 [171], where he proposed the development of tissue (morphogenesis) was driven by diffusion and chemical reaction, and based on these observations subsequent mathematical models of tissue pattern formation have been formulated [34, 99, 171].

In the mid-19th century Adolf Fick derived Fick's laws of diffusion to describe the relationship between diffusive flux and concentration. Under the assumption of a steady state, Fick postulated that spatial variance is proportional to the magnitude of the flux moving from a high concentration to a low concentration [82, 176].

$$\frac{\partial \phi}{\partial t} = -D\frac{\partial^2 \phi}{\partial x^2}, \tag{2.1}$$

where D represents a diffusion coefficient (rate) and ϕ represents substance (per unit volume). This equation is commonly referred to as Fick's first law of diffusion, or the heat equation, and is used to describe the diffusive behaviour of cell populations where cell motility can be described as a diffusive process, with ϕ representing a cell density (per unit volume).

Fick's second law is widely used as a backbone in the area of mathematical modelling for regenerative medicine and has been used to form a basis for many reaction-diffusion models. Reaction-diffusion models explain how the concentration of several substances changes due to chemical reactions and diffusion [82, 99]. The typical form of a reaction-diffusion equation comprises a diffusion term, as detailed by Fick's first law, and reaction terms [176].

$$\frac{\partial \phi}{\partial t} = -D\frac{\partial^2 \phi}{\partial x^2} + R, \tag{2.2}$$

where R represents the reaction terms (rates). Reaction terms can be used to describe certain cell characteristics such as cell proliferation, differentiation, and apoptosis i.e. a cell proliferation rate, as obtained from experimental data, modelled proportional to the cell population, ϕ.

Also fundamental to the formulation of reaction diffusion models is Michaelis-Menten kinetics, a principle that relates reaction rate to substrate concentration. This modelling approach is widely used when describing the saturation of cell nutrient uptake rates and random motility of cells when attached to a substrate, along with other cell behaviours [48, 79, 148, 149, 178].

The relationship between substrate and reaction rate is given by:

$$\frac{\mathrm{d}[P]}{\mathrm{d}t} = \frac{V_{max}[S]}{(K_m + [S])} \tag{2.3}$$

where $[P]$ is product formation, $[S]$ substrate concentration, V_{max} the maximum reaction rate at enzyme saturation, and K_m the Michaelis-Menten constant defined as the substrate concentration at half V_{max}.

An example of how these modelling principles can be used together in reaction diffusion modelling is for cell behaviour where cell diffusion (motility) is dependent on extracellular matrix density, relevant to our problem of chondral and osteochondral defect regeneration, i.e.,

$$\frac{\partial \phi}{\partial t} = -D_\phi \Big(\frac{m}{m^2 + m_1^2} \Big) \frac{\partial^2 \phi}{\partial x^2} + R\phi, \tag{2.4}$$

where D_ϕ represents cell diffusion coefficient (rate), ϕ represents a cell density (per unit volume), m represents extracellular matrix density (per unit volume), m_1 represents a reference matrix density (per unit volume), and R the proliferation (rate) of ϕ.

This models cell behaviour where cells proliferate with a specified rate R, and diffuse dependent on the matrix density, with cell diffusion formulated to increase for low matrix densities and decrease for high matrix densities [119].

Types of Solutions for Partial Differential Equation (PDE) systems For the above system we have formulated a PDE, where boundary ($\phi_x(x = x_0, t) = \phi_0$) and initial (i.e. $\phi(x, t = 0) = \phi_{init}$) conditions are applied to create a PDE problem, that can have 2 forms of solution:

(1.) *Analytical solution*, where the solution is a mathematical function that can be solved exactly.

(2.) *Numerical solution*, where the solution is not a mathematical function, and is therefore solved by numerical approximation of the analytical solution, with high accuracy.

For many systems of PDEs, and much of the literature that follows in the remainder of this chapter and the mathematical models that are formulated within this thesis, a numerical approximation of the solution is the chosen approach, as no analytical solution exists (i.e., the PDE systems are non-linear). An example of a numerical scheme that can be used to solve a system of PDEs is the *Method of Lines* (MOL), where we replace the spatial derivatives in the PDE with approximations in algebraic form:

The *First step* is to approximate the spatial derivative with an algebraic expression, using a second order central *finite difference* approximation, such as

$$\frac{\partial^2 \phi}{\partial x^2} \approx \frac{\phi_{i+1} - 2\phi_i + \phi_{i-1}}{h^2} \tag{2.5}$$

Where i represents the location along the grid $x \leq i \leq \chi$. For the minimum value of x, $i = 1$,

and for the maximum value of x, $i = \chi$, meaning the grid has χ points. *Then* we have

$$\frac{\partial \phi}{\partial t} = -D_{\phi}\Big(\frac{m}{m^2 + m_1^2}\Big)\frac{\phi_{i+1} - 2\phi_i + \phi_{i-1}}{h^2} + R\phi, \qquad x \leq i \leq \chi. \tag{2.6}$$

We have replaced the spatial derivatives by a system of ordinary differential equations (ODEs) that approximates the original PDE. *Then*, all boundary and initial conditions must also be approximated using the same above method. *Finally,* we are ready to integrate the system over t. The solution of this ODE system outputs χ functions $\phi_1(t), ..., \phi_\chi(t)$.

The numerical scheme detailed above is the method used for the mathematical models formulated in this thesis, solved in in MATLAB (Release 2013a, The MathWorks, Inc., Natick, Massachusetts, United States) using the stiff ODE solver *ode15s*.

NB. Other methods of finite difference approximation include first-order forward, first-order backward, second-order forward and second-order backward. The method shown here is the method undertaken in the remainder of the thesis.

Reaction-Diffusion models of cartilage and bone regeneration

Most relevant to the works undertaken in this thesis, Lutianov *et al.* [119] formulated a mathematical model of the regeneration of cartilage after cell therapy, most specifically when an ACI or ASI procedure is undertaken, as detailed in 2.1.4, for which a mathematical model had not been previously developed [119]. A continuum, reaction-diffusion-type mathematical model was formulated to better understand the repair of cartilage once previously expanded chondrocytes or mesenchymal stem cells are inserted into a chondral defect, with the hope of regenerating usually irreparable or highly degradable cartilage. The mechanical loading

environment and growth factors were not considered in this model despite their important roles in the regrowth of damaged cartilage. Modulating cell proliferation, differentiation and migration, the mechanical loading can influence the overall structure of the tissue and the extracellular matrix production. Growth factors belonging to the TGF-β superfamily, more specifically TGF-β1, FGF-1,2 are well documented for their abilities to increase the formation of cartilaginous tissue and chondrogenesis, but are not considered here for simplicity. Their mathematical model follows the framework of a reaction-diffusion process with reaction terms consisting of cell proliferation, cell differentiation and apoptosis, with nutrient uptake and cell diffusion modelled using Michaelis-Menten kinetic terms to simulate limiting behaviour associated with these processes.

They first simulated chondrocyte implantation, corresponding to ACI, with cells initially seeded along the subchondral bone interface. Over longer time periods, due to low chondrocyte proliferation, diffusion is the main cause of chondrocytes reaching the top of the defect. As there is a large supply of nutrients matrix is produced at a high rate, and consequently the density of chondrocytes is restricted due to the larger volume of matrix present. At around 36 months, the chondrocytes and matrix in the defect have diffused to a steady state with a large volume of regenerated matrix present, almost filling the entirety of the defect. Next, they consider an initial implantation of mesenchymal stem cells, corresponding to ASI. Nutrients are utilised much faster at early times and as a result stem cells diffuse to the top of the defect where more nutrients are available. The implanted mesenchymal stem cells then continue to proliferate and eventually differentiate into chondrocytes once they have surpassed their differentiation threshold value, with matrix deposition following soon after. Their findings show there is minimal difference in healing time between chondrocytes or mesenchymal stem cells being initially implanted into the chondral defect, but observe differences

in the evolution of healing. In fact, they conclude that due to stem cells needing to take up a large amount of nutrients to differentiate into chondrocytes, the case where chondrocytes are implanted is a more optimal route to take during a cell implantation surgery. When stem cells are implanted there is a delay in the production of chondrocytes but still a large amount of nutrients being utilised, meaning when matrix begins to be produced in larger volumes once the stem cells have exceeded their differentiation threshold, there are less nutrients for the matrix and as such limits the matrix production rate. This leads to the conclusion that stem cell implantation might not be optimal in comparison to the initial implantation of chondrocytes alone. The results obtained by Lutianov *et al.* [119] are justified by findings from animal models and previous clinical studies and successfully capture the key characteristics of chondral healing. This model will act as a basis for the work undertaken in Chapters 3 & 4, where the equations (and modifications) will be stated and modelling justifications detailed.

Bailon-Plaza and Van der Meulen [7] developed a mathematical model focusing on fracture healing and the effects cytokines and growth factors have on this process. The main growth factors that have been identified to regulate the fracture healing process are TGF-β and BMPs. Their equations modelled the evolution of chondrocytes and osteoblasts residing in the fracture callus. They assumed, following an assumption of rotational symmetry about the marrow cavity, that their problem was two-dimensional. Their work is based on underlying principles seen in earlier literature of fracture healing, hypothesising that cartilage and bone formation is dependent on the level of mechanical stress and strain in various regions within the callus and occurs via endochondral ossification. For this mathematical model cell proliferation, differentiation and migration, growth factor production and diffusion, and ECM synthesis and degradation are simulated at the fracture site over time. The approach taken for this mathematical model follows the earlier work of Olsen *et al.* 1996, 1997 [147, 146], and

Murray 1993 [138], in which models for wound healing, tumour morphogenesis and angiogenesis have been outlined. These models have given an indispensable understanding of how growth factors and extracellular matrix regulate these processes. This mathematical model is formed to further extend the knowledge of the effects on the healing response of the initial concentrations of the released growth factors. The effects of the mechanical environment in the callus, along with interactions between ECM, receptors and growth factors were not considered for simplicity. In addition, during fracture healing more tissue forming cells and ECM types are present than are considered in this model. Despite this, the model presented was able to successfully simulate fracture healing histology observed in rats via the process of endochondral ossification.

Obradovic *et al.* [144] formulated a mathematical model of glycosaminoglycan (GAG) deposition in engineered cartilage, specifically cartilage produced from chondrocytes seeded onto a biodegradable scaffold cultivated in bioreactors. Their model and experiments were developed to understand the relationship between GAG expression and oxygen concentration, where GAG production was used as a marker for chondrogenesis. Their model utilised a reaction-diffusion type approach and Michaelis-Menten principles to model chondrocyte uptake of oxygen. Their model successfully supported their hypothesis of glycosaminoglycan synthesis and oxygen expression, demonstrating low oxygen levels inhibit good cartilage formation as proposed in the literature, and approximated the processes occurring in engineered cartilage formation that mediate development.

Garzon-Alvardo *et al.* [64] undertook a reaction-diffusion modelling approach to describe the process of long bone growth, occurring via endochondral ossification, under the influence of

important biochemical signalling pathways such as PTHrP and Ihh and mechanical stresses and strains. Their model predicts diaphysis growth and epiphysis formation of a long bone with spatial distribution of chondrocytes shown to influence bone morphology. Despite making several simplifications, their model corresponds to experimental findings and data.

Other more recent modelling studies have highlighted the importance of growth factors and MSC-chondrocyte interactions within chondral defect regeneration. Kimpton *et al.* [96] showed how different cell seeding strategies and growth factors affect the spatial distribution of cells within a hydrogel inserted into a chondral defect. Chen *et al.* [27] explored the interactions between MSCs, chondrocytes and TGF-β. They demonstrated how adopting this strategy combining growth factors produced by the cells and exogenous addition of growth factors has advantages over each individual strategy.

Multiphase modelling and Mixture theory Multiphase modelling is a mathematical modelling technique used to describe multiphase flow scenarios, i.e. tissue growth with multiple tissue types (phases). Mixture theory uses the theories of continuum mechanics to model complex multiphase systems, with major application in regenerative medicine. It is derived from early work in the mid 1800's by Fick and Stefan [33]. The theory of mixtures considers solid and liquid phases to be present at any point within a continuum, meaning these points are not distinguishable from one another. A mixture is comprised of at least 2 ingredients and can be classed as either immiscible, when the particles remain identifiable, and miscible if they lose their identity within the mixture [33]. Mixture theory requires constitutive laws to describe the type of phase. For example, a liquid phase can be modelled as either Newtonian or non-Newtonian by the viscosity, the measurement of the resistance to gradual deformation

when under shear or tensile stress. Corresponding to each constituent of a mixture, Truesdell and Toupin [170] formulated energy balance equations of momentum, mass and energy. The equations for a multiphase modelling approach are formulated using spatial averaging with variables including true density, pressure, velocity and stress. The sum of the liquid and solid fractions are equal to one [85]. The theory of mixtures has been applied to several different areas of tissue engineering such as tumour growth, which uses the specific assumption of a fluid model [81]. Other applications of mixture theory include models for incompressible fluid-particle suspensions, interstitial tissue growth and nutrient depletion [33, 85, 108].

Multiphase modelling of cartilage and bone regeneration

Mow *et al.* [133] formulated a mathematical model of biphasic interactions within articular cartilage. At this time articular cartilage was considered to have no or very little internal interactions between phases due to its lack of blood supply, nerves and lymphatic system. In this work, Mow *et al.* hypothesise biphasic theory, a theory that specifically focuses on the interactions between the interstitial fluid phase and solid matrix phase of articular cartilage using the theory of mixtures. They derive their equations using balance of momentum, constitutive mass laws, energy balance and entropy inequality, linear deformation theory and the assumption that the organic solid matrix and the interstitial fluids are intrinsically incompressible. Their biphasic theory model was the first to accurately predict the deformation of articular cartilage, although at the time of the research some of their assumptions had not been experimentally verified.

Kelly and Prendergast [91] built on biphasic poroelastic finite element models of spontaneous repair applied to osteochondral defects in the knee, specifically focusing on the mechano-

biological influence on stem cell differentiation. This mathematical model focuses on a relationship between the diffusion, differentiation, proliferation and eventual apoptosis of mesenchymal stem cells and the mechanical environment. Kelly and Prendergast model the formation of bone through both endochondral and intramembranous ossification at the bottom of the defect, the formation of cartilage in the centre of the defect and fibrous tissue formation at the top of the defect, with a greater amount of fibrous tissue predicted to grow in larger osteochondral defects. The results obtained from the model demonstrated that osteogenesis (bone formation) is initiated due to the osteochondral defect being protected initially by adjacent cartilage that is still in-tact. Once the repair tissue starts to stiffen, mechanical loads can be supported and chondrogenesis commences in the centre of the defect. Direct intramembranous and endochondral ossification at the base of the defect begins a progression leading to fibrous tissue forming at the articular cartilage surface because of the fluid flow and strain in this area. The volume of cartilage in the defect is then predicted to decrease due to areas containing cartilage differentiating into fibrous tissue, and endochondral ossification increasing bone formation. Despite the achievements of this model, there are many simplifications, i.e. the effects of growth factors such as TGF-β and BMPs being ignored (unlike in earlier work [7]), and additionally an initial cartilage fill is not observed here but is shown to occur in animal experiments [120, 161]. The model still accurately simulated the differentiation observed in cells during osteochondral defect healing experiments, and as such can be successfully used to develop a theory to explain the rapid degradation of osteochondral defect repair.

Zhang *et al.* [193] formulated a mathematical model focusing on the chemical and mechanical stimuli moderating the healing of bone fractures. They proposed a model investigating the repair of a fracture callus that is treated as a multiphase mixture comprised of liquid, solid

and solute phases, modelled as a combination of diffusion and advection equations. The liquid phase represents interstitial fluid, thought to be the most likely stress-derived factor that informs the bone cells of mechanical loading. The solid phase and solute phase represents ECM and growth factors, such as IGFs (Insulin-like Growth Factors), respectively. Their computational model considers the fracture conditions such as shape, position and size, the method of fixation used for the fracture along with loads exerted due to the patient's natural movement. The solid phase in this model is assumed to be linearly elastic which, although is justifiable for simple modelling, is not feasible due to the fracture callus being a heterogeneous material; for a more practical and refined model this assumption would have to be improved upon to consider the fracture callus more realistically.

2.2.2 Mathematical modelling of tissue growth and regeneration

Here we consider mathematical models with a broader application within regenerative medicine, i.e. those concerned with tumour growth, epidermal wound healing and engineered tissue growth. We include these models to show more examples of the modelling approaches undertaken in the following chapters of this thesis and how these methods can be applied to various scenarios within regenerative medicine.

Lemon *et al.* [109] formulated a framework for the modelling of porous flow for *in vitro* tissue growth. Focusing on the microscopic level, they chose to model the tissue growth and dynamics involved in this process, and ignore the interactions between cells and other materials. Each tissue constituent has a corresponding equation formulated of mass and force equations. Interphase and intraphase pressure terms are derived from mechanical interactions at the microscopic level between the tissue constituents. Inertial effects are neglected

along with water being assumed as an inviscid fluid. Their constituents are considered to have no voids, i.e. they sum to 1. They derive a general equation for an *ith* phase using an equation for mass transfer, and once summing over all of the i phases we obtain a conservation condition. Porous flow models are now used to relate the dynamics of the phases at any non-specific point within the *in vitro* tissue, through which each phases' motion is in reaction to the stresses within its phase, and also by the pressures applied from the other phases. The interphase forces, defined as the forces influencing the interfaces joining each pair of phases, are modelled with forces comprised in terms of drag components and interphase pressures. Later in 2007 Lemon and King expand on their multiphase porous flow model to apply it to cell behaviour on artificial scaffolds [108]. Their work concentrates on the effects of non-uniform porosity and the depletion of nutrients. For their model they assume the cells act as a viscous fluid, the scaffold is porous and rigid with its porosity inconsistent and water as an inviscid fluid. Their simulations show that without a notable effect on the total cell yield that a better penetration of cells into the scaffold can be achieved by increasing the motility of cells.

Prendergast *et al.* [152] formulated a mathematical model focused on the biophysical stimuli on cells during tissue differentiation at implant interfaces. They outline a mathematical model based on the biphasic theory represented by Mow *et al.* [133] to describe how cell differentiation is mediated by stimulus from the surrounding mechanical environment. It is thought this stimulus can alter cell shape and influence the motility of bioactive factors, but the influence on cell differentiation had not yet been explored. Prendergast *et al.* assume all constituents of their mixture are present at all material points and as such can assume that the sum of the volume fraction is 1, following from the biphasic and mixture theories. They formulate their equations using the conservation of linear momentum, thermodynamic constraints and Darcy's law. Their model is formulated using the previous work of Kelly, 1964

[93], Cowin & Hegedus, 1976 [32, 77] and Mow *et al.* [133] to derive their equations for the mixture. They use a finite element model to analyse the peri-implant tissues and push-out tests were implemented to calculate the Young's modulus of the interface tissues. Push-out tests are conducted to test for the adhesion of the implant with the bone. It was seen that tissue differentiation increased as the Young's modulus of the interfacial tissue was intensified. Their mixture theory model predicts their hypothesis; the mechanical environment has influence on the differentiation of tissue, indicating there may be boundaries between mechanical states with reactions taking place once a boundary is crossed, initiating differentiation from one tissue type to another.

Orme and Chaplain [148] developed a mathematical model describing vascular tumour growth and invasion. Their model details how a tumour grows and forms a necrotic core due to high nutrient demand, leaving central cells dead and outer cells still proliferating; this results in the tumour growth stopping. The tumour can undergo angiogenesis, the formation of new blood vessels, which gives the tumour a new supply of nutrition, supressing its inactive state. Orme and Chaplain touched upon other pathological conditions in which angiogenesis can be undertaken such as chronic inflammation, arthritis and diabetic retinopathy. Their mathematical model follows Liotta *et al.* [114] using conservation of mass laws to formulate their equations. They formulate their model under the assumption tumour cells react to blood vessels as observed in taxis, the movement of continuous living systems in response to a stimulus such as nutrients. Previous models assume the tumour to be modelled as a diffusive term but this is not applicable here. In this case, the tumour cells are moving upward a capillary gradient. Because of this, the tumour cell flux is modelled as the sum of a diffusion term and a taxis term. Assumptions also made include rapid proliferation of the tumour, providing there is a sufficient amount of nutrients available, and when the tumour is in its

avascular stage it becomes dormant and has reached its largest possible size. It is also assumed that the tumour is radially symmetrical. After running simulations, it is noted that the model reproduced the key events that occur during vascular tumour growth. Diffusion, migration and proliferation of tumour cells causes the cells to advance across the host tissue field. Liotta *et al.* [114] shows that cells not reaching the centre of the tumour fast enough explains the formation of a necrotic core. Once vascularisation has taken place the entirety of the tumour is crossed with capillaries. Orme and Chaplain later discuss the restrictions of their model stating that some assumptions made and mechanisms neglected call for the model to be not entirely accurate, such as cell to matrix interactions and the development of an age-structured model where two ages of cells would be observed. Despite this, the model successfully replicates the results of *in vivo* observations.

Many other models describing the various mechanisms occurring during tumour growth have been formulated since, such as those by Ward *et al.*, 1997 [178], and Hubbard and Byrne, 2012 , [81]. A mathematical model was formulated by Ward *et al.* to describe deterministic tumour growth, with the tumour assumed to be an conglomeration of living and dead cells (two phases), a modelling approach of tumour growth that had not been previously attempted. A velocity field is created within the tumour from expansion generated by living cells, and contraction generated by cell death. They modelled cell growth and division to be dependent on nutrient availability, described using Michaelis-Menten principles. Their model successfully demonstrated an initial exponential growth that becomes linear over time. They deduce that nutrient diffusion is highly important in the phases of growth, and also demonstrate a correlation between their model results and experimental data. In more recent work by Hubbard and Byrne [81] a multi-dimensional model of avascular tumour growth using a multiphase continuum approach is proposed. They consider the tissue to be comprised of 4

distinct phases: healthy cells, tumour cells, blood vessels and extracellular matrix. All phases are assumed to act as a viscous fluid. Applying the principles of conservation of mass and momentum a two-dimensional model is formulated which is then discretised using a finite element/volume scheme. Their simulations indicate the mathematical model formulated accurately replicates the characteristic pattern of vascular tumour growth. This model could be successfully applied to other biological problems including tissue engineering and wound healing.

2.3 Summary

It has been demonstrated in this chapter there is a large body of literature studying mathematical modelling of fracture healing, tumour growth and angiogenesis, bone regeneration and growth, and engineered tissue growth. However, very little literature focuses on mathematical modelling of osetochondral defect regeneration, in particular using the reaction-diffusion modelling approach, reproducing the sequential healing process as described in the literature [120, 161], and considering the effects of cell implantation. Additionally, there is no mathematical model to describe the effects of growth factors on the chondral healing process, or how co-implantation of MSCs and chondrocytes might impact defect healing, despite literature indicating co-implantation could result in a trophic healing scenario through the effect of important growth factors [184]. The mathematical models formulated in the following chapters of this thesis aim to bridge these gaps in the literature, with the effects of growth factors and co-implantation of mesenchymal stem cells and chondrocytes on chondral healing being explored in chapters 3 & 4, following the work of Lutianov *et al.* [119]. Chapter 5 sees a novel mathematical model formulated to describe osteochondral defect regeneration after

cell implantation, following the modelling approaches demonstrated in chapters 3 & 4 and relevant literature discussed in this chapter, particularly those that use a reaction-diffusion modelling approach [7, 119].

Chapter 3

Mathematical model of chondral defect regeneration after cell therapy – the influence of growth factors

Within this chapter we will develop a mathematical model to explore the hypothesis that the mutual growth factor mediated interaction between mesenchymal stromal cells (MSCs) and chondrocytes, after implanting these cells into a cartilage defect, affects the pattern of cartilage matrix production over the time-frame needed to achieve repair. The hypothesised nature of the interaction and its short-term effects (up to 1 month) on matrix production will be based on the *in vitro* experimental findings of Wu *et al.*[184]. The various rate constants required in the mathematical model will be based on *in vitro* or *in vivo* data where possible, otherwise an assumption will be made. For all model parameters, sensitivity analyses will be

performed to determine the influence of the parameter value on the model outcomes. The specific role of the mathematical model is to find the extent to which short-term (1-2 months) effects on matrix production persist in the longer term (1-2 years).

Firstly, the model formulation is discussed with explanation for modelling choices of the growth factors provided, along with details of non-dimensionalisation and parameter choices. Next, we present the results of the model and make comparison to simulations not including the effects of growth factors in order to highlight the impact of their inclusion. Following on from this, we conduct a sensitivity analysis to validate our parameter choices, and discuss in more detail those parameters that exhibit particularly interesting characteristics when varied. Finally, we summarise the findings of this work, with main discussion located in Chapter 6.

3.1 Introducing the problem

Autologous Chondrocyte Implantation (ACI) is a commonly used cell-based therapy mainly used in the treatment of cartilage damage in the knee, first implemented clinically in 1987 [17]. The treatment involves obtaining chondrocytes from a biopsy of healthy cartilage, culturing and expanding these chondrocytes *in vitro* for several weeks to an amount in excess of 5-10 million [190], and a surgical implantation procedure of these cultured cells into the damaged (or defect) region [15, 17].

The geometry represented in Fig 3.1 represents an *in vivo* scenario. The rationale for the 1D assumption is based on evidence from large-animal models that variations in cell and matrix density or nutrient concentration during and following repair primarily occur along the depth of the defect, as labelled in Fig. 3.1, whereas relatively little variation occurs along the width of the defect [143, 179]. We acknowledge that chondral defects can vary greatly in dimension,

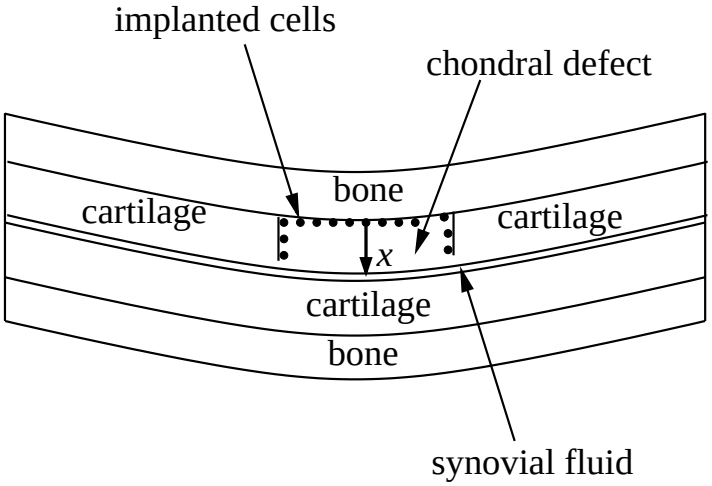

Figure 3.1: Schematic of a cross-section of the defect. The diameter of the defect is approximately 10-20mm and its thickness 2-3mm. After debridement of the defect, chondrocytes or MSCs are implanted into the defect along the bottom and sides. The initial number of cells implanted are around 10^6 cells/cm^2 of defect area [58].

from small *mm*-sized lesions of articular cartilage to *cm*-sized defects of full thickness that penetrate through to the calcified cartilage zone. However, cell therapy is only advised when defects are at least 2 cm^2 (equivalent to 1.6cm diameter) [60] and in practice only defects down to or into the subchondral bone are treated [142]. Hence, a model based on a 1-D geometry that covers the full depth of a defect can concentrate on the essential processes of cartilage repair following cell implantation, while neglecting the dimensions where little variation is observed.

The chondrocytes proliferate (by taking-up nutrients) and migrate, in the process forming extracellular matrix (ECM) and new cartilage. In the case of MSCs, the process of forming new cartilage is initiated only after the stem cells first differentiate into chondrocytes. Growth factors, such as those from the Transforming Growth Factor-beta (TGF-β) family, e.g., TGF-β-1 and Bone Morphogenetic Protein (BMP-2), and Fibroblast Growth Factor, FGF-1 and FGF-2, are also known to regulate cell migration, proliferation and differentiation, although their mechanisms are not clearly understood.

As detailed in Chapter 2, Wu [184] showed increase in matrix deposition when co-culturing mesenchymal stem cells (MSCs) and chondrocytes *in vitro*. Their findings show that when culturing a mixture of stem cells and chondrocytes, an increase in matrix deposition is observed. This increase can be approximately quantified to be 50% for a 50:50 ratio of MSCs to chondrocytes, and 30% for an 80:20 ratio in comparison to a 100% MSC seeding at 4 weeks. They identified two growth factors, FGF-1, produced by the MSCs and is shown to influence the proliferation of the chondrocyte population, and, BMP-2, produced by the chondrocytes and is shown to induce chondrogenesis of MSCs. These two growth factors are hypothesised to mediate the mutual chondrocyte and MSC interaction as shown in Fig. 5.4 [187, 188, 185, 186, 107]. This hypothesis assumes that the increased matrix production is explained by the increased number of chondrocytes due to the actions of both growth factors. The same authors also found evidence that FGF-1 leads to increased matrix production per chondrocyte, which could also explain the increased matrix deposition in their experiments.

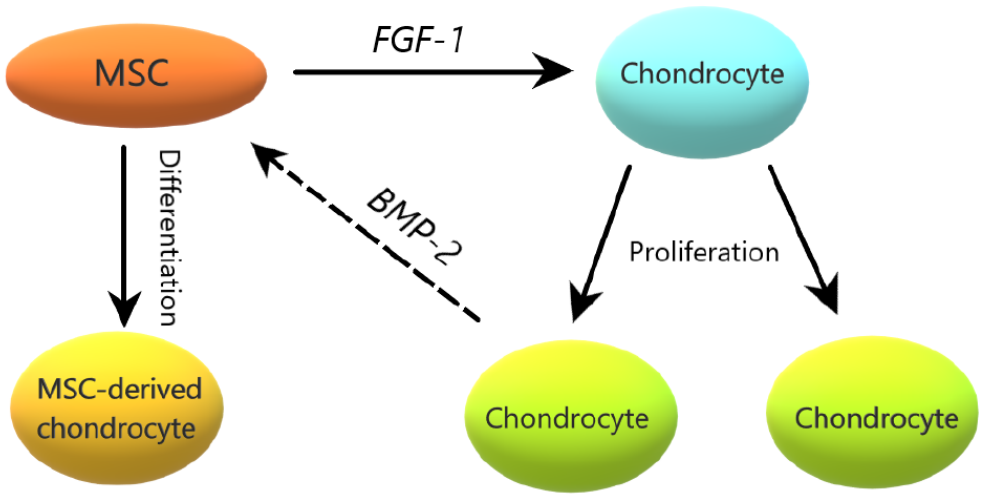

Figure 3.2: Schematic of hypothesised crosstalking between chondrocytes and MSCs mediated by FGF- 1 and BMP-2. Adapted from Wu *et al.* [184]

In 2011, Lutianov *et al.* [119] formulated a mathematical model to describe the various processes involved in the regeneration of a cartilage defect following the implantation of chondrocytes (ACI) or MSCs (ASI). This model showed that during the healing process there is very little difference in the overall time taken to heal the defect between the two cell therapies, suggesting that regeneration using stem cells alone is no better or worse than that using chondrocytes. The stem cells need to first differentiate into chondrocytes before forming ECM and new cartilage, a process that is initiated only after the stem cell density exceeds a threshold value. The overall healing time frame of about 18 months for the defect to reach full maturation corresponds with results from clinical studies and demonstrated that cartilage regeneration is a slow process. The only stem cell-chondrocyte interaction considered in this work was the one-way interaction in which MSCs differentiated to form chondrocytes once a threshold stem cell density was exceeded. This work did not include the influence of growth factors, as well as MSC-chondrocyte interaction.

The focus of this chapter, encouraged by the findings of Wu [184], is to investigate the role of growth factors and MSC-chondrocyte interactions in the regeneration of cartilage after stem cell implantation (ASI). Once stem cells differentiate into chondrocytes we can expect to see the same cell-to-cell interaction observed in co-cultures of MSCs and chondrocytes with similar trophic effects [187, 188, 185, 186, 107]. In Chapter 4, we will consider a co-implantation of MSCs and chondrocytes to see how this impacts matrix deposition compared with ACI and ASI cell therapies, motivated by a potentially earlier healing time. To achieve this, we first seek to address the specific question of the impact of growth factors, released via cell-to-cell interaction, on the deposition of matrix during chondral healing. Co-implantation of MSCs and chondrocytes could have important implications on how clinicians approach surgical procedures of the regeneration of cartilage, indicating a potentially superior procedure

could be implemented involving a mixture of MSCs and chondrocytes. We extend Lutianov *et al.* [119] to include the actions of growth factors BMP-2 and FGF-1 and investigate their mediating role on chondrocyte and MSC interaction hypothesised by Wu [184] and shown in Fig. 5.4. Including their proposed stem cell-chondrocyte interaction into our model would also enable validation of the enhanced matrix levels observed [184].

3.2 Mathematical model

3.2.1 Formulation

A typical cartilage defect has a small thickness depth to length ratio. This enables us to simplify to a one-dimensional problem where cell growth is modelled along the defect thickness only, shown as the x-direction in Fig. 3.1. The variables in our model are: the stem cell density, C_S (cells/mm^3), chondrocyte density, C_C (cells/mm^3), matrix density, m (g/mm^3), nutrient concentration, n (moles/mm^3), FGF-1 concentration, g (g/mm^3), and BMP-2 concentration, b (g/mm^3). Our model includes two types of cells, MSCs and chondrocytes. Both cell types in the model are able to migrate non-directionally (randomly) and proliferate via the uptake of nutrients. MSCs are able to differentiate and chondrocytes can deposit cartilage matrix. In order to explore the hypothesis that a mutual growth factor mediated interaction between MSCs and chondrocytes affects cartilage production, we include a further mechanism that models the soluble growth-factor mediated influence of chondrocytes on MSC differentiation and that of MSCs on chondrocyte proliferation. We do not include the biomechanical and biochemical effects discussed in Chapter 2. We also do not explicitly include directed cell migration (chemotaxis), the migration of a cell up or down the gradient of a stimulant (such as nutrient) or repellent. In this model, and the models formulated in the subsequent

chapters, the motility of cells is modelled proportional to the nutrient concentration, with cell proliferation and differentiation ceasing to occur when nutrient levels are low, meaning cell motility is the driving force of evolution at these times, migrating towards locations of higher nutrient concentration.

We follow the model of Lutianov *et al.* [119] to describe the evolution of the cell and matrix densities and nutrient concentration in time, t, and space, x, measured along the thickness of the defect (see Fig. 3.1). We state with brief comments the equations, with details of their results and model implications described in Chapter 2.

The rate of change of stem cell density, based on proliferation by uptake of nutrients, migration and differentiation into chondrocytes, is modelled as

$$\frac{\partial C_S}{\partial t} = \frac{\partial}{\partial x}\left(D_S(m)\frac{\partial C_S}{\partial x}\right) + p_1\left(m, \frac{C_S}{C_{S,max}(m)}\right)\frac{n}{n+n_0}C_S H(n-n_1) \\ - p_2 C_S H(C_S - C_{S_0}(b)) - p_3 C_S H(n_1 - n). \tag{3.1}$$

The third term on the right of Eq. (3.1) models stem cell differentiation into chondrocytes at a rate p_2 (assumed constant). This process is initiated once C_S exceeds a threshold density C_{S_0} modelled using the Heaviside function $H(C_S - C_{S_0})$, which takes the unit value when $C_S > C_{S_0}$ and zero otherwise. We assume that the BMP-2 growth factor concentration modulates stem cell differentiation by reducing the threshold density and is modelled as

$$C_{S_0}(b) = (C_{S_{0,max}} - C_{S_{0,min}})e^{-\alpha b} + C_{S_{0,min}}, \tag{3.2}$$

where $C_{S_{0,max}}$ and $C_{S_{0,min}}$ are maximum and minimum threshold densities, respectively,

and α is a decay constant. Alternatively, one could also model this modulation by making the stem cell differentiation rate, p_2, dependent on the BMP-2 growth factor concentration, keeping C_{S_0} fixed. We do not consider this here but briefly mention any sensitivity to this in section 3.3.2 on *Sensitivity of parameters and initial conditions*. The first, second and fourth terms on the right of Eq. (3.1) model stem cell migration (modelled as a diffusion process), proliferation and cell death, respectively, where D_s is the stem cell random motility (diffusion) coefficient (assumed to depend on the matrix density), p_1 is the stem cell proliferation rate (assumed to depend on the matrix and stem cell densities) and p_3 is the stem cell death rate (assumed constant) [119]. Following Lutianov *et al.* [119], we choose

$$D_S(m) = D_{S_0}\frac{m}{m^2+m_1^2}, \;\; p_1\left(m, \frac{C_S}{C_{S,max}(m)}\right) = A(m)\left(1-\frac{C_S}{C_{S,max}(m)}\right),$$
$$A(m) = p_{1_0}\frac{m}{m^2+m_2^2}, \;\; C_{S,max}(m) = C_{S,max_0}\left(1-\frac{m}{m_{max}}\right)$$

where D_{S_0} and p_{1_0} are reference migration and proliferation rates, respectively, m_1 and m_2 are reference matrix densities, and C_{S,max_0} and m_{max} are a maximum stem cell and matrix density, respectively. Diffusion is modelled to be dependent on the matrix density, as done in the related literature [7]. Cell motility is expected to increase for lower matrix densities and decrease for higher densities [119].

Similar to the above, the rate of change of chondrocyte density is modelled as

$$\frac{\partial C_C}{\partial t} = \frac{\partial}{\partial x}\Big(D_C(m)\frac{\partial C_C}{\partial x}\Big) + p_4\left(m, g, \frac{C_C}{C_{C,max}(m)}\right)\frac{n}{n+n_0}C_C H(n-n_1)$$
$$+ p_2 C_S H(C_S - C_{S_0}(b)) - p_5 C_C H(n_1 - n), \tag{3.3}$$

where D_C is the chondrocyte random motility (diffusion) coefficient, p_4 is the chondrocyte

proliferation rate and p_5 is the chondrocyte death rate, as in Lutianov *et al.* [119]. We use similar expressions as above for

$$D_C(m) = D_{C_0}\frac{m}{m^2+m_1^2},\;\; p_4\left(m, g, \frac{C_C}{C_{C,max}(m)}\right) = B(m,g)\left(1-\frac{C_C}{C_{C,max}(m)}\right),$$
$$B(m,g) = \left(p_{4_0}\frac{m}{m^2+m_2^2} + p_{4_{00}}\frac{g}{g+g_0}\right),\;\; C_{C,max}(m) = C_{C,max0}\left(1-\frac{m}{m_{max}}\right)$$

where D_{C_0} is a reference diffusion rate, p_{4_0} is a reference proliferation rate, m_1 and m_2 are reference matrix densities and C_{C,max_0} is a maximum chondrocyte density [119]. The additional contribution to chondrocyte proliferation due to the influence of the FGF-1 growth factor is modelled by the second term in the expression for $B(m,g)$ in Eq. (3.4). Here $p_{4_{00}}$ and g_0 are a reference proliferation rate and FGF-1 concentration, respectively (Table 3.1). When g is small, $p_{4_{00}}\dfrac{g}{g+g_0}$ increases linearly, saturating to a limiting value of $p_{4_{00}}$ for larger values of g. A similar term representing the effect of growth factors on proliferation is used by Bailon-Plaza and Vander Meulen [7], and replicates a Michaelis-Menten-type saturation term. We assume the biological effect of the growth factor is an additive contribution to that from the matrix density, hence we add it to the original proliferation term, $p_{4_0}\dfrac{m}{m^2+m_2^2}$.

The rate of change of nutrient concentration and matrix density are as detailed below, adapted from Lutianov *et al.* [119] with minor changes made to our m equation. The rate of change of nutrient concentration is modelled by a Fickian-type diffusion term with nutrient uptake terms proportional to chondrocyte and stem cell densities, with a Michaelis-Menten type nutrient saturation. The rate of change of matrix density is similarly comprised of a diffusion term, a production term proportional to the chondrocyte density that is limited by a Michaelis-Menten type nutrient saturation term.

$$\frac{\partial n}{\partial t} = D_n \frac{\partial^2 n}{\partial x^2} - \frac{n}{n+n_0}(p_6 C_S + p_7 C_C), \tag{3.4}$$

$$\frac{\partial m}{\partial t} = D_m \frac{\partial^2 m}{\partial x^2} + p_8(m,g)\frac{n}{n+n_0} C_C, \tag{3.5}$$

where D_n and D_m are the nutrient and matrix diffusion coefficients, respectively (assumed constant), n_0 is a reference nutrient concentration, p_6 and p_7 represent the nutrient uptake rate by stem cells and chondrocytes, respectively (assumed constant) and $p_8(m,g) = (p_{8_0} - p_{8_1} m)(1 + p_{8_{00}} \frac{g}{g+g_0})$ is the matrix synthesis rate, where p_{8_0} is a matrix production rate, p_{8_1} is a matrix degradation rate and the last term in the brackets accounts for any additional matrix directly produced by FGF-1 with a pre-factor $0 < p_{8_{00}} < 1$ [119]. The main effect of FGF-1 is thought to be indirectly through the increase in chondrocyte proliferation modelled in Eq. (3.3). For our simulations we set $p_{8_{00}} = 0$ and explore the effects of non-zero values of $p_{8_{00}}$ in the section *Sensitivity of parameters and Initial conditions.*

The growth factor FGF-1 is produced by the stem cells, it migrates along the defect, degrades and then diffuses out of the upper end of the defect. Using this information, we model the rate of change of FGF-1 as

$$\frac{\partial g}{\partial t} = D_g \frac{\partial^2 g}{\partial x^2} + p_9 C_S - p_{11} g. \tag{3.6}$$

The first term on the right of Eq. (3.6) models diffusion of FGF-1 along the defect, with D_g (assumed constant) representing its diffusion coefficient. The second term on the right of Eq. (3.6) models the production of FGF-1, assumed proportional to the stem cell density, with production rate p_9. The third term on the right of Eq. (3.6) models the degradation of FGF-1 at a constant rate p_{11}. The growth factor BMP-2 is produced by the chondrocytes,

it can migrate along the defect and degrades. Using this information, we model the rate of change of BMP-2 as

$$\frac{\partial b}{\partial t} = D_b \frac{\partial^2 b}{\partial x^2} + p_{12} C_C - p_{13} b. \tag{3.7}$$

The first term on the right of Eq. (3.7) models diffusion of BMP-2 along the defect, with D_b (assumed constant) representing its diffusion coefficient. The second term on the right of Eq. (3.7) models the production of BMP-2, assumed proportional to the chondrocyte density, with production rate p_{12}. The third term on the right of Eq. (3.7) models the degradation of BMP-2 at a constant rate p_{13}.

3.2.2 Boundary conditions

We need to prescribe two boundary conditions for each variable. These boundary conditions are specified at the lower end of the defect, x =0 (subchondral bone interface), and upper end of the defect, x =d (normal cartilage surface), where d is the thickness of the defect. At $x = 0$ we impose no flux of cells, matrix, nutrients and growth factors, i.e.,

$$-D_S(m)\frac{\partial C_s}{\partial x} = -D_C(m)\frac{\partial C_c}{\partial x} = -D_n \frac{\partial n}{\partial x} = -D_m \frac{\partial m}{\partial x} = -D_g \frac{\partial g}{\partial x} = -D_b \frac{\partial b}{\partial x} = 0.$$

At $x = d$ we impose

$$-D_S(m)\frac{\partial C_s}{\partial x} = -D_C(m)\frac{\partial C_c}{\partial x} = -D_m \frac{\partial m}{\partial x} = 0, n = N_0, \;\; -Dg\frac{\partial g}{\partial x} = \gamma g, \;\; -Db\frac{\partial b}{\partial x} = \chi b.$$

The first, second and third boundary conditions represent no flux of stem cells, chondrocytes and matrix, respectively, from the normal cartilage interface. We assume that a reservoir of nutrients with concentration, N_0, is always available at this end.

A small flux of growth factors FGF-1 and BMP-2 are allowed to diffuse out of the defect and is

modelled to be proportional to the respective growth factor concentrations with constants of proportionality, γ and χ (assumed constant). A sensitivity analysis has been performed on γ and χ in section 3.3.2 *Sensitivity of parameters and Initial conditions*, with their approximate values given in Table 3.1.

3.2.3 Initial conditions

The initial conditions at $t = 0$ are prescribed as follows:

$$C_S = C_S^{(0)} h(x), \;\; C_C = C_C^{(0)}, \;\; n = N_0, \;\; m = m_3, g = g_{init}, \;\; b = b_{init}. \tag{3.8}$$

Here, $C_S^{(0)}$ and $h(x)$ are an initial stem cell density and profile, respectively. $C_C^{(0)}$, m_3, g_{init} and b_{init} are some initial chondrocyte and matrix densities, and growth factor concentrations (assumed to be uniformly distributed in the defect). The initial nutrient concentration is uniform with value N_0. The values of $C_S^{(0)}, C_C^{(0)}, N_0, m_3, g_{init}$, and b_{init} are stated and referenced in Table 3.1.

3.2.4 Non-dimensionalisation

There are several dimensional parameters appearing in the model. Their estimated values and the references from which they are obtained are provided in Table 3.1. All approximated parameters are disclosed in the table and references are given where available.

Once we have non-dimensionalised the system of equations all parameters are scaled against one another, meaning parameters with particularly large or small magnitude in non-dimensional space can be identified, indicating which mechanisms are likely to be most important to the investigated scenario. Non-dimensionalisation also makes it easier to observe how parameters

change in relation to one another, i.e. during a sensitivity analysis. Non-dimensionalisation can also be used to reduce the amount of parameters in a model, which can lead to simplification from a system of PDEs to ODEs. We do not use non-dimensionalisation for reduction in this thesis.

dimensional parameters	**estimated value**, *source type*
d, defect thickness	2 mm
D_S, maximum stem cell migration (or diffusion) coefficient	$3.6 \times (10^{-4}$ - $10^{-3})$ mm^2/hr [144], *in silico*
D_C, maximum chondrocyte migration (or diffusion) coefficient	3.6×10^{-4} mm^2/hr [144] *in silico*
$D_{S_0} = 2m_1 D_S$, stem cell migration (or diffusion) constant,	$7.2 \times (10^{-9}$-$10^{-8})$ (mm^2/hr) (g/mm^3) (assuming $m_1 = 10^{-5}$ g/mm^3)
$D_{C_0} = 2m_1 D_C$, chondrocyte migration (or diffusion) constant,	7.2×10^{-9} (mm^2/hr) (g/mm^3) (assuming $m_1 = 10^{-5}$ g/mm^3)
D_n, nutrient diffusion coefficient	4.6 mm^2/hr [195], *mathematical model*
D_m, matrix diffusion coefficient	2.5×10^{-5} mm^2/hr [144], *in silico*
D_g, FGF-1 diffusion coefficient	2×10^{-3} mm^2/hr [7], *mathematical model*
D_b, BMP-2 diffusion coefficient	2×10^{-3} mm^2/hr [7], *mathematical model*
p_1, maximum stem cell proliferation rate	0.2 cell/hr or 5 cells/day [7], *mathematical model*
$p_{1_0} = 2m_2 p_1$, stem cell proliferation constant	4×10^{-6} g/mm^3/hr (assuming $m_2 = 10^{-5}$ g/mm^3) [119], *mathematical model*
p_2, stem cell differentiation rate	3.75×10^{-3}/hr [144], *in silico*
p_3, stem cell death rate	3.75×10^{-3}/hr (guess)
p_4, maximum chondrocyte proliferation rate	2×10^{-4}/hr (guess)
$p_{4_0} = 2m_2 p_4$, chondrocyte proliferation constant	4×10^{-9} g/mm^3/hr [119], *mathematical model*
p_5, chondrocyte death rate	3.75×10^{-3}/hr (guess)

p_9, FGF-1 production constant	10^{-17}(g/mm^3)/((Nc/mm^3) hr) (guess)
p_{11}, FGF-1 degradation rate	5.8$\times$ 10^{-2} /hr (based on an approximate 12hr half-life, [38], *in vitro*)
p_{12}, BMP-2 production constant	10^{-17}(g/mm^3)/((Nc/mm^3) hr) (guess)
p_{13}, BMP-2 degradation rate	5.8$\times$ 10^{-2} /hr (based on an approximate 12hr half-life, [14], *in vitro*)
$p_{4_{00}}$, chondrocyte proliferation rate (from FGF-1)	2 $\times$ 10^{-4} /hr (guess)
p_{8_0}, matrix production constant	3.75 $\times$ 10^{-13}(g/mm^3)/((Nc/mm^3) hr)[144], *in silico*
p_{8_1}, matrix degradation constant	3.75 $\times$ 10^{-13}(g/mm^3)/((Nc/mm^3) hr) [144], *in silico*
p_6, nutrient uptake constant by stem cells	1.5 $\times$ 10^{-14}Nm/(Nc hr) [195], *mathematical model*
p_7, nutrient uptake constant by chondrocytes	1.5 $\times$ 10^{-14}Nm/(Nc hr) [195], *mathematical model*
$p_{8_{00}}$, FGF-1 matrix deposition rate	0 - 1 (guess)
C_{total,max_0}, maximum total cell density	10^6 Nc/mm^3 (assuming 10μm cell diameter)
C_{S,max_0}, maximum stem cell density	$0 - 10^6$ Nc/mm^3
C_{C,max_0}, maximum chondrocyte density	$0 - 10^6$ Nc/mm^3
m_{max}, maximum matrix density	10^{-4} g/mm^3 [7], *mathematical model*
$C_S^{(0)}$, initial stem cell density	2.5 $\times$ 10^5 Nc/mm^3 (based on 10^6 cells in 20mm x 20mm x 10μm volume)
$C_C^{(0)}$, initial cartilage cell density	10^2 Nc/mm^3 (10^{-2}% of total cell density)
$C_{S_{0_{max}}}$, threshold stem cell density	C_{total,max_0}/2 Nc/mm^3 (guess)

$C_{S_{0min}}$, threshold stem cell density	90% of $C_{S_{0max}}$ (guess)
m_1, matrix density	10^{-5} g/mm^3 (assumed $m_{max}/10$)[119], *mathematical model*
m_2, matrix density	10^{-5} g/mm^3 (assumed $m_{max}/10$)[119], *mathematical model*
m_3, initial matrix density	10^{-8} g/mm^3 (assumed $m_{max}/10^4$)[119], *mathematical model*
N_0, initial nutrient concentration	$(2.85 - 9.5) \times 10^{-11}$ Nm/mm^3 [195], *mathematical model*
g_{init}, initial FGF-1 concentration	10^{-12} g/mm^3 [7], *mathematical model*
b_{init}, initial BMP-2 concentration	10^{-12}g/mm^3 [7], *mathematical model*
n_0, threshold nutrient concentration	2.3×10^{-11} Nm/mm^3 [195], *mathematical model*
n_1, critical nutrient concentration	9.5×10^{-12} Nm/mm^3 (assumed $N_0/10$)
α, threshold stem cell density reduction factor	10^{10} /(g/mm^3) (guess)
g_0, FGF-1 reference concentration	10^{-10} g/mm^3 [7], *mathematical model*
b_0, BMP-2 reference concentration	10^{-10} g/mm^3 [7], *mathematical model*
γ, FGF-1 flux coefficient	10^{-2} mm/hr (guess)
χ, BMP-2 flux coefficient	10^{-2} mm/hr (guess)

Table 3.1: Estimated values of dimensional parameters. In the above, N_C represents number of cells and N_m is number of moles.

We non-dimensionalise Eqs. (3.1)- (3.8) by introducing the following dimensionless variables based on characteristic quantities for each variable.

$$\begin{aligned} &\bar{x} = x/d,\ \bar{t} = t(p_{8_0} C_{total,max_0}/m_{max}),\ (\bar{C}_S, \bar{C}_C) = (C_S, C_C)/C_{total,max_0}, \\ &\bar{m} = m/m_{max}, \bar{n} = n/N_0,\ \bar{g} = g/g_0,\ \bar{b} = b/b_0 \end{aligned} \tag{3.9}$$

where the overbars represent dimensionless quantities. The characteristic quantities used to measure the spatial variable, x, cell densities, matrix density and nutrient and growth factor concentrations are the defect thickness, d, the reference maximum total cell density, $C_{total,max0}$, the maximum matrix density, m_{max}, the initial nutrient concentration, N_0 and reference growth factor concentrations, g_0 and b_0, respectively. We choose to measure time, t, based on the matrix production time scale, $m_{max}/(p_{8_0} C_{total,max_0})$. Using the parameter values in Table 3.1, we estimate this time scale to be approximately 11 days. Henceforth, a unit of time corresponds to approximately 11 days. For each variable a sensitivity analysis was undertaken by increasing and decreasing their tabulated values given in Table 3.2 and investigating the effect on matrix production.

The dimensionless equations using the above non-dimensionalisation are:

$$\frac{\partial \bar{C}_S}{\partial \bar{t}} = \frac{\partial}{\partial \bar{x}}\Big(\bar{D}_S(\bar{m})\frac{\partial \bar{C}_S}{\partial \bar{x}}\Big) + \bar{p}_1\Big(\bar{m}, \frac{\bar{C}_S}{\bar{C}_{S,max}(\bar{m})}\Big)\frac{\bar{n}}{\bar{n}+\bar{n}_0}\bar{C}_S H(\bar{n}-\bar{n}_1)$$

$$- \bar{p}_2\bar{C}_S H(\bar{C}_S - \bar{C}_{S_0}(\bar{b})) - \bar{p}_3\bar{C}_S H(\bar{n}_1 - \bar{n}), \tag{3.10a}$$

$$\frac{\partial \bar{C}_C}{\partial \bar{t}} = \frac{\partial}{\partial \bar{x}}\Big(\bar{D}_C(\bar{m})\frac{\partial \bar{C}_C}{\partial \bar{x}}\Big) + \bar{p}_4\Big(\bar{m}, \bar{g}, \frac{\bar{C}_C}{\bar{C}_{C,max}(\bar{m})}\Big)\frac{\bar{n}}{\bar{n}+\bar{n_0}}\bar{C_C}H(\bar{n}-\bar{n_1})$$

$$+ \bar{p_2}\bar{C_S}H(\bar{C_S} - \bar{C}_{S_0}(\bar{b})) - \bar{p_5}\bar{C}_C H(\bar{n}_1 - \bar{n}), \tag{3.10b}$$

$$\frac{\partial \bar{n}}{\partial \bar{t}} = \bar{D}_n\frac{\partial^2 \bar{n}}{\partial \bar{x}^2} - \frac{\bar{n}}{\bar{n}+\bar{n}_0}(\bar{p}_6\bar{C}_S + \bar{p}_7\bar{C}_C), \tag{3.10c}$$

$$\frac{\partial \bar{m}}{\partial \bar{t}} = \bar{D}_m\frac{\partial^2 \bar{m}}{\partial \bar{x}^2} + \bar{p}_8(\bar{m},\bar{g})\frac{\bar{n}}{\bar{n}+\bar{n_0}}\bar{C_C}, \tag{3.10d}$$

$$\frac{\partial \bar{g}}{\partial \bar{t}} = \bar{D}_g\frac{\partial^2 \bar{g}}{\partial \bar{x}^2} + \bar{p}_9\bar{C}_S - \bar{p}_{11}\bar{g}, \tag{3.10e}$$

$$\frac{\partial \bar{b}}{\partial \bar{t}} = \bar{D}_b\frac{\partial^2 \bar{b}}{\partial \bar{x}^2} + \bar{p}_{12}\bar{C}_C - \bar{p}_{13}\bar{b}, \tag{3.10f}$$

where

$$\bar{p}_1\left(\bar{m}, \frac{\bar{C}_S}{\bar{C}_{S,max}(\bar{m})}\right) = \bar{A}(\bar{m})\left(1 - \frac{\bar{C}_S}{\bar{C}_{S,max}(\bar{m})}\right),\ \bar{A}(\bar{m}) = \bar{p}_{1_0}\frac{\bar{m}}{\bar{m}^2 + \bar{m}_2^2},$$

$$\bar{p}_4\left(\bar{m}, \bar{g}, \frac{\bar{C}_C}{\bar{C}_{C,max}(\bar{m})}\right) = \bar{B}(\bar{m},\bar{g})\left(1 - \frac{\bar{C}_C}{\bar{C}_{C,max}(\bar{m})}\right),\ \bar{B}(\bar{m},\bar{g}) = \bar{p}_{4_0}\frac{\bar{m}}{\bar{m}^2+\bar{m}_2^2} + \bar{p}_{4_{00}}\frac{\bar{g}}{\bar{g}+1},$$

$$\bar{C}_{S,max}(\bar{m}) = \bar{C}_{S,max_0}(1-\bar{m}),\ \ \bar{C}_{C,max}(\bar{m}) = \bar{C}_{C,max_0}(1-\bar{m}),$$

$$\bar{C}_{S,max_0} + \bar{C}_{C,max_0} = 1, \bar{p}_8(\bar{m},\bar{g}) = (1-\bar{p}_{8_1}\bar{m})(1 + p_{\bar{8}_{00}}\frac{\bar{g}}{\bar{g}+1}),$$

$$\bar{D}_S(\bar{m}) = \bar{D}_{S_0}\frac{\bar{m}}{\bar{m}^2+\bar{m}_1^2},\ \bar{D}_C(\bar{m}) = \bar{D}_{C_0}\frac{\bar{m}}{\bar{m}^2+\bar{m}_1^2},$$

$$\bar{C}_{S_0}(\bar{b}) = (\bar{C}_{S_{0,max}} - \bar{C}_{S_{0,min}})e^{-\bar{\alpha}\bar{b}} + \bar{C}_{S_{0,min}}.$$

(3.11)

The non-dimensional boundary and initial conditions are:

$$-\bar{D}_S(\bar{m})\frac{\partial \bar{C}_S}{\partial \bar{x}} = -\bar{D}_C(\bar{m})\frac{\partial \bar{C}_C}{\partial \bar{x}} = -\bar{D}_n\frac{\partial \bar{n}}{\partial \bar{x}} = -\bar{D}_m\frac{\partial \bar{m}}{\partial \bar{x}} = -\bar{D}_g\frac{\partial \bar{g}}{\partial \bar{x}} = -\bar{D}_b\frac{\partial \bar{b}}{\partial \bar{x}} = 0, \quad (3.12a)$$

(at $\bar{x} = 0$),

$$-\bar{D}_S(\bar{m})\frac{\partial \bar{C}_S}{\partial \bar{x}} = -\bar{D}_C(\bar{m})\frac{\partial \bar{C}_C}{\partial \bar{x}} = -\bar{D}_m\frac{\partial \bar{m}}{\partial \bar{x}} = 0, \;\; \bar{n} = 1, \;\; -\bar{D}_g\frac{\partial \bar{g}}{\partial \bar{x}} = \bar{\gamma}\bar{g}, \;\; -\bar{D}_b\frac{\partial \bar{b}}{\partial \bar{x}} = \bar{\chi}\bar{b}, \quad (3.12b)$$

(at $\bar{x} = 1$),

$$\bar{C}_S = \bar{C}_S^{(0)}\bar{h}(\bar{x}), \;\; \bar{C}_C = \bar{C}_C^{(0)}\bar{h}(\bar{x}), \;\; \bar{n} = 1, \;\; \bar{m} = \bar{m}_3, \;\; \bar{g} = \bar{g}_{init}, \;\; \bar{b} = \bar{b}_{init}, \quad (3.12c)$$

(at $\bar{t} = 0$).

The dimensionless parameters and their estimated values are provided in Table 3.2.

dimensionless parameters	estimated value
stem cell migration (or diffusion) constant, $\bar{D}_{S_0} = D_{S_0}/(p_{8_0} C_{total,max_0} d^2)$	10^{-3} - 10^{-2}
chondrocyte migration (or diffusion) constant, $\bar{D}_{C_0} = D_{C_0}/(p_{8_0} C_{total,max_0} d^2)$	10^{-3}
nutrient diffusion coefficient, $\bar{D}_n = D_n m_{max}/(p_{8_0} C_{total,max_0} d^2)$	$(1-3) \times 10^2$
matrix diffusion coefficient, $\bar{D}_m = D_m/(p_{8_0} C_{total,max_0} d^2)$	10^{-3}-10^{-2}
FGF-1 diffusion coefficient, $\bar{D}_g = D_g m_{max}/(p_{8_0} C_{total,max_0} d^2)$	1.14
BMP-2 diffusion coefficient, $\bar{D}_b = D_b m_{max}/(p_{8_0} C_{total,max_0} d^2)$	1.14
stem cell proliferation constant, $\bar{p}_{1_0} = p_{1_0}/(p_{8_0} C_{total,max_0})$	12
stem cell differentiation rate, $\bar{p}_2 = p_2 m_{max}/(p_{8_0} C_{total,max_0})$	1
stem cell death rate, $\bar{p}_3 = p_3 m_{max}/(p_{8_0} C_{total,max_0})$	1
chondrocyte proliferation constant, $\bar{p}_{4_0} = p_{4_0}/(p_{8_0} C_{total,max_0})$	0.012
chondrocyte death rate, $\bar{p}_5 = p_5 m_{max}/(p_{8_0} C_{total,max_0})$	1

FGF-1 production constant, $\bar{p}_9 = p_9 m_{max}/(p_{8_0} g_0)$	26.67
FGF-1 degradation rate, $\bar{p}_{11} = p_{11} m_{max}/(p_{8_0} C_{total,max_0})$	15.4
BMP-2 production constant, $\bar{p}_{12} = p_{12} m_{max}/(p_{8_0} b_0)$	26.67
BMP-2 degradation rate, $\bar{p}_{13} = p_{13} m_{max}/(p_{8_0} C_{total,max_0})$	15.4
chondrocyte proliferation rate (from FGF-1), $\bar{p}_{4_{00}} = p_{4_{00}} m_{max}/(p_{8_0} C_{total,max_0})$	0.012
matrix degradation constant, $\bar{p}_{8_1} = p_{8_1} m_{max}/p_{8_0}$	1
nutrient uptake constant by stem cells, $\bar{p}_6 = p_6 m_{max}/(p_{8_0} N_0)$	10^4
nutrient uptake constant by chondrocytes, $\bar{p}_7 = p_7 m_{max}/(p_{8_0} N_0)$	10^4
FGF-1 matrix deposition rate, $\bar{p_{8_{00}}}$	0 - 1
threshold nutrient concentration, $\bar{n}_0 = n_0/N_0$	0.24-0.81
critical nutrient concentration, $\bar{n}_1 = n_1/N_0$	0.1
threshold stem cell density, $\bar{C}_{S_{0_{max}}} = C_{S_{0_{max}}}/C_{total,max_0}$	0.35

threshold stem cell density, $\bar{C}_{S_{0_{min}}} = C_{S_{0_{min}}}/C_{total,max_0}$	0.315
initial stem cell density, $\bar{C}_S^{(0)} = C_S^{(0)}/C_{total,max_0}$	0.25
initial chondrocyte density, $\bar{C}_C^{(0)} = C_C^{(0)}/C_{total,max_0}$	10^{-4}
maximum stem cell density, $\bar{C}_{S,max_0} = C_{S,max_0}/C_{total,max_0}$	0.6
maximum chondrocyte density, $\bar{C}_{C,max_0} = C_{C,max_0}/C_{total,max_0}$	0.4
matrix density, $\bar{m}_1 = m_1/m_{max}$	10^{-1}
matrix density, $\bar{m}_2 = m_2/m_{max}$	10^{-1}
initial matrix density, $\bar{m}_3 = m_3/m_{max}$	10^{-4}
initial FGF-1 concentration, $\bar{g}_{init} = g_{init}/g_0$	10^{-2}
initial BMP-2 concentration, $\bar{b}_{init} = b_{init}/b_0$	10^{-2}
FGF-1 flux coefficient, $\bar{\gamma} = \gamma/(p_{8_0}C_{total,max_0}d/m_{max})$	1
BMP-2 flux coefficient, $\bar{\chi} = \chi/(p_{8_0}C_{total,max_0}d/m_{max})$	1
threshold stem cell density reduction factor, $\bar{\alpha} = \alpha b_0$	100

Table 3.2: Estimated values of dimensionless parameters.

3.3 Results and parameter sensitivity analysis

3.3.1 Methods

We use a second order accurate finite difference discretisation scheme to discretise the spatial variable x in Eqs. (3.10)-(3.12), keeping the time derivative t continuous. The resulting ordinary differential equations are solved in MATLAB (Release 2013a, The MathWorks, Inc., Natick, Massachusetts, United States) using the stiff ODE solver *ode15s*. Table 3.2 provides the non-dimensional parameter values.

3.3.2 Numerical results

We first consider the case where the defect is only seeded with stem cells and there are no growth factors present. These results will be used as a baseline case to compare with the case which includes the influence of growth factors. We re-run these simulations from Lutianov *et al.* [119], where a flux of mesenchymal stem cells entering from the bottom of the defect, thought to be sourced by the surrounding defect, was considered. Here, we omit this flux, as clinical guidelines state the underlying subchondral bone of a chondral defect is to be left intact, meaning we would not necessarily observe this flux [15].

Initially, stem cells are seeded close to the subchondral bone side of the defect ($x = 0$), and the nutrient concentration is uniform (Panel 1 in Fig. 3.3). The nutrient we consider in our model is oxygen, assumed to be diffusing in from the surrounding synovium of the joint. We also assume a small density of chondrocytes and matrix ($\bar{C}_C^{(0)} = \bar{m}_3 = 10^{-4}$) uniformly distributed across the defect in order to activate the cell and matrix evolution. Figs. 3.3 and 3.4 show the evolution of the stem cell density, C_S ($\times 10^6$ cells/mm^3), chondrocyte density, C_C

($\times 10^6$ cells/mm^3), matrix density, m ($\times 10^{-4}$ g/mm^3), and nutrient concentration, n ($\times 10^{-11}$ moles/mm^3), for time ranging between 2 to 18 months. Over the first few days (not shown here) the initial seeding of stem cells start to proliferate by taking up nutrients resulting in a gradual decline of nutrients near $x = 0$. The stem cells are also observed to slowly diffuse away from this end. Up until 2 months the stem cells have not yet proliferated enough to exceed their differentiation threshold value ($\bar{C}_{S_0} = 0.35$). As a result, there are no chondrocytes formed from stem cell differentiation and hence no matrix deposition. From approximately 2 months onwards, the stem cells have now exceeded their threshold value near $x = 0$ and we observe rapid formation of chondrocytes which in turn increases the matrix deposition at a rapid rate (Panel 2 in Fig. 3.3). We observe the formation of two fronts in the stem cell and chondrocyte densities which gradually migrate up the defect where a higher concentration of nutrients is available (Panel 3 in Fig. 3.3). The stem cell density front migrates faster than the chondrocyte front owing to its higher diffusion coefficient [144]. We also observe that where the nutrient concentration surpasses its critical value there is a peak in stem cells, and as a result a peak in chondrocyte density (Panels 2 and 3 in Fig. 3.3). The peak in chondrocytes is also due to the stem cells exceeding their differentiation threshold. Over the course of the first few months, we clearly observe an increase in matrix levels (Panels 2 and 3 in Fig. 3.3). At later times (4 months and beyond), an increase in matrix density is observed near the upper end of the defect due to this increase in chondrocyte formation observed from the peak in stem cells. This is enabled by the large amount of nutrients available (Panel 1 in Fig. 3.4). From approximately 9 months onwards matrix production continues gradually filling up the entire defect from the upper end down (Panels 2 and 3 in figure 3.4).

We now consider the influence of growth factors FGF-1 and BMP-2 on the evolution of the cell and matrix densities. We have an initial seeding of stem cells at the bottom of the defect with a small concentration of both the growth factors ($\bar{g}_{init} = \bar{b}_{init} = 10^{-2}$),

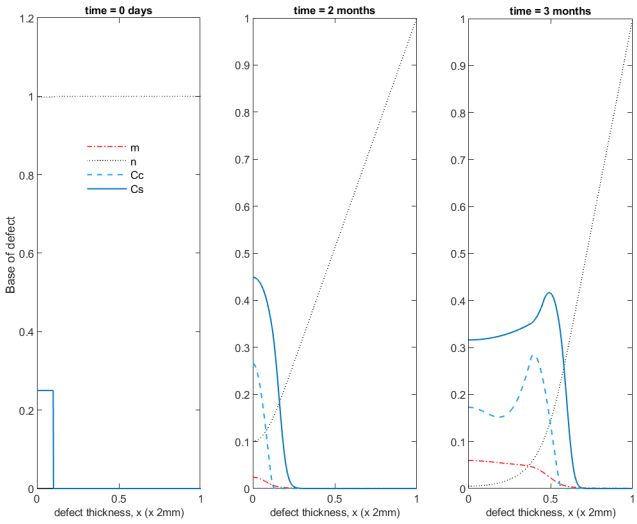

Figure 3.3: Evolution of cell and matrix densities, and nutrient concentration at times, $t =$ 0 days, 2 months, 3 months. $x = 0$ in the figure represents the location of the base of the defect, $x = 1$ represents the surface of articular cartilage.

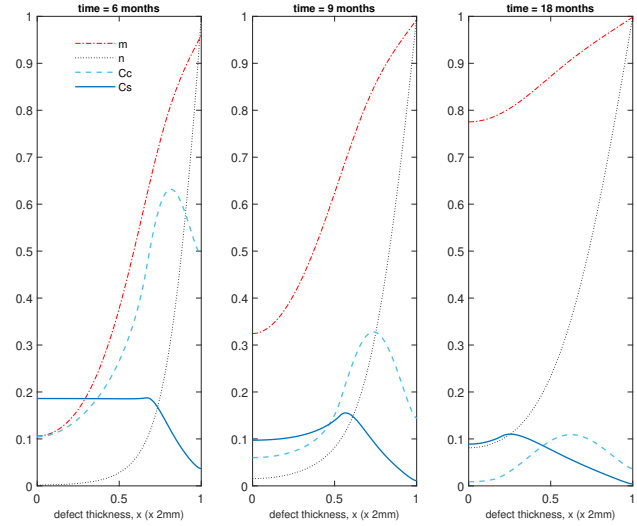

Figure 3.4: Evolution of cell and matrix densities, and nutrient concentration at times, $t =$ 6, 9, 18 months. $x = 0$ in the figure represents the location of the base of the defect, $x = 1$ represents the surface of articular cartilage.

and chondrocytes and matrix ($\bar{C}_C^{(0)} = \bar{m}_3 = 10^{-4}$) pre-existing uniformly within the defect (Panel 1 in Fig. 3.5). Similar to the early time behaviour observed in the previous case, the stem cells start to proliferate with a slow decline of nutrients in the first few days. These proliferating stem cells produce FGF-1 which gradually increases in concentration near the bottom of the defect. This has a minor influence on chondrocyte proliferation, though. The initial seeding of chondrocytes, however, produce sufficient BMP-2 which reduces the stem cell density threshold for differentiation into chondrocytes at an earlier time compared to the previous case. This resultant increase in the production of chondrocytes through stem cell differentiation in turn speeds up the matrix production process. This increase in chondrocyte and matrix density at early time ($t = 2$ months) is clearly observed in Panel 2 of Fig. 3.5 (also see Figs. 3.7(b, c) for comparison with the case when no growth factors are present). Also, at this time point we already observe a diffusion front in the stem cell density starting to form (Panel 2 in Fig. 3.5; also see Fig. 3.7(a) for comparison with the case when no growth factors are present). The growth factor concentrations are much higher near the bottom of the defect owing to the higher density of stem cells and chondrocytes there (Panel 2 in Fig. 3.5). The relative abundance of BMP-2 here, in particular, further lowers the threshold stem cell density to its minimum value, $\bar{C}_{S_{0min}}$, which increases the chondrocyte density (compare the chondrocyte densities in Panel 2 in Figs. 3.3, 3.5). From 2 months onwards, we observe the two fronts in the stem cell and chondrocyte density to gradually migrate up the defect where a higher concentration of nutrients are available (Panel 3 in Fig. 3.5 shows the evolution at $t = 3$ months). We note that these fronts are slightly ahead compared to those from the previous results (Panel 3 in Fig. 3.3) at this time point. This is due to the diffusion fronts forming earlier for this case as described above. Additionally, there is a larger volume of matrix in the defect at time points between two and three months (see Panels 2 and 3 in Fig. 3.5; also see Fig. 3.7(c) for comparison with the case when no growth factors

are present). The evolution past six months shown in Panel 1 of Fig. 3.6 is similar to the previous set of results, albeit with slightly higher levels of matrix at comparable time points. This might be due to the FGF-1 growth factor concentration enhancing the chondrocyte proliferation resulting in additional matrix. We note here that there is no contribution from stem cell differentiation since the stem cell density has fallen well below its minimum threshold density, $\bar{C}_{S_{0min}} = 0.315$, for differentiation into chondrocytes. For time twelve months and beyond, the matrix formation continues until the defect eventually fills up with matrix (see Panels 2 and 3 in Fig. 3.6).

We now highlight the differences at early time observed in the cell and matrix densities in the two sets of simulations above. We pick a representative time point at $t = 2$ months to depict this. We will also look at cases where either FGF-1 or BMP-2 alone are included to determine which growth factor has a stronger influence, if at all, on the system. In Fig. 3.7(a) we observe that the stem cell density near the bottom of the defect is lower when growth factors are included. This suggests that stem cell differentiation has occurred earlier for this case due to the lowering of the threshold density. The higher level of stem cell density for the case when growth factors are absent implies delay in stem cell differentiation due to the threshold density not being exceeded. Looking at the chondrocyte levels in Fig. 3.7(b) we observe that including growth factors results in a slightly higher chondrocyte density near the bottom of the defect compared to that without growth factors. These additional chondrocytes are produced by stem cell differentiation which occurs earlier in the presence of growth factors. This increase in chondrocyte density results in a significantly larger amount of matrix being formed compared to that without growth factors (Fig. 3.7(c)). Moreover, there is no discernible difference in the cell and matrix densities when comparing the cases where both growth factors are included to that where BMP-2 alone is included. This indicates that BMP-2 alone has a much more significant influence on the system than FGF-1 alone

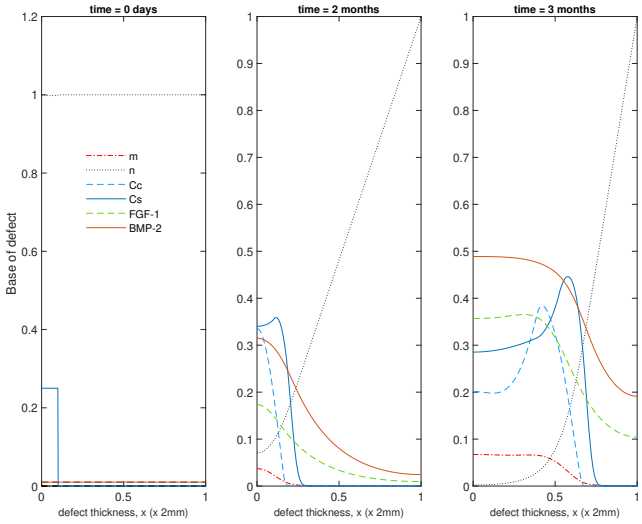

Figure 3.5: Evolution of cell and matrix densities, and nutrient and growth factor concentrations at times, $t = 0$ days, 2 months, 3 months. $x = 0$ in the figure represents the location of the base of the defect, $x = 1$ represents the surface of articular cartilage.

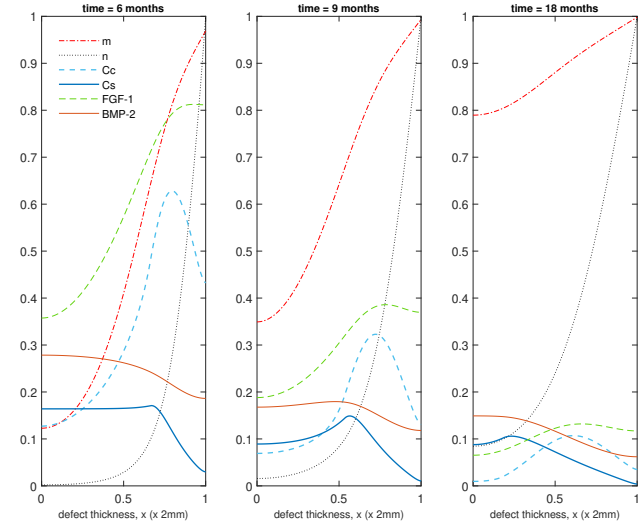

Figure 3.6: Evolution of cell and matrix densities, and nutrient and growth factor concentrations at times, $t = 6$, 9, 18 months. $x = 0$ in the figure represents the location of the base of the defect, $x = 1$ represents the surface of articular cartilage.

at least at an early time point. This is mainly due to the lowering of the threshold density for stem cell differentiation into chondrocytes. However, at a later time point this influence gradually decreases as the stem cell density falls well below its minimum threshold density for differentiation. Past 4 months the system then evolves similarly to that without growth factors.

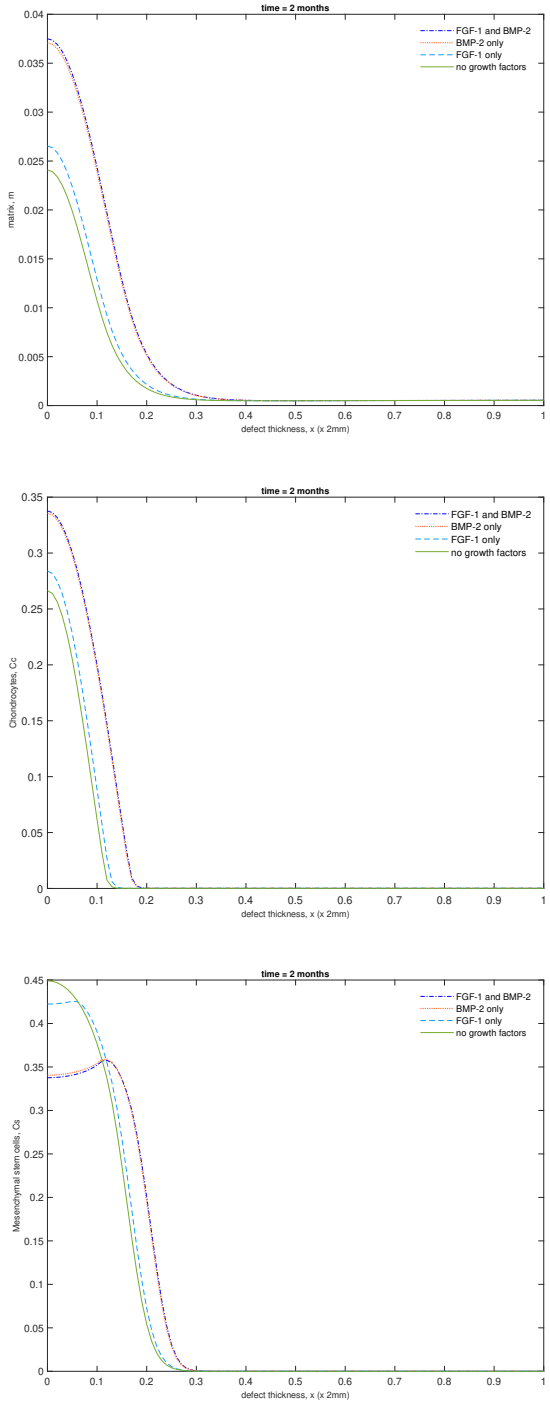

Figure 3.7: Comparison of (a) matrix (b) chondrocyte and (c) stem cell densities at t =2 months when including FGF-1 and BMP-2 (dot-dashed lines), BMP-2 alone (dotted lines), FGF-1 alone (dashed lines) and no growth factors (solid lines). $x = 0$ in the figure represents the location of the base of the defect, $x = 1$ represents the surface of articular cartilage.

To further highlight the effects of FGF-1 and BMP-2 on the system, we show comparisons of the overall densities of chondrocytes, C_C, mesenchymal stem cells, C_S and extracellular matrix (ECM), m, with and without the effects of growth factors over 24 months.

These results allow us to quantify the percentage difference between the cell and matrix types, with and without the effects of growth factors, enabling us to quantify our specific research question posed in the *Introduction* section. This gives us an indication of how considering these growth factors in a co-culture will impact matrix deposition.

Figure 3.8(a) shows overall matrix densities between 1 month and 2 years in time increments of 1 month. From this figure it is clear the main difference in matrix densities is at early times, with effects seeming to subside after around 4-5 months. At time 2 months we have a 65% increase in matrix density when growth factors are included, declining to 34% increase at 4 months. From 4 months onwards the percentage change of matrix density is still greater with growth factors, but decreases in magnitude.

Figure 3.8(b) shows the difference in chondrocyte levels within the defect up to 24 months. Chondrocyte proliferation and MSC differentiation into chondrocytes are mechanisms both effected by the growth factors, meaning we expect to see a pronounced increase in this cell type in the defect during healing. At time 2 months we see a 66% increase in chondrocyte levels, declining to only a 19% increase at time 4 months. The main increase in overall chondrocyte densities is primarily observable up to 4 months and subsides thereafter.

Figure 3.8(c) shows MSC densities within the defect over 2 years. The stem cell differentiation into chondrocytes mechanism is directly affected by BMP-2, meaning we expect to see lower MSC levels in the defect at times that growth factors are most effective. At times

1-3 months we see a slight increase in overall MSC levels, but Fig. 3.7(a) shows a diffusion front of MSCs forming sooner than without growth factors at 2 months due to the effects of FGF-1 and BMP-2. This indicates that MSC differentiation has been initiated sooner. Additionally, at this time chondrocyte densities are markedly higher than without growth factors (Figure 3.7(b)), meaning more BMP-2 is being produced. This implies evolution of MSCs is accelerated due to the effects of the growth factors during this time frame. At time 4 months we see a 13% decrease in MSC density, which is due to BMP-2 effects increasing due to increased chondrocyte densities around this time. After 4 months a consistent trend of lower MSCs is observed in the defect for the case with growth factors.

These results indicate and validate that the timeframe for FGF-1 and BMP-2 effects to be significant is at early times, primarily up until 4 months. The effects of growth factors subside thereafter, as demonstrated by the similarity between Figs. 3.4 and 3.6. The experiments of Wu *et al.*[184] are *in vitro*, and therefore performed over short periods of time. This therefore corroborates the effects they observe. It is likely the effects of FGF-1 and BMP-2 decline due to other limiting factors in the model such as nutrient concentration and motility of cells (Figs. 3.5 and 3.6).

Convergence analysis

A convergence analysis has been performed in space, x, with results showing the numerical scheme is reliable. For the simulations shown above the numerical scheme is performed over $n = 100$ grid points. Increasing n by a factor of 10 results in a slower runtime in the ODE15s solver, with the solution path unchanged. Convergence in time has also been explored, with a steady state obtained where the constituents of the regenerated defect remain full (at 1),

with the cartilage filling the entirety of the defect.

3.3.3 Sensitivity of parameters and initial conditions

The model is used to simulate a variety of parameter values and initial conditions. A sensitivity analysis will help in pinpointing those parameters that the system is sensitive to, which could indicate biological significance. In addition, a parameter whose value has been approximated and not deemed to be sensitive to change, then indicates that this approximate value is a good representation of that parameter value. Here, we only consider the sensitivity of the model to variations in the FGF-1 and BMP-2 parameters and initial conditions. These are described briefly in Table 3.3 and the ones which most influenced model results are discussed in detail below. The sensitivity to the other parameters and initial conditions are similar to that discussed in Lutianov *et al.* [119] and we refer the reader to Table 3 in this chapter.

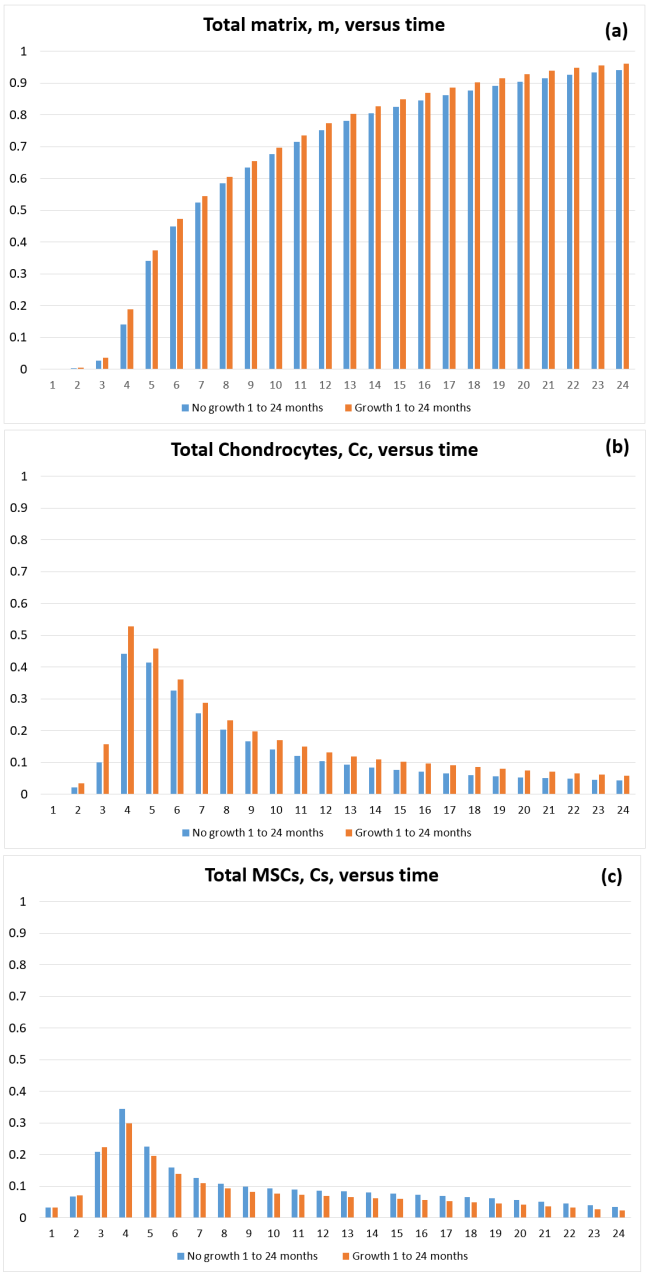

Figure 3.8: Total densitites integrated over the thickness of the defect of (a) matrix, m, (b) chondrocytes, C_C, MSCs, C_S, as a function of the time, in months, from 1-24 months for simulations with (orange) and without (blue) growth factors. $x = 0$ in the figure represents the location of the base of the defect, $x = 1$ represents the surface of articular cartilage.

Parameters	Sensitivity description
Initial FGF-1 concentration, $\bar{g}_{init}$	Increasing $\bar{g}_{init}$ results in a small increase in chondrocyte proliferation and matrix deposition at very early times; thereafter no change is observable.
Initial BMP-2 concentration, $\bar{b}_{init}$	Increasing $\bar{b}_{init}$ has no effect on the system since it degrades quickly before it has the chance to take effect; it starts being produced again when a sufficient level of chondrocyte density is reached to counteract its degradation.
FGF-1 production constant, $\bar{p}_9$	Increasing $\bar{p}_9$ results in a minor increase in chondrocyte proliferation and matrix levels at early time; decreasing $\bar{p}_9$ decreases matrix levels marginally at early time; no noticeable difference thereafter.
BMP-2 production constant, $\bar{p}_{12}$	see details in text.
FGF-1 degradation rate, $\bar{p}_{11}$	Increasing/decreasing $\bar{p}_{11}$ has no significant change to cell density levels and evolution characteristics.
BMP-2 degradation rate, $\bar{p}_{13}$	see details in text.
FGF-1/BMP-2 diffusion coefficient, $D_{g,b}$	Increasing $D_{g,b}$ have no significant change to cell density levels and evolution characteristics.
FGF-1/BMP-2 flux coefficient, $\bar{\gamma}$, $\bar{\chi}$	Increasing/decreasing $\bar{\gamma}$, $\bar{\chi}$ have no significant change to cell density levels and evolution characteristics.

FGF-1 matrix deposition rate, $\bar{p}_{8_{00}}$	Increasing $\bar{p}_{8_{00}}$ up to 1 has minor effects to overall matrix levels. We see higher matrix levels primarily at the bottom of the defect indicating main effect at early time. The general evolution remains unchanged and earlier healing time is not achieved.
minimum threshold stem cell density, $\bar{C}_{S_{0_{min}}}$	see details in text.
threshold stem cell density reduction factor, $\bar{\alpha}$	see details in text.
stem cell differentiation rate, $\bar{p}_2$	Variations (including assumed dependency on BMP-2 concentration) only resulted in minor differences in cell and matrix densities and accelerated growth; general evolution characteristics remain unchanged.

Table 3.3: Sensitivity of parameters. Those highlighted in bold are further described in the text.

We described earlier that the increased levels of chondrocyte and matrix densities observed at early time in the presence of growth factors was primarily due to the reduction of the threshold stem cell density for differentiation into chondrocytes (Figs. 3.7$(a-c)$). We have further investigated variations in the parameters we found that this reduction was most sensitive to the BMP-2 growth factor production constant, $\bar{p}_{12}$, the BMP-2 degradation rate, $\bar{p}_{13}$, the minimum threshold stem cell density, $\bar{C}_{S_{0min}}$, and the threshold stem cell density reduction factor, $\bar{\alpha}$ (last function, Eq. 3.11).

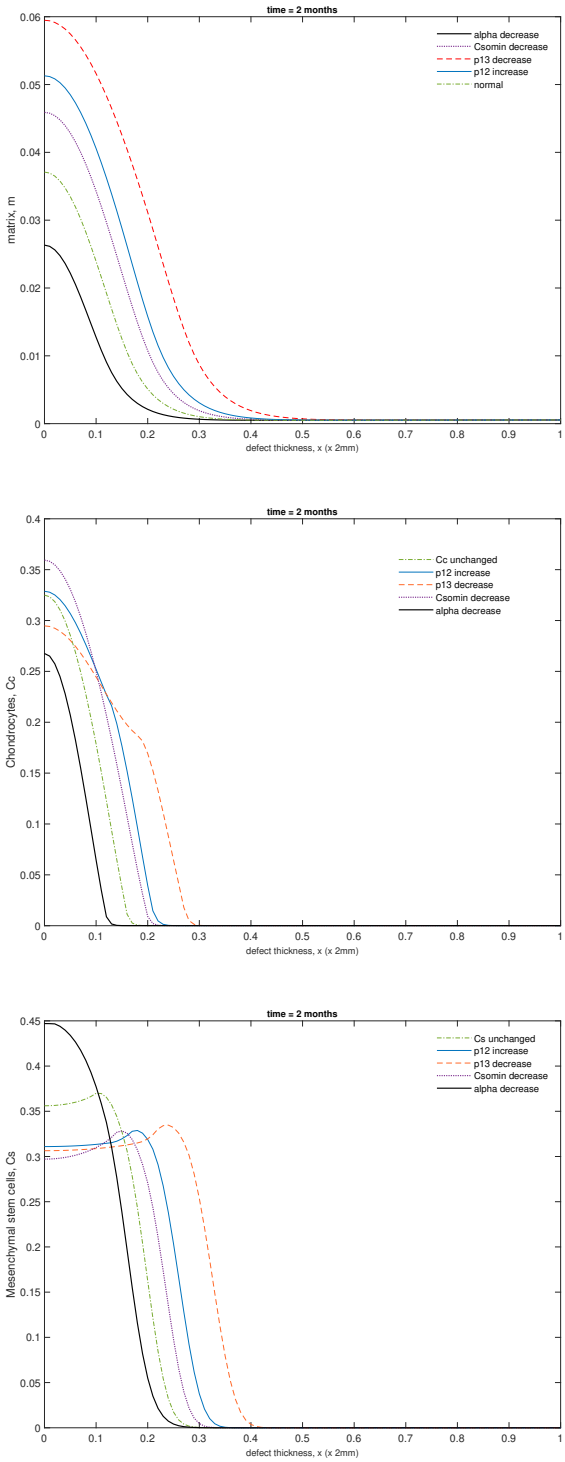

Figure 3.9: Comparison of (a) stem cell, (b) chondrocyte and (c) matrix densities at t =2 months when varying the BMP-2 growth factor production constant, $\bar{p}_{12}$ (darker solid lines), the BMP-2 degradation rate, $\bar{p}_{13}$ (dashed lines), the minimum threshold stem cell density, $\bar{C}_{S_{0_{min}}}$ (dotted lines), and the threshold stem cell density reduction factor, $\bar{\alpha}$ (lighter solid lines) independently from their base values (dot-dashed lines). See text for parameter values used. $x = 0$ in the figure represents the location of the base of the defect, $x = 1$ represents the surface of articular cartilage.

Figure 3.9(a, b, c) show the stem cell, chondrocyte and matrix density, respectively, at time t =2 months by varying $\bar{p}_{12,13}$, $\bar{C}_{S_{0min}}$ and $\bar{\alpha}$ independently from their base values. In the simulations shown, $\bar{p}_{12} = 267$ (10 fold increase from its base value), $\bar{p}_{13} = 0.154$ (100 fold decrease from its base value), $\bar{C}_{S_{0min}} = 0.28$ (reduces $\bar{C}_{S_0}$ by 20% in comparison to its base value which imposes a 10% reduction) and $\bar{\alpha} = 1$ (100 fold decrease from its base value). Increasing $\bar{p}_{12}$ and decreasing $\bar{p}_{13}$ and $\bar{C}_{S_{0min}}$ resulted in stem cell differentiation to occur much earlier in comparison to their base values (Fig. 3.9(a)). Moreover, stem cell differentiation was most delayed when α was decreased. The chondrocyte density levels appeared less sensitive to variations in these parameters (Fig. 3.9(b)). The diffusion of chondrocytes away from the defect was observed slightly earlier when $\bar{p}_{12}$ was increased, and $\bar{p}_{13}$ and $\bar{C}_{S_{0min}}$ were decreased compared to the base values and when α was decreased. This was a consequence of the stem cell differentiation occurring earlier when these parameters were varied. The matrix density levels shown in Fig. 3.9(c) show slightly enhanced levels compared to the base value and when α was decreased. This was again due to stem cell differentiation into chondrocytes occurring early and subsequently producing more matrix.

An alternative method to implement the effect of BMP-2 on stem cell differentiation is to vary the stem cell differentiation rate, $\bar{p}_2$ with the BMP-2 concentration, while keeping the threshold stem cell density, $\bar{C}_{S_0}$ fixed. As detailed in Table 3.3, we found no significant influence of this on the system and the model results appeared much less sensitive to variations in $\bar{p}_2$ than to the stem cell density threshold variation considered in this work.

The sensitivity analysis indicates the values we have approximated, are also not extremely sensitive to change, hence a good representation of that parameter value. Identifying the

sensitive parameters from the sensitivity analysis could provide important information for *in vitro* studies, indicating which mechanisms need to be focused on or manipulated experimentally to produce a desired effect, such as increased cell and/or matrix densities.

3.4 Summary & Conclusions

In this chapter have extended the model proposed by Lutianov *et al.* [119] to consider the influence of two growth factors, BMP-2 and FGF-1 on the regeneration of a cartilage defect. These two growth factors serve as examples that embody the type of interactions that can occur between mesenchymal stem cells and chondrocytes, which would typically affect stem cell and chondrocyte proliferation, differentiation and matrix production. The interactions in the model are those hypothesised by Wu *et al.* [184], which they formulated on the basis of their and others' experimental data. Our simulations show that the interactions from the growth factors enhance matrix production at early times. This is consistent with *in vitro* results of Wu *et al.* [184], who's findings show increased GAG (glycosaminoglycan) levels in co-culture pellets of mesenchymal stem cells and chondrocytes up to 4 weeks after culture, indicative of increased matrix deposition. Of course, unlike the co-culture experiments which start with a mixture of stem cells and chondrocytes, our initial conditions represented implantation of only stem cells. However, once stem cells differentiated into chondrocytes in our model, they displayed the same stem cell-chondrocyte interaction observed in the co-culture experiments with similar trophic effects [184].

The consideration of growth factors and their mediating influence on cell-to-cell interactions is an important step towards looking at more complex models such as implantations of a mixture of cells. The work of Wu *et al.* [184] shows how inserting mixtures of stem cells and chondrocytes together into a defect can promote matrix deposition, and therefore a faster healing time due to the trophic effects growth factors such as BMP-2 and FGF-1 have on the system. This is the topic of Chapter 4.

Chapter 4

Mathematical model of chondral defect regeneration after cell therapy – the influence of cell co-implantation

In this chapter, we further use the mathematical model, developed in Chapter 3, to explore the hypothesis that the pattern of cartilage matrix production over time in a cartilage defect into which a mixture of chondrocytes and MSCs was implanted, depends on the chondrocyte:MSC ratio and that an optimal ratio maximising matrix production exists. Like chapter 3, we will use the observations of Wu *et al.*[184] from an *in vitro* experimental model to model the growth factor mediated interaction between chondrocytes and MSCs to obtain short-term results at specific chondrocyte:MSC ratios[184]. As in Chapter 3, the various rate constants in the mathematical model will be based on *in vitro* or *in vivo* data where possible, otherwise

an assumption will be made. For relevant parameters, sensitivity analyses will be performed to determine the influence of the parameter value on the model outcomes. The role of the mathematical model in this Chapter is to determine if an optimal chondrocyte:MSC ratio to maximize cartilage matrix production over time exists, and to what extent it may speed up cartilage defect healing.

Chapter 3 describes in detail the modelling choices of the growth factors with details of non-dimensionalisation and parameter choices, hence we simply state the relevant equations in this chapter. We present the results of the model and compare several different implantation ratios to see if an optimal ratio can be identified and demonstrate the differences between low and high concentrations of each cell type. Following on from this, we compare the matrix densities of our co-implantation procedures at various times to those corresponding to ACI and ASI, as shown in Chapter 3 [21] and in [119]. Finally, we summarise the findings of this work, with main discussion located in Chapter 6.

4.1 Introducing the problem

As is now widely recognised, the implantation of MSCs into a chondral defect does not only contribute to the repair process via their differentiation into chondrocytes but also via their secretion of growth factors and cytokines, termed as their "trophic" effect [23, 41]. Work by Wu *et al.* [184] identifies two growth factors, FGF-1 and BMP-2, as particularly important during cartilage regeneration. These two growth factors were identified when investigating the effect of co-cultures of MSCs and chondrocytes on cartilage formation [184]. They are released by MSCs and chondrocytes and mediate MSC-to-chondrocyte interaction, enhancing chondrocyte proliferation and mesenchymal stem cell chondrogenesis (see Fig. 3

for a schematic of this cell-to-cell interaction in Chapter 3 & [21]). Their observations were modelled mathematically in Chapter 3, which studied the effects of these growth factors after MSC implantation (ASI) into the defect [21]. Our simulations showed that matrix formation following ASI was enhanced at early times when cell-to-cell interactions mediated by these growth factors were taken into account. This was mainly due to the presence of BMP-2, resulting in increased formation of chondrocytes via increased chondrocyte proliferation and MSC chondrogenesis, and hence enhancing early matrix production in comparison to the case when no growth factors are present. At later time points no differences were found.

Several *in vitro* studies have suggested that co-culturing a mixture of MSCs and chondrocytes increases matrix formation [9, 42, 41, 115]. In these mixtures, the chondrocytes could immediately start forming cartilage and trophic effects due to the growth factors released in the system would boost this further [184]. However, these *in vitro* studies are by necessity short-term studies and it is therefore not clear how these differences develop in the longer term and if they are maintained. To our knowledge, the only *in vivo* study used a rat model and found no difference in quality of cartilage defect repair 12 weeks after implanting scaffolds with either a 90:10 MSC:chondrocyte mixture or pure chondrocytes but did not study other time points [35].

In this chapter we aim to explore the longer term patterns over time of cartilage defect healing following implantation of mixtures of MSCs and chondrocytes at various ratios, and investigate the differences between them. The plan of this chapter is as follows. In the section 4.2 *Mathematical model*, we state the model equations, boundary and initial conditions. Next, 4.3 *Results* shows the results of simulations for five co-implantation ratios and their comparison with respect to matrix density levels over healing time. Results showing sensitivity to variations in co-implantation ratios are also considered here, in particular, comparisons are

made with 100% stem cells (ASI) and 100% chondrocytes (ACI) implantations. Finally, section 4.4 *Summary & discussion* explores the implications of the model results on co-culture cell therapy and future work. We refer the reader to Chapter 3 [21] where full details of non-dimensionalisation and a sensitivity analysis of the model has been conducted, which will not be shown here.

4.2 Mathematical model

Our mathematical model follows the same formulation as in Chapter 3 [21] with the initial cell implantation profile changed to accommodate a varying ratio of stem cells and chondrocytes. We only state the dimensionless equations, and boundary and initial conditions here. For more information on the formulation and non-dimensionalisation of these equations and assumptions made, the reader is referred to Chapter 3 [21] and Lutianov *et al.* [119].

We consider a cartilage defect with a small depth to diameter ratio (see Fig. 3.1) which enables us to simplify to a one-dimensional problem where cell growth is modelled along the defect depth x only, with $x = 0$ at the base of the defect. The variables in our model are: the stem cell density C_S, the chondrocyte density C_C, the matrix density m, the nutrient concentration n, the FGF-1 concentration g and the BMP-2 concentration b. Cell density is measured in number of cells per unit volume, matrix density and growth factor concentration are measured as mass per unit volume and nutrient concentration is measured in number of moles per unit volume.

Following the non-dimensionalisation given in Chapter 3, the dimensionless equations (overbars omitted), boundary and initial conditions for the evolution of the cell and matrix densities and nutrient concentration in time, t, and space, x are given by:

$$\frac{\partial C_S}{\partial t} = \frac{\partial}{\partial x}\Big(D_S(m)\frac{\partial C_S}{\partial x}\Big) + p_1\Big(m, \frac{C_S}{C_{S,max}(m)}\Big)\frac{n}{n+n_0}C_S H(n-n_1)$$
$$- p_2 C_S H(C_S - C_{S_0}(b)) - p_3 C_S H(n_1 - n), \tag{4.1a}$$
$$\frac{\partial C_C}{\partial t} = \frac{\partial}{\partial x}\Big(D_C(m)\frac{\partial C_C}{\partial x}\Big) + p_4\Big(m, g, \frac{C_C}{C_{C,max}(m)}\Big)\frac{n}{n+n_0}C_C H(n-n_1)$$
$$+ p_2 C_S H(C_S - C_{S_0}(b)) - p_5 C_C H(n_1 - n), \tag{4.1b}$$
$$\frac{\partial n}{\partial t} = D_n\frac{\partial^2 n}{\partial x^2} - \frac{n}{n+n_0}(p_6 C_S + p_7 C_C), \tag{4.1c}$$
$$\frac{\partial m}{\partial t} = D_m\frac{\partial^2 m}{\partial x^2} + p_8(m,g)\frac{n}{n+n_0}C_C, \tag{4.1d}$$
$$\frac{\partial g}{\partial t} = D_g\frac{\partial^2 g}{\partial x^2} + p_9 C_S - p_{11} g, \tag{4.1e}$$
$$\frac{\partial b}{\partial t} = D_b\frac{\partial^2 b}{\partial x^2} + p_{12} C_C - p_{13} b, \tag{4.1f}$$

where

$$p_1\left(m, \frac{C_S}{C_{S,max}(m)}\right) = A(m)\left(1 - \frac{C_S}{C_{S,max}(m)}\right),\ A(m) = p_{1_0}\frac{m}{m^2+m_2^2},$$
$$p_4\left(m, g, \frac{C_C}{C_{C,max}(m)}\right) = B(m)\left(1 - \frac{C_C}{C_{C,max}(m)}\right),\ B(m) = p_{4_0}\frac{m}{m^2+m_2^2} + p_{4_{00}}\frac{g}{g+1},$$
$$C_{S,max}(m) = C_{S,max_0}(1-m),\ \ C_{C,max}(m) = C_{C,max_0}(1-m),$$
$$C_{S,max_0} + C_{C,max_0} = 1, p_8(m,g) = (1 - p_{8_1}m)(1 + p_{8_{00}}\frac{g}{g+1}),$$
$$D_S(m) = D_{S_0}\frac{m}{m^2+m_1^2},\ D_C(m) = D_{C_0}\frac{m}{m^2+m_1^2},$$
$$C_{S_0}(b) = (C_{S_{0,max}} - C_{S_{0,min}})e^{-\alpha b} + C_{S_{0,min}}.$$

(4.2)

The estimated values of the parameters in dimensional form and the dimensionless parameters

are provided in the Chapter 3 (Tables 3.1 and 3.2) and Campbell *et al.* [21].

The non-dimensional boundary and initial conditions are:

$$-D_S(m)\frac{\partial C_S}{\partial x} = -D_C(m)\frac{\partial C_C}{\partial x} = -D_n\frac{\partial n}{\partial x} = -D_m\frac{\partial m}{\partial x} = -D_g\frac{\partial g}{\partial x} = -D_b\frac{\partial b}{\partial x} = 0, \quad \text{(4.3a)}$$

(at $x = 0$),

$$-D_S(m)\frac{\partial C_S}{\partial x} = -D_C(m)\frac{\partial C_C}{\partial x} = -D_m\frac{\partial m}{\partial x} = 0,\ n = 1,\ -D_g\frac{\partial g}{\partial x} = \gamma g,\ -D_b\frac{\partial b}{\partial x} = \chi b, \quad \text{(4.3b)}$$

(at $x = 1$),

$$\mathbf{C_S} = (\mathbf{1} - \mathbf{p_c})\mathbf{C_S^{(0)}}\mathbf{h}(\mathbf{x}),\ \mathbf{C_C} = \mathbf{p_c}\mathbf{C_C^{(0)}}\mathbf{h}(\mathbf{x}),\ n = 1,\ m = m_3,\ g = g_{init},\ b = b_{init}, \quad \text{(4.3c)}$$

(at $t = 0$).

with γ and χ representing the flux of growth factors leaving the top of the defect into the synovial fluid.

The new initial conditions representing the different co-culture ratios of stem cells and chondrocytes are highlighted in bold in Eq. (4.3). Here, $C_S^{(0)}$and $C_C^{(0)}$ are the initial stem cell and chondrocyte densities, $h(x)$ is the initial profile and p_c ($0 \leq p_c \leq 1$) represents the proportion of chondrocytes implanted in the defect (e.g. a 35% chondrocyte proportion means $p_c = 0.35$, a mixture consisting of 65% stem cells and 35% chondrocytes at $t = 0$).

We used a second order accurate finite difference scheme to discretise the spatial derivatives in x over 100 grid points in Eqs. 4.1-4.3, keeping the time derivative t continuous. The resulting ordinary differential equations were solved in MATLAB (Release 2013a, The MathWorks Inc., Natick, Massachusetts, United States) using the stiff ODE solver *ode15s*. The dimensionless parameter values used in our simulations are given in Table 3.2.

The initial stem cell and chondrocyte density spatial profile is $C_S(x,0) = C_S^{(0)}(1-\mathbf{p_c})[1-\tanh(A(x-x_0))]/2$ and $C_C(x,0) = C_C^{(0)}\mathbf{p_c}[1-\tanh(A(x-x_0))]/2$, with $A = 10^4$ and $x_0 = 0.1$. Dimensionally, this is equivalent to a combined chondrocyte and stem cell density of 2.5×10^5 cells/mm^3, restricted to an area of thickness 200μmm near $x = 0$, and zero elsewhere. We also assumed a small density of matrix ($m_3 = 10^{-4}$), FGF-1 ($g = g_{init}$) and BMP-2 ($b = b_{init}$) uniformly distributed across the defect.

The general evolution characteristics of the cell and matrix densities, nutrient and growth factor concentrations using this model are described in Chapter 3 of this thesis [21, 119] and hence are not repeated in detail here. The main focus of our simulations is to vary the initial stem cell and chondrocyte implantation densities through the parameter p_c, keeping the other parameters fixed.

We simulate cartilage repair following implantation of five mixtures, namely $p_c = 0.1$ (90% stem cells and 10% chondrocytes, hereafter referred to as 90:10), $p_c = 0.3$ (70% stem cells and 30% chondrocytes, hereafter referred to as 70:30), $p_c = 0.5$ (50% stem cells and 50% chondrocytes, hereafter referred to as 50:50), $p_c = 0.7$ (30% stem cells and 70% chondrocytes, hereafter referred to as 30:70) and $p_c = 0.9$ (10% stem cells and 90% chondrocytes, hereafter referred to as 10:90).

4.3 Results

4.3.1 Numerical results

Co-implantation of 90% stem cells and 10% chondrocytes

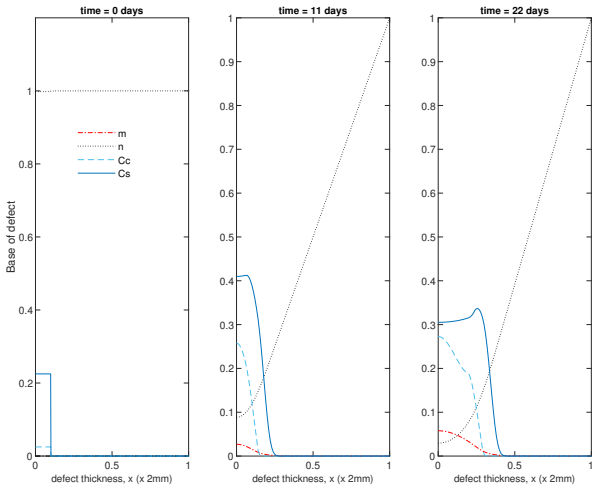

Figure 4.1: Evolution of cell and matrix densities, and nutrient concentration at times t =0, 11 and 22 days following co-implantation of 90% stem cells and 10% chondrocytes. $x = 0$ in the figure represents the location of the base of the defect, $x = 1$ represents the surface of articular cartilage.

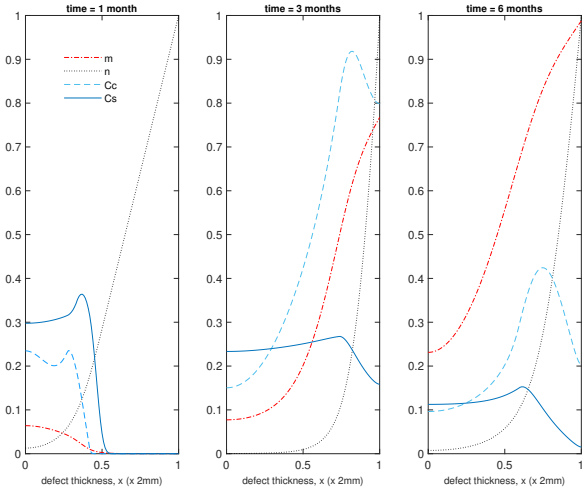

Figure 4.2: Evolution of cell and matrix densities, and nutrient concentration at times t =1, 3 and 6 months following co-implantation of 90% stem cells and 10% chondrocytes. $x = 0$ in the figure represents the location of the base of the defect, $x = 1$ represents the surface of articular cartilage.

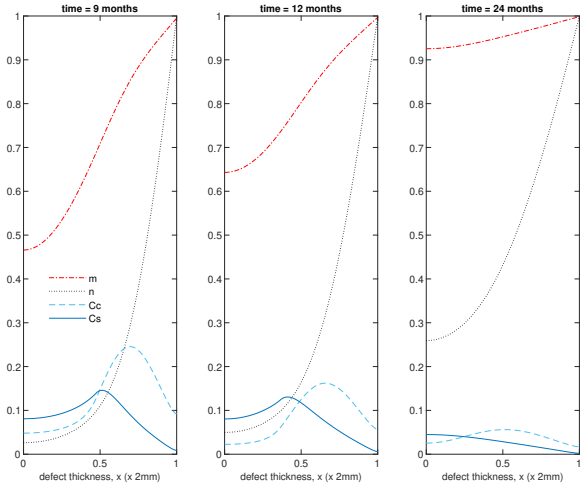

Figure 4.3: Evolution of cell and matrix densities, and nutrient concentration at times t =9, 12 and 24 months following co-implantation of 90% stem cells and 10% chondrocytes. $x = 0$ in the figure represents the location of the base of the defect, $x = 1$ represents the surface of articular cartilage.

We first show the simulations corresponding to $p_c = 0.1$ (90% stem cells and 10% chondrocytes; 90:10). Panels 2 and 3 in Fig. 4.1 show the evolution at $t = 11$ and 22 days, respectively. Matrix production near $x = 0$ is seen after only a few days, mainly due to a rapid increase in chondrocyte density (almost 10 times the initial number within 11 days; see Panel 2 in Fig. 4.1). This early matrix production is of comparable magnitude to that produced for $p_c = 1.0$ (implantation of 100% chondrocytes; see Panel 2 in Fig. 2 of Lutianov *et al.* [119]), but using a far smaller number of chondrocytes and occurs much earlier than for $p_c = 0$ (implantation of 100% stem cells), which requires 2 months to achieve similar matrix levels (Fig. 3.5 in Chapter 3 also see Fig. 4.18 below).

Over the course of the first few months, chondrocyte density is generally larger in the co-implantation case compared to the 100% stem cell and 100% chondrocyte implantation cases (compare Fig. 4.2 with Fig. 3.5 in Chapter 3 and Fig. 3 in Lutianov *et al.* [119]). This larger chondrocyte density comes with increased matrix production but also with increased uptake of nutrients. The latter results in a drop of chondrocyte density towards the bottom of the

defect once the nutrient concentration falls below the minimum threshold level $n_1 = 10^{-1}$), increasing chondrocyte death and slowing down chondrocyte proliferation. The net result is a slowing down of matrix production at the bottom of the defect. On the other hand, chondrocyte density continues to grow at the top of the defect due to the local abundance of nutrients there, resulting in a continued increase in matrix density near the top of the defect (see Panels 2 and 3 in Fig. 4.2).

At later times (Fig. 4.3), matrix deposition slows down and the defect fills up in 18-24 months. This time scale is similar to the two single cell type implantation cases (Fig. 4 in Lutianov *et al.* [119] and Fig. 3.6 in Chapter 3).

Co-implantation of 70% stem cells and 30% chondrocytes

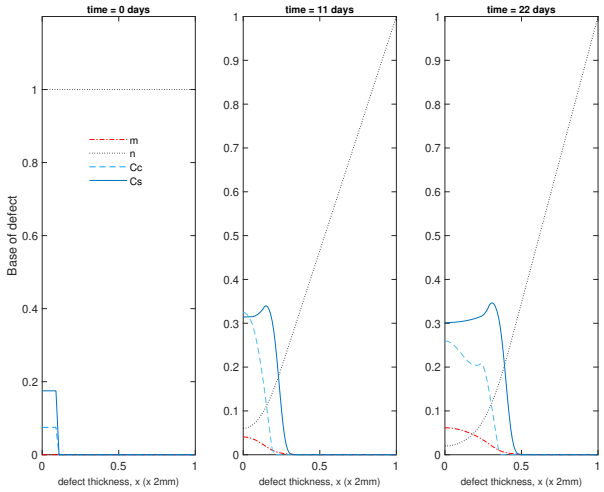

Figure 4.4: Evolution of cell and matrix densities, and nutrient concentration at times t =0, 11 and 22 days following co-implantation of 70% stem cells and 30% chondrocytes. $x = 0$ in the figure represents the location of the base of the defect, $x = 1$ represents the surface of articular cartilage.

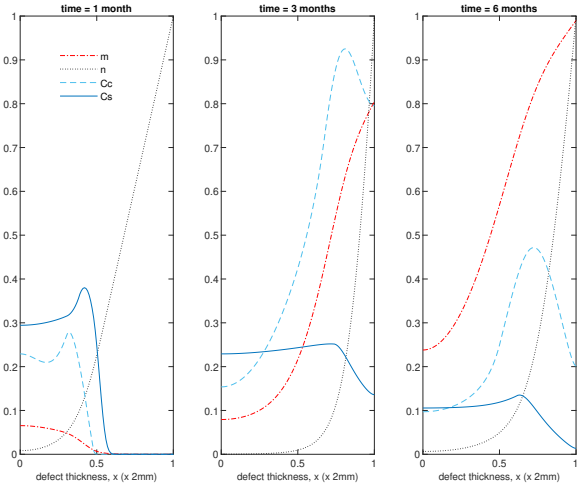

Figure 4.5: Evolution of cell and matrix densities, and nutrient concentration at times t =1, 3 and 6 months following co-implantation of 70% stem cells and 30% chondrocytes. $x = 0$ in the figure represents the location of the base of the defect, $x = 1$ represents the surface of articular cartilage.

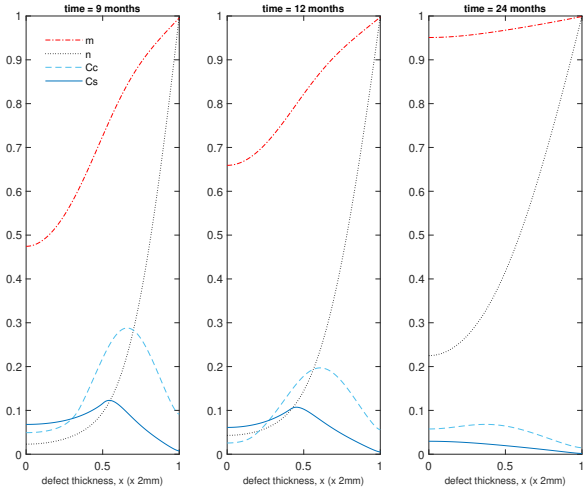

Figure 4.6: Evolution of cell and matrix densities, and nutrient concentration at times t =9, 12 and 24 months following co-implantation of 70% stem cells and 30% chondrocytes. $x = 0$ in the figure represents the location of the base of the defect, $x = 1$ represents the surface of articular cartilage.

Next we show simulations of $p_c = 0.3$ corresponding to 70% stem cells 30% chondrocytes (70:30). Figures 4.4-4.6 show the evolution of the cell and matrix densities and nutrient concentration for time ranging between 11 days and 24 months. Similar to the 90:10 case (Figs. 4.1-4.3) we see enhanced matrix production at early time points with the nutrient concentration falling below the critical condition, $n_1 = 10^{-1}$, as early as 11 days at the bottom of the defect. This large consumption of nutrients is due to cell proliferation and MSC differentiation, which is enhanced due to FGF-1 and BMP-2 [21, 184]. This decreases chondrocyte proliferation at the bottom of the defect, meaning diffusion of cells to higher concentrations of nutrients will be the main driver of defect healing. As time continues, we see the general evolutionary characteristics of the simulations remain similar to our 90:10 case, albeit with slightly higher matrix levels due to the higher proportion of chondrocytes inserted into the defect. The defect is observed to fill-up with new cartilage within 18-24 months, which is in line with our previous results (Chapter 3, [21]).

Co-implantation of 50% stem cells and 50% chondrocytes

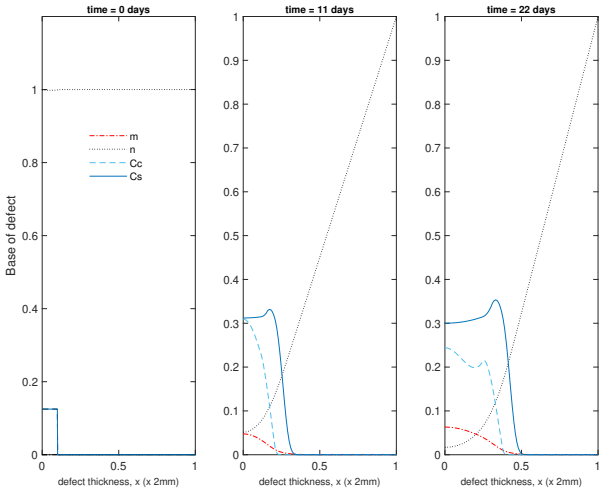

Figure 4.7: Evolution of cell and matrix densities, and nutrient concentration at times t =0, 11 and 22 days following co-implantation of 50% stem cells and 50% chondrocytes. $x = 0$ in the figure represents the location of the base of the defect, $x = 1$ represents the surface of articular cartilage.

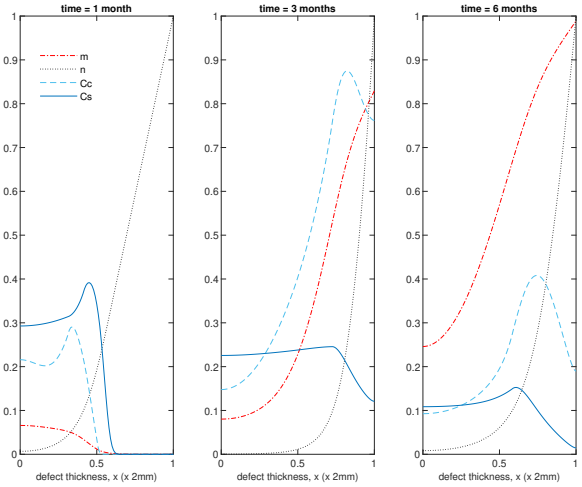

Figure 4.8: Evolution of cell and matrix densities, and nutrient concentration at times t =1, 3 and 6 months following co-implantation of 50% stem cells and 50% chondrocytes. $x = 0$ in the figure represents the location of the base of the defect, $x = 1$ represents the surface of articular cartilage.

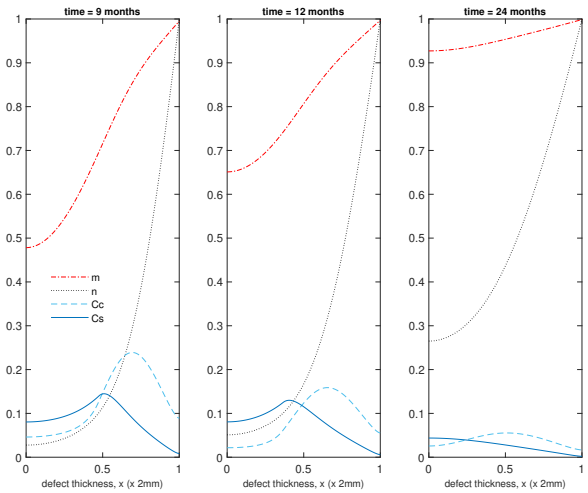

Figure 4.9: Evolution of cell and matrix densities, and nutrient concentration at times t =9, 12 and 24 months following co-implantation of 50% stem cells and 50% chondrocytes. $x = 0$ in the figure represents the location of the base of the defect, $x = 1$ represents the surface of articular cartilage.

We next show the simulations corresponding to $p_c = 0.5$ (50% stem cells and 50% chondrocytes; 50:50). Figures 4.7-4.9 show the evolution of the cell and matrix densities and nutrient concentration for this case at early and late time points. The evolution characteristics are identical to the 90:10 and 70:30 cases, except that the overall matrix density is slightly higher, particularly at earlier times (compare Panel 2 Fig. 4.7 and Fig. 4.1). This is a consequence of the larger proportion of implanted chondrocytes and the subsequent increase in chondrocyte density due to a combination of growth factor enhanced proliferation and stem cell differentiation. However, at later time points the increased nutrition demand from the larger overall cell density causes the nutrient concentration close to the bottom of the defect to fall below the minimum threshold level $n_1 = 10^{-1}$, in turn slowing down cell proliferation and matrix production rates. Thus, the matrix density at later times is very similar to the 90:10 and 70:30 cases (compare Fig. 4.8 with Fig. 4.2 and Fig. 4.5).

Co-implantation of 30% stem cells and 70% chondrocytes

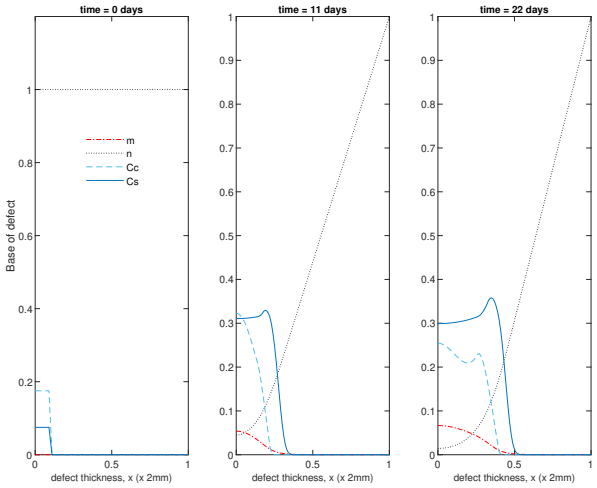

Figure 4.10: Evolution of cell and matrix densities, and nutrient concentration at times t =0, 11 and 22 days following co-implantation of 30% stem cells and 70% chondrocytes. $x = 0$ in the figure represents the location of the base of the defect, $x = 1$ represents the surface of articular cartilage.

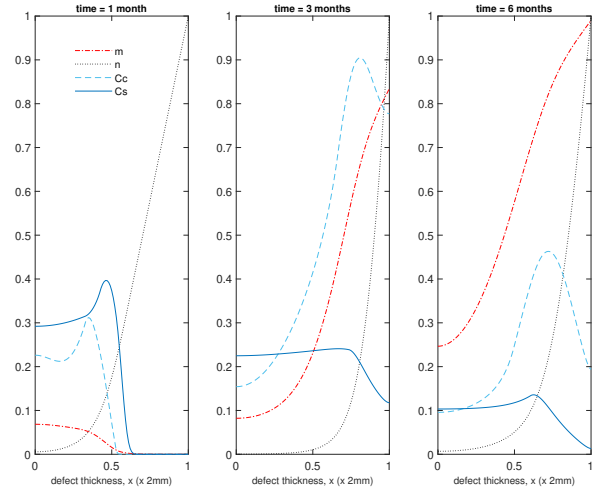

Figure 4.11: Evolution of cell and matrix densities, and nutrient concentration at times t =1, 3 and 6 months following co-implantation of 30% stem cells and 70% chondrocytes. $x = 0$ in the figure represents the location of the base of the defect, $x = 1$ represents the surface of articular cartilage.

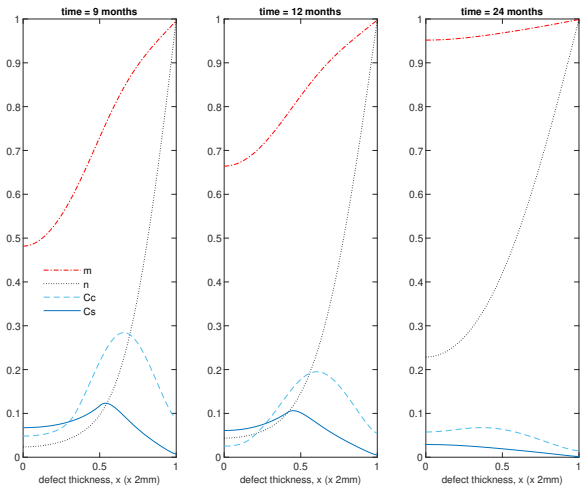

Figure 4.12: Evolution of cell and matrix densities, and nutrient concentration at times t =9, 12 and 24 months following co-implantation of 30% stem cells and 70% chondrocytes. $x = 0$ in the figure represents the location of the base of the defect, $x = 1$ represents the surface of articular cartilage.

Figures 4.10-4.12 show cell and matrix densities, and nutrient concentration for $p_c = 0.7$ simulations corresponding to 30% stem cells 70% chondrocytes (30:70). Here we observe high levels of matrix at early times. As with the other cases, nutrients are a limiting factor on healing, falling below the critical concentration and switching off cell proliferation by 11 days. MSCs appear to begin diffusing towards the top of the defect sooner in this case when compared with the 90:10 case (Fig. 4.1), for instance, likely to be due to higher matrix density allowing for cell motility. Once cell diffusion to the top of the defect has begun, we observe similar trends to the previous cases (Figs. 4.2, 4.5, 4.8). By 9 months (Fig. 4.12) matrix densities are similar to those of our previous cases (Figs. 4.3, 4.6, 4.9), indicating the differences we see at early times are not maintained as time continues. This could be due to limited nutrient concentration, which is consistently low during the evolution.

Co-implantation of 10% stem cells and 90% chondrocytes

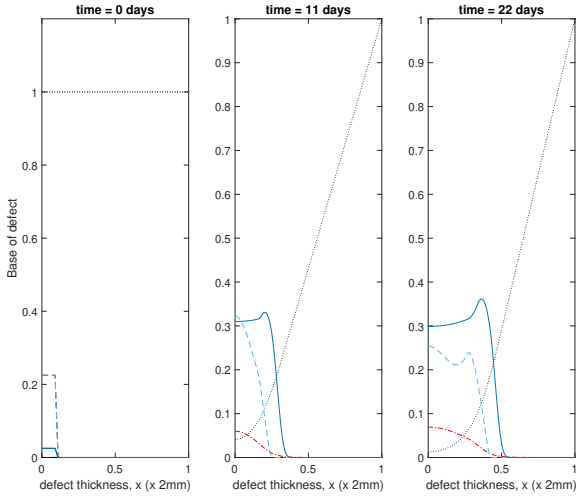

Figure 4.13: Evolution of cell and matrix densities, and nutrient concentration at times t =0, 11 and 22 days following co-implantation of 10% stem cells and 90% chondrocytes. $x = 0$ in the figure represents the location of the base of the defect, $x = 1$ represents the surface of articular cartilage.

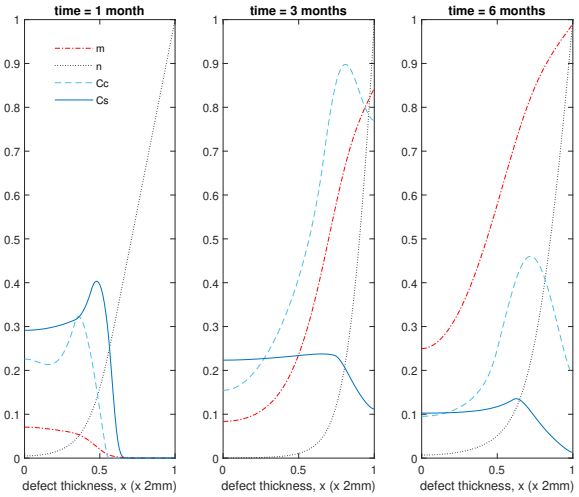

Figure 4.14: Evolution of cell and matrix densities, and nutrient concentration at times t =1, 3 and 6 months following co-implantation of 10% stem cells and 90% chondrocytes. $x = 0$ in the figure represents the location of the base of the defect, $x = 1$ represents the surface of articular cartilage.

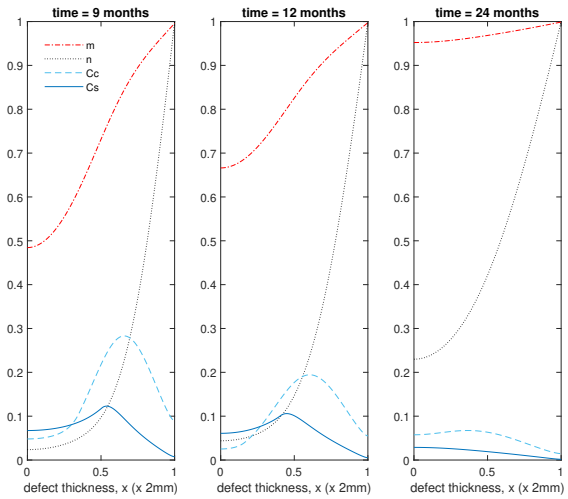

Figure 4.15: Evolution of cell and matrix densities, and nutrient concentration at times t =9, 12 and 24 months following co-implantation of 10% stem cells and 90% chondrocytes. $x = 0$ in the figure represents the location of the base of the defect, $x = 1$ represents the surface of articular cartilage.

We finally show the results for a 10% MSC and 90% chondrocyte mixture corresponding to $p_c = 0.9$ (10:90) (Figures 4.13, 4.14, 4.15). Here we have the highest proportion of chondrocytes inserted into the defect, and as such have the highest matrix levels at early times. This is likely due to increased matrix formation primarily occurring at early times during our simulations, when nutrients are more readily available in the defect. This means a higher implanted chondrocyte density, as demonstrated here, could be desirable to increase matrix levels. Despite this, as with our previous co-implantation cases, increased matrix deposition appears to slow at later times, with nutrient concentration and cell diffusion being the main regulatory factors of healing.

Next, we make a comparison between the five co-implantation cases with ACI and ASI to identify both spatial and temporal differences in matrix and cell densities.

4.3.2 Comparison of matrix density of co-implantation, ACI and ASI at early times

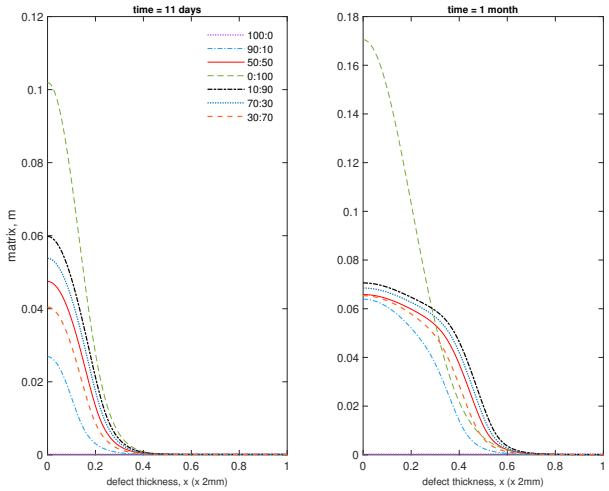

Figure 4.16: Comparison of matrix density profiles for all cases at times $t = 11$ days and 1 month. $x = 0$ in the figure represents the location of the base of the defect, $x = 1$ represents the surface of articular cartilage.

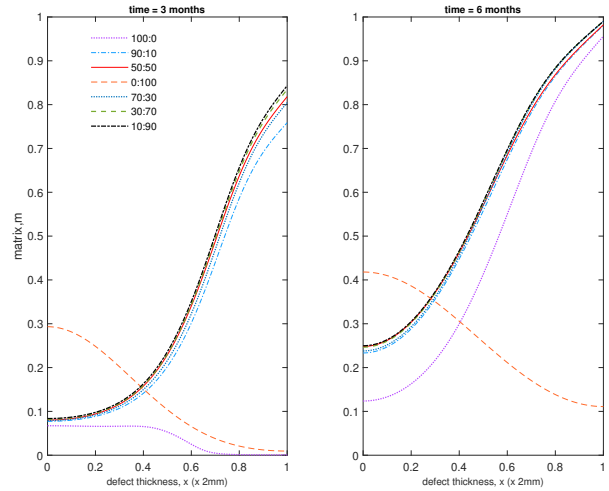

Figure 4.17: Comparison of matrix density profiles for all cases at times $t = 3$ and 6 months. $x = 0$ in the figure represents the location of the base of the defect, $x = 1$ represents the surface of articular cartilage.

Figures 4.16 and 4.17 compare matrix densities at early times for five co-implantation cases with ACI and ASI.

Up to 1 month, the 100% chondrocyte case (0:100) has the largest amount of matrix (Fig. 4.16). Although at 11 days the chondrocyte density in the 90:10 case is close to that of other co-implantation cases containing higher chondrocyte densities, and even higher than in the 0:100 case (compare Figs. 4.1, 4.4, 4.7, 4.10, 4.13 and Fig 2 in Lutianov *et al.* [119]), the additional nutrient demands of the stem cells brings the nutrient concentration below the minimum threshold value, resulting in matrix densities much lower than the 0:100 case (Fig. 4.16). In the 100:0 case, the stem cells have not yet differentiated into chondrocytes at these early time points and hence no matrix at all is produced (Fig. 4.16).

The 10:90 case has the highest levels of matrix at 3 months (Panel 1 in Fig. 4.17), consistent with the observations in Figures 4.13, 4.14, 4.15. The five co-implantation cases produce more matrix than the 0:100 case, despite the 0:100 case having the largest matrix density at earlier times and the highest implantation of chondrocytes. The 100:0 implantation, relevant to ASI, still has the lowest matrix levels, indicating that the implantation of mesenchymal stem cells alone delays healing initially (Panel 1 in Fig. 4.17).

These findings highlight the importance of early matrix deposition, as it is clear at late times the differences we observe in matrix levels between our co-implantation cases are more moderate (Figs. 4.3, 4.6 4.9, 4.12, 4.15, Panel 2 in 4.17). At late times our simulations are more likely to be constrained by low nutrient concentrations, therefore slowing the rate of healing down. At early times more nutrients are available within the defect, primarily at the top, where formation of cartilage is most notable in our ASI and co-implantation cases. We find our ACI case forms matrix primarily at the bottom of the defect as nutrient levels never become very low here, unlike for our other cases, meaning cells are not forced to diffuse to areas of higher nutrient concentration to continue proliferating (Fig. 4.17). Chondrocytes also have a lower cell motility rate in comparison to MSCs, meaning diffusion to the top of

the defect will be slower.

Comparing mean cell and matrix densities versus time for co-implantation, ACI and ASI

Here we compare the mean matrix, chondrocyte and MSC densities over a period of 24 months for 4 cases: 0:100 (ACI), 100:0 (ASI), and 2 co-implantation strategies, 90:10 and 10:90. We choose to focus on 90:10 and 10:90 as they represent our two most extreme co-implantation cases, with all other results, i.e 70:30, 50:50 and 30:70, lying within the bounds of these two sets of results (see Figs. 4.16 and 4.17). The two single-cell implantation cases are investigated in Lutianov *et al.* [119] and Chapter 3 of this thesis [21].

In Figure. 4.18(a), at 1 month, the mean matrix density produced is largest for the 0:100 case (blue). This is not only because this case has the largest concentration of chondrocytes directly producing matrix from the beginning, but also because only chondrocytes are seeded in the defect. The co-implantation cases also have a population of stem cells competing for nutrients, thus reducing the average matrix production by the chondrocytes. At 2 months the 100:0 (yellow) case has produced barely any matrix due to MSCs having to first differentiate into chondrocytes before matrix deposition can begin. Also at this time, our co-implantation cases (90:10 grey, 10:90 orange) have already surpassed the matrix levels of 0:100 despite containing less implanted chondrocytes. This is due to growth factors being released by the cell-to-cell interaction of the MSCs and chondrocytes (Chapter 3 [21]) and the balance of the effects of cell proliferation and nutrient levels. In our model MSCs have a high demand for nutrients to support their high proliferation rate and their differentiation into chondrocytes. In the 90:10 case the large concentration of MSCs therefore consume a large amount of nutrients, leaving less for the chondrocytes to produce matrix. On the other hand, in the 10:90 case the MSC density is lower and therefore these cells consume less nutrients, leaving

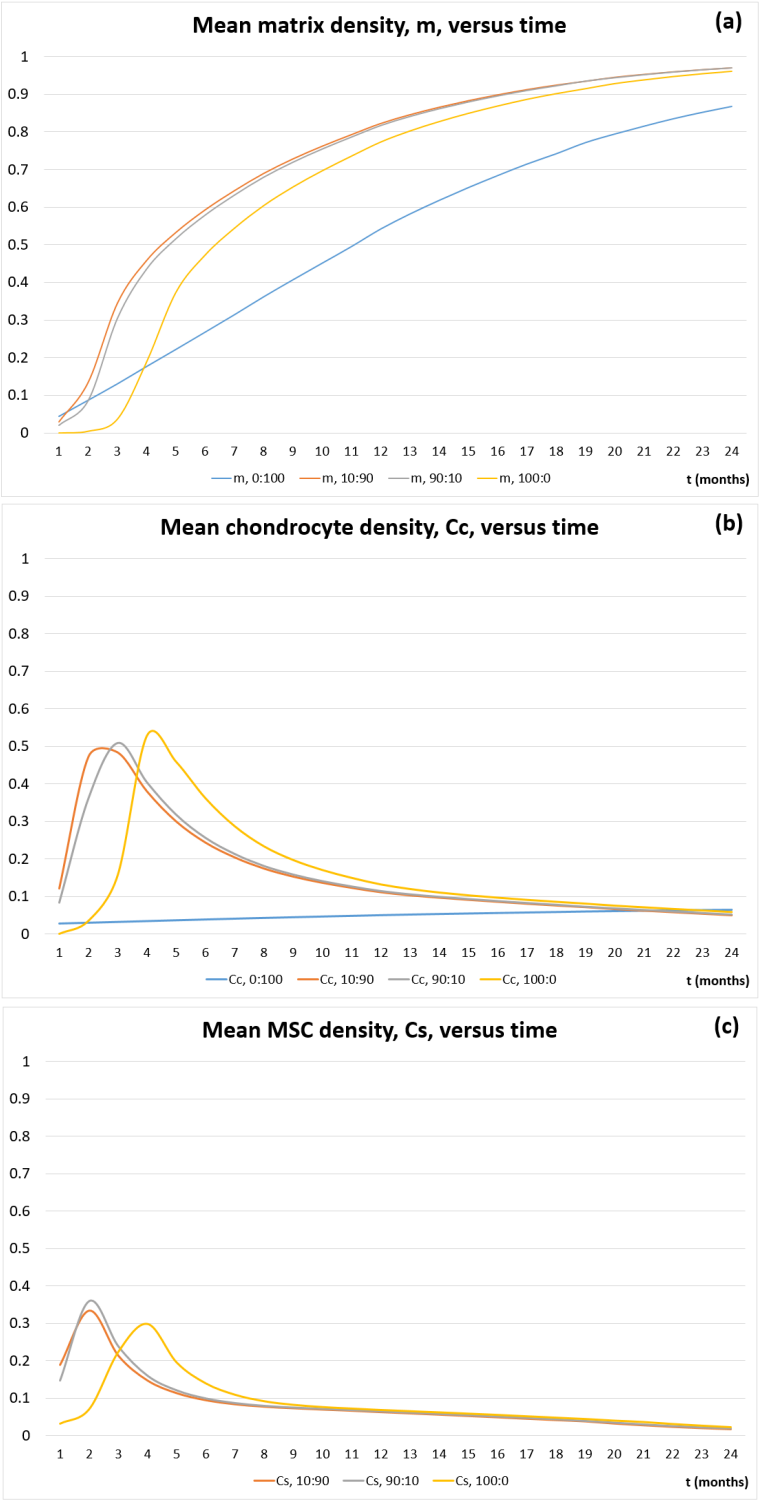

Figure 4.18: Mean densitites of (a) matrix, m, (b) chondrocytes, C_C, (c) MSCs, C_S, as a function of the time, in months, from 1-24 months for 0:100 (ACI, blue), 10:90 (orange), 90:10 (grey) and 100:0 (ASI, yellow). $x = 0$ in the figure represents the location of the base of the defect, $x = 1$ represents the surface of articular cartilage.

more nutrients for the chondrocytes to proliferate and deposit matrix. This difference is mainly observable at early times.

At 3 months the mean matrix density for 90:10 (grey) case is 136% more than in the 0:100 case (blue), and an even higher percentage difference when compared with the 100:0 case (yellow). This marked increase in matrix density is due to the effects of the growth factors [21]. We see a higher percentage difference when compared to 100:0 due to lower mean chondrocyte density at this time compared to 90:10 and 0:100 (see Fig. 4.18(b) for the mean chondrocyte density comparison between the co-implantation cases and ACI and ASI). Beyond 3 months this increase in mean matrix levels is sustained for the co-implantation cases with an 80% increase at 12 months when compared with 0:100 for our 90:10 case. The percentage difference is smaller when compared with the 100:0 case, with a 5.5% increase at 12 months. 12-24 months we see the co-implantation cases maintain the highest mean matrix levels, which is an accumulation of the differences in matrix levels at early times.

In Fig. 4.18(b) we compare the mean chondrocyte densities for the 10:90 (orange), 90:10 (grey) and 100:0 (yellow) cases. We do not show the evolution of the mean cell density of the 0:100 case since it is more localised to the bottom of the defect and therefore not a good comparison for mean cell levels. We see at 1 month that the 10:90 case (orange) has the highest levels of chondrocytes, but despite this matrix deposition is slow initially due to nutrient levels falling below the critical condition, $n_1 = 10^{-1}$ (Fig. 4.8). This effect is also observable in the 90:10 case (orange). At 3 months chondrocyte levels have increased dramatically in our co-implantation cases, indicating MSC differentiation has been initiated, thus leading to these cases having the highest matrix density (Fig 4.18(a)).

In Fig. 4.18(c) we compare the mean MSC densities for the 10:90 (grey) and 90:10 (orange) co-implantation and 100:0 (yellow) cases. The 0:100 contains no MSCs. At 1 month the 90:10 case has the highest density of MSCs, despite the 100:0 case having the highest implantation of MSCs. In the 10:90 and 90:10 cases cell-to-cell interaction releases growth factors almost immediately, meaning chondrocyte proliferation and MSC differentiation is enhanced [184, 21]. This is likely to be the cause of the marked increase in MSC levels in the defect at this time.

4.4 Summary & Conclusions

This chapter aimed to develop a mathematical model to explore the longer term patterns over time of cartilage defect healing following implantation of mixtures of MSCs and chondrocytes at various ratio's, and investigate the differences between them. Firstly, our simulations suggest that co-implanting MSCs and chondrocytes will increase matrix deposition within the first half year of healing when compared with 100% mesenchymal stem cell (ASI) or 100% chondrocyte (ACI) implantation therapies, indicating a chondral defect could fill with new cartilage at earlier times when a co-culture procedure is the chosen treatment. Although 10:90 appears to have the highest matrix density at early times, clinically a co-implantation ratio that uses less chondrocytes is desirable if the aim would be to develop a single-stage autologous chondrocyte implantation procedure [9]. Opting for the lower proportion of chondrocytes in these co-implantation therapies could mean sufficient chondrocytes can be isolated from the cartilage harvest obtained during arthroscopy for a successful co-implantation procedure [175]. This alleviates the need for expansion of cells *in vitro* if the fresh chondrocytes are combined with allogeneic stem cells, allowing cells to be harvested and inserted into the defect region during one procedure [44]. Alternatively, the fresh chondrocytes can be mixed with fresh bone marrow, which despite the lower total cell number has been suggested to be clinically effective [163].

Current cell implantation methods such as ACI and ASI have their drawbacks. Autologous Chondrocyte Implantation results in a very slow and steady fill of matrix in the defect, where nutrients are rarely low with healing taking closer to 24 months. Articular Stem Cell Implantation has an exceedingly slow start with matrix only being deposited after around 2 months due to MSCs first having to differentiate into chondrocytes before healing can begin. Despite its slow start, ASI does however fill the defect with new cartilage well within the 18-24 month

time frame, exceeding matrix levels of ACI from around 5 months onwards. Motivation for a new, better procedure is clear, with both current procedures having their own disadvantages [21, 191]. Combining both MSCs and chondrocytes to create a new cell therapy is hoped to result in good matrix deposition at earlier times, as with ACI, and good intermediate matrix deposition, as with ASI, which our model has achieved.

Chapter 5

Mathematical model of osteochondral defect regeneration after cell therapy

In this chapter, we develop a mathematical model to explore the hypothesis that the repair of osteochondral defects uses the process of endochondral ossification seen in the growth plate. This hypothesis is based on the findings of Lydon *et al.* [120], who observed in an *in vivo* ovine experimental model that osteochondral defect regeneration is driven by endochondral ossification. However, the mathematical model specifically explores the hypothesis that the PTHrP-Ihh feedback loop identified in the growth plate [103] can also regulate endochondral defect healing. We will use the *in vivo* experimental results from Lydon *et al.* to compare the general pattern of cartilage and bone formation between our mathematical model and the repair process *in vivo* at various time points, in particular if the mathematical model captures the observed key processes of osteochondral defect healing, i.e. cartilage fill, calcification and bone production. As in Chapters 3 & 4, the various rate constants in the mathematical model

will be based on *in vitro* or *in vivo* data where possible, otherwise an assumption will be made. For relevant parameters, sensitivity analyses will be performed to determine the influence of the parameter value on the model outcomes. The specific role of the mathematical model is to address the hypothesis that PTHrP production in the surface layer of cartilage is a key determinant of cartilage thickness in the repaired defect.

Firstly, we summarise the clinical problem osteochondral defects pose, giving details of the proposed healing mechanism and growth factors PTHrP and Ihh, and detail the plan of the chapter. Then, we formulate the model, giving details of modelling and parameter choices along with non-dimensionalisation. Next we present the results of the model, whilst also conducting a sensitivity analysis, highlighting the important mechanisms within the model and validating our parameter choices and approximations. Finally, we briefly summarise the findings of this work, with main discussion located in Chapter 6.

5.1 Introducing the problem

General understanding of osteochondral defect healing is of important clinical significance, with little experimental data in humans available and reliable treatment strategies lacking. Once a joint afflicted with an osteochondral defect is osteoarthritic, surgical intervention is problematic and treatment options are limited [70]. Some treatment options for osteochondral defects include Autologous Chondrocyte Implantation (ACI), Osteochondral Autograft Transplantation (OATS), microfracture, with others [16, 36, 43]. Of these, only ACI and OATS are able to achieve the hyaline-type cartilage needed when regenerating chondral or osteochondral tissue, and are the treatments most used in clinical practice, with ACI determined to be an effective treatment strategy for large knee lesions due to the durability of the regenerated tissue [12, 16, 40].

Lydon *et al* recently demonstrated osteochondral defects in ovine models healing via endochondral ossification [120]. The findings of Lydon *et al* show healing begins with cartilage formation first occurring along the edges of the defect, filling from the sides inwards and upwards until the defect fills and forms a cartilage model. Once this process has completed, chondrocytes undergo hypertrophy and ossification takes place, with a layer of cartilage left remaining along the top of the defect. Other earlier studies support this hypothesis, such as those by Gotterbarm *et al* using the Gottingen mini-pig model (GMP) that show defects located in the trochlear groove of the knee heal via endochondral ossification [73, 86]. Shapiro *et al* also observed an endochondral ossification-like process occurring from the base of osteochondral defects in rabbit models, where hypertrophic chondrocytes were observed to be exhibiting behaviour akin to an endochondral process [161].

As detailed in Chapter 2, transcription factor Ihh (Indian Hedgehog) and growth factor PTHrP (Parathyroid hormone-related Protein) have an important mediatory role during the process of endochondral ossification. Indian hedgehog (Ihh) stimulates chondrocyte proliferation, along with chondrocyte and osteoblast differentiation [103]. Indian hedgehog is secreted when chondrocytes are exiting their proliferative state to undergo hypertrophy, whereas parathyroid hormone-related protein (PTHrP) is secreted by chondrocytes at the articular surface [84, 193]. PTHrP keeps chondrocytes in their proliferative state, which inhibits the production of Ihh and chondrocyte hypertrophy, forming a negative feedback loop [173]. Additionally, an external regulator to initiate chondrocyte hypertrophy, indicating the initiation of the endochondral ossification process, has been reported in various works. Kerkhofs *et al.* [94] explore the regulatory effects controlling endochondral ossification within the growth plate, and identify a sequential process where the PTHrP-Ihh feedback loop takes effect once

an external regulator initiates hypertrophy. Geris *et al.* [66] include a critical cartilage density in their bio-regulatory fracture healing model to initiate cartilage calcification based on earlier observations by Einhorn [50], where cartilage mineralisation is proposed to occur in the abundance of cartilage, akin to a critical density being achieved. Another example is by Carlier *et al.* [24], where in their computational fracture healing model a critical cartilage density is reached before endochondral ossification can occur, similar to [66]. Kozhemyakina *et al.* [100] describes how chondrocytes convert from a proliferative to a hypertrophic state within the growth plate, where this process is thought to be regulated by C-type natriuretic peptide (CNP) (and also its antagonistic feedback with FGF-18) that is produced by pre-hypertrophic and proliferative chondrocytes. The hypotheses we discuss above are perhaps regulated by differing factors, whether it be an abundance of cartilage matrix or a critical growth factor level, but the result remains the same; an external regulator outside the PTHrP-Ihh loop initiates the conversion of proliferation to hypertrophy in chondrocytes. In our model, we decide to use a critical cartilage density.

The focus of our work is to formulate a mathematical model to describe the osteochondral defect healing process after undergoing Autologous Chondrocyte Implantation (ACI). With this model, we aim to encapsulate the main characteristics of healing as described in the literature by focusing on the endochondral ossification healing pathway, and explore the importance of the above signalling pathway within the healing process. In Chapters 3 and 4 mathematical models were formulated to explore the processes involved in chondral defect healing after cell therapy. Lutianov *et al.* [119] successfully simulated cartilage regeneration following Autologous Chondrocyte Implantation and Articular Stem Cell Implantation, an ACI-like therapy where mesenchymal stem cells are implanted in the place of chondrocytes. The simulations compared the two cell therapies to demonstrate how they differed during

healing, with their conclusions stating there was no difference in overall healing time, but successfully highlighted differences in cell behaviour and healing evolution. Following on from this work, we incorporated the effects of growth factors to this model and simulated the implantation of chondrocytes and mesenchymal stem cells in a co-implantation cell therapy procedure [22, 21]. This work built on the *in vitro* experiments by Wu *et al.* [184] and highlighted the importance of growth factors released by cell-to-cell interactions within chondral healing between mesenchymal stem cells and chondrocytes, and how the co-implantation of these two cell types had a trophic effect on healing at early times. Despite these effects, we found no difference in overall healing time.

Current mathematical models of osteochondral defects are primarily concerned with various aspects of mechanical influence, with work exploring the properties of relevant scaffolds used in defect repair [92] and the mechanical influence of mesenchymal stem cell differentiation within a defect [91]. Another model was formulated to predict the effect of location of osteochondral defects within knees that are arthritic, using a finite element modelling approach [150]. Though these models explore some aspects of the healing process, this work will produce a novel mathematical model to depict the key mechanisms of osteochondral defect healing including endochondral ossification.

The plan of this chapter is as follows. In section 5.2 §*Mathematical model* we describe the basic model and the assumptions made, the boundary and initial conditions used, estimates of the parameter values and the scalings used to non-dimensionalise the equations. The results of our simulations are discussed in section 5.3 §*Results and sensitivity analysis*, where a thorough sensitivity analysis will be undertaken to validate our parameters and highlight those most

sensitive to change within the model. Finally, in section 5.4 §*Discussion & conclusions*, we explore the implications of the model, its limitations, and future work.

5.2 Mathematical model

A typical osteochondral defect has a small aspect thickness depth to length ratio. This enables us to simplify to a one-dimensional problem where we model cell growth along the defect thickness only, shown as the x-direction in Fig. 5.1.

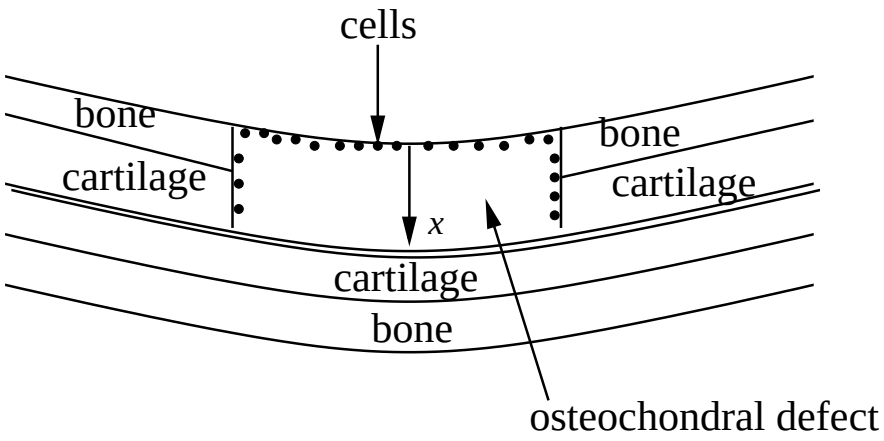

Figure 5.1: Schematic of a cross-section of the osteochondral defect. After debridement of the defect, cells such as chondrocytes or mesenchymal stem cells are seeded along the defect walls.

The variables in our model are: the chondrocyte density, C_C (cells/mm^3), the mature (or hypertrophied) chondrocyte density, C_H (cells/mm^3), the osteoblast density, C_B (cells/mm^3), the total matrix density, m (g/mm^3), which consists of the cartilage matrix density, m_C (g/mm^3), the bone matrix density, m_B (g/mm^3), and the calcified cartilage density, m_{Ca} (g/mm^3), the nutrient concentration, n (moles/mm^3), the hypertrophy-inducing growth factor concentration, g_{HI} (g/mm^3), the hypertrophy-suppressing growth factor concentration, g_{HS} (g/mm^3) and the hypertrophy modulating concentration (g/mm^3), g_{HM}. Our model assumes a healing osteochondral defect can be populated by three cell types, namely chondrocytes, hypertrophied chondrocytes and osteoblasts, which each produce their specific matrix:

cartilage, calcified cartilage or bone. Depending on cell type, the cells are able to migrate non-directed (random) and depending on cell type proliferate via the uptake of nutrients, differentiate, undergo hypertrophy and deposit matrix via nutrient uptake. In order to explore our central hypothesis that the PTHrP-Ihh feedback loop is important in endochondral ossification also controls the healing of osteochondral defects, we include a particular mechanism representing the growth factors in this feedback loop and their stimulatory and suppressive influence on chondrocyte hypertrophy. We do not include the biomechanical and other biochemical effects discussed in Chapter 2, which are known to influence bone resorption and remodelling as well as patterns of endochondral ossification, even though they may also relate to the repair process we are modelling. We also do not explicitly include chemotaxis (directed motility). As with the model formulated in Chapter 3, the motility of cells (assumed to occur through diffusion) is modelled proportional to the nutrient concentration, with cell proliferation and differentiation ceasing to occur when nutrient levels are low, meaning cell motility is the driving force of evolution at these times, migrating towards locations of higher nutrient concentration.

We now develop a mathematical model for the evolution of each species in time, t, and space, x, where x is measured along the thickness of the defect (see Figure 5.1). Much of the model formulation follows from our previous chapters and other models of chondral defect regeneration [21, 22, 119].

We focus here on the cartilage-to-calcified cartilage-to-bone formulation (endochondral ossification) pathway and the role of growth factors mediating this. To achieve a sequential healing process, we allow for processes described to occur during osteochondral defect repair to be

regulated by certain factors: For example, we will allow our osteochondral defect to first fill entirely with cartilage, therefore forming the cartilage model, before chondrocyte hypertrophy and eventual conversion into bone can occur [24, 66]. Factors that regulate these stages are growth and transcription factors, such as PTHrP and Ihh, represented in the model by g_{HI}, g_{HM}, g_{HS}.

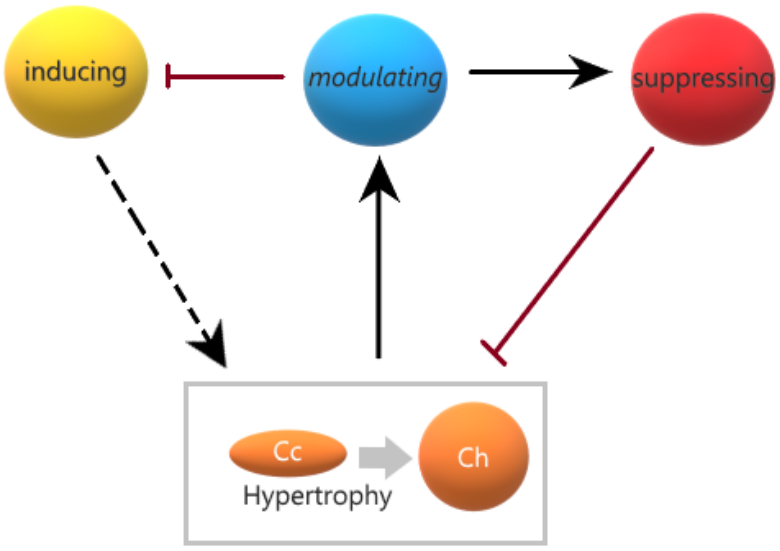

Figure 5.2: Schematic of a growth factor feedback loop akin to PTHrP and Ihh, modelled as inducing, modulating and suppressing growth factors. Black arrows indicate inducing, maroon lines represent inhibiting. Cc and Ch represent chondrocytes and hypertrophic chondrocytes, respectively.

Here we use g_{HI} to represent the growth factor that regulates hypertrophy. Once hypertrophic chondrocytes are being produced modulating growth factor is released, g_{HM}, that acts as an intermediate step within the signalling pathway; this growth factor inhibits our inducing growth factor, g_{HI}, but also produces suppressing growth factor, g_{HS}, that inhibits the hypertrophy, representing effects similar to PTHrP suppressing hypertrophy by keeping chondrocytes proliferating [94].

Additionally, we include a critical cartilage density, $m_{C_{crit}}$, acting as an external regulator

that allows chondrocytes to switch from a proliferative to a hypertrophic state whilst also initiating the conversion of cartilage to calcified matrix and the endochondral ossification process. Once $m_{C_{crit}}$ is achieved, taken in our model to be 95% of $m_{C_{max}}$, cartilage can begin conversion into calcified matrix which is subsequently remodelled to bone as seen in bone fracture healing [24, 66]. This conversion of cartilage to calcified matrix can occur at locations where m_C reaches $m_{C_{crit}}$, allowing chondrocytes to convert from a proliferative to a hypertrophic state.

The mechanisms we include in our model are detailed below. We do not include the biomechanical and biochemical effects discussed in Chapter 2 of this thesis. We do not explicitly include chemotaxis in the nutrient field.

Chondrocytes can proliferate by uptake of nutrients, they can migrate and can undergo hypertrophy. Based on these processes, the rate of change of chondrocyte density is modelled as

$$\begin{aligned}\frac{\partial C_C}{\partial t} = \frac{\partial}{\partial x}\left(D_{C_C}(m)\frac{\partial C_C}{\partial x}\right) + p_5\left(m, \frac{C_C}{C_{C,max}(m)}\right)C_C\frac{n}{n+n_0}H\left(n-n_1\right) \\ - p_6 C_C H\left(g_{HI}-g_{HI_0}\right)H\left(g_{HS_0}-g_{HS}\right) - p_7 C_c H\left(n_1-n\right),\end{aligned} \tag{5.1}$$

The first term on the right of Eq. (5.1) represents random chondrocyte migration, modelled as a diffusion process, with an effective chondrocyte random motility coefficient, D_{C_C}. This coefficient is assumed to depend on the total matrix density, m, where $m = m_C + m_B + m_{Ca}$. This is based on the argument that cells can only migrate by attaching to a substrate (in this case, matrix). We use a density-weighted formula for the effective chondrocyte diffusion

coefficient, D_{C_C}, based on the diffusivity through cartilage, $D_{C_{C,C}}$, calcified cartilage, $D_{C_{C,Ca}}$, and bone matrix, $D_{C_{C,B}}$, using a mixtures rule, analogous to the overall resistance of resistors in parallel in an electrical circuit. We follow [147] and [7] in choosing expressions for $D_{C_{C,C}}$, $D_{C_{C,Ca}}$ and $D_{C_{C,B}}$.

$$\frac{1}{D_{C_C}(m)} = \left(\frac{m_C}{m}\right)^{\alpha} \frac{1}{D_{C_{C,C}}(m_C)} + \left(\frac{m_B}{m}\right)^{\alpha} \frac{1}{D_{C_{C,B}}(m_B)} + \left(\frac{m_{Ca}}{m}\right)^{\alpha} \frac{1}{D_{C_{C,Ca}}(m_{Ca})}, \quad \alpha \geq 2,$$

$$D_{C_{C,C}}(m_C) = D_{C_{C,C_0}} \frac{m_C}{m_C^2 + m_{C,1}^2}, \quad D_{C_{C,B}}(m_B) = D_{C_{C,B_0}} \frac{m_B}{m_B^2 + m_{B,1}^2},$$

$$D_{C_{C,Ca}}(m_{Ca}) = D_{C_{C,Ca_0}} \frac{m_{Ca}}{m_{Ca}^2 + m_{Ca,1}^2} \tag{5.2}$$

where $(D_{C_{C,C_0}}, D_{C_{C,B_0}}, D_{C_{C,Ca_0}})$ are reference diffusion ratios of chondrocyte through cartilage, bone and calcified cartilage, respectively, and $(m_{C,1}, m_{B,1}, m_{Ca,1})$ are reference matrix densities.

The exponent $\alpha \geq 2$ is chosen so that we mimic the low motility of cells for the limiting cases when there is no cartilage (or bone) present and for large cartilage (or bone) matrix densities.

The second term on the right of Eq. (5.1) represents chondrocyte proliferation.
Cell proliferation is assumed to be proportional to the chondrocyte density and the nutrient concentration. This process is assumed to start only when the nutrient concentration exceeds a critical value, n_1 (or, alternatively, cell proliferation is switched-off when the nutrient concentration falls below this critical value). This is modelled by the Heaviside function, $H(n - n_1)$, which takes the unit value when $n > n_1$ and zero otherwise. The chondrocyte proliferation rate is given by p_5. The proliferation rate is assumed to depend on both the

chondrocyte and total matrix densities. We choose

$$
\begin{aligned}
&p_5\left(m, \frac{C_C}{C_{C,max}(m)}\right) = p_{5,m}\left(1 - \frac{C_C}{C_{C,max}(m)}\right), \\
&\frac{1}{p_{5,m}(m)} = \left(\frac{m_{C_{tot}}}{m}\right)^{\alpha} \frac{1}{p_{5,C}(m_{C_{tot}})} + \left(\frac{m_B}{m}\right)^{\alpha} \frac{1}{p_{5,B}(m_B)}, \quad \alpha \geq 2, \\
&p_{5,C}(m_{C_{tot}}) = p_{5,C_0} \frac{m_{C_{tot}}}{m_{C_{tot}}^2 + m_{C,2}^2}, \quad p_{5,B}(m_B) = p_{5,B_0} \frac{m_B}{m_B^2 + m_{B,2}^2}, \\
&C_{C,max}(m) = C_{C,max0}\left(1 - \frac{m}{m_{max}}\right),
\end{aligned}
\tag{5.3}
$$

The dependence of p_5 on the total matrix density is represented by $p_{5,m}(m)$. A density-weighted formula (similar to the effective cell diffusion coefficient) is used to model the effective proliferation rate based on cell proliferation rate in the presence of cartilage (represented by $p_{5,C}$) and bone (represented by $p_{5,B}$). The dependence of $(p_{5,C}, p_{5,B})$ on the matrix density $(m_{C_{tot}}, m_B)$ are chosen so that $(p_{5,C}, p_{5,B}) = 0$ when $(m_{C_{tot}}, m_B) = 0$, $(p_{5,C}, p_{5,B}) \to 0$ for large $(m_{C_{tot}}, m_B)$ and $(p_{5,C}, p_{5,B})$ attain a maximum at some intermediate matrix density, $(m_{C_{tot}}, m_B) = (m_{C,2}, m_{B,2})$. The coefficients, p_{5,C_0}, p_{5,B_0}, represent chondrocyte proliferation rates in the presence of cartilage and bone, respectively. We assume that $p_{5,C}$ depends on the total cartilage matrix density, $m_{C_{tot}} = m_C + m_{Ca}$ and not on the cartilage type, i.e., whether regular or calcified cartilage. The dependence of p_5 on the chondrocyte density is assumed to follow a logistic growth model with the proliferation rate decreasing as the chondrocyte density approaches its maximum value, $C_{C,max}$. This maximum chondrocyte density is assumed to decrease linearly with total matrix density, m, because the presence of matrix will limit the space for cells. C_{C,max_0} is a reference maximum chondrocyte density.

The third term on the right of Eq. (5.1) models chondrocyte hypertrophy. This is assumed to be proportional to the chondrocyte density and is regulated by the hypertrophy-inducing and suppressing growth factors, g_{HI} and g_{HS}, respectively. The maturation rate is p_6, and is assumed constant. The dependence on these growth factor concentrations is modelled

using the Heaviside function, $H(g_{HI} - g_{HI_0})$ and $H(g_{HS_0} - g_{HS})$, where g_{HI_0} and g_{HS_0} are a threshold hypertrophy-inducing and suppressing growth factor concentration, respectively. The first Heaviside function promotes hypertrophy once the hypertrophy-inducing growth factor concentration exceeds its threshold value, g_{HI_0}, and the second suppresses hypertrophy once the hypertrophy-suppressing growth factor concentration exceeds its threshold value, g_{HS_0}.

The last term in Eq. (5.1) represents cell death due to lack of adequate nutrients. This process starts when the nutrient concentration falls below the critical value, n_1, and is modelled using the Heaviside function, $H(n_1 - n)$, which takes the unit value when $n < n_1$ and zero otherwise. The cell death rate, p_7, is assumed constant.

The rate of change of mature hypertrophic chondrocyte density is written as

$$\frac{\partial C_H}{\partial t} = \frac{\partial}{\partial x}\left(D_{C_H}(m)\frac{\partial C_H}{\partial x}\right) - p_8 C_H + p_6 C_C H\left(g_{HI} - g_{HI_0}\right) H\left(g_{HS_0} - g_{HS}\right), \tag{5.4}$$

where D_{C_H} is the migration (diffusion) coefficient and p_8 is the death rate. We use similar expressions as in Eqs. (5.3) for the diffusion coefficient D_{C_H} through cartilage and bone, given by

$$\begin{aligned}
&\frac{1}{D_{C_H}(m)} = \left(\frac{m_C}{m}\right)^{\alpha}\frac{1}{D_{C_{H,C}}(m_C)} + \left(\frac{m_B}{m}\right)^{\alpha}\frac{1}{D_{C_{H,B}}(m_B)} + \left(\frac{m_{Ca}}{m}\right)^{\alpha}\frac{1}{D_{C_{H,Ca}}(m_{Ca})}, \quad \alpha \geq 2,\\
&D_{C_{H,C}}(m_C) = D_{C_{H,C_0}}\frac{m_C}{m_C^2 + m_{C,1}^2}, \quad D_{C_{H,B}}(m_B) = D_{C_{H,B_0}}\frac{m_B}{m_B^2 + m_{B,1}^2},\\
&D_{C_{H,Ca}}(m_{Ca}) = D_{C_{H,Ca_0}}\frac{m_{Ca}}{m_{Ca}^2 + m_{Ca,1}^2},
\end{aligned} \tag{5.5}$$

where $D_{C_{H,C_0}}, D_{C_{H,B_0}}, D_{C_{H,Ca_0}}$ are reference diffusion ratios of hypertrophic chondrocytes

through cartilage, bone and calcified cartilage, respectively,

The last term in Eq. (5.4) models the formation of hypertrophic chondrocytes modulated by the hypertrophy-inducing and suppressing growth factor concentrations.

The rate of change of osteoblast density is written as

$$\begin{aligned}\frac{\partial C_B}{\partial t} &= \frac{\partial}{\partial x}\left(D_{C_B}(m)\frac{\partial C_B}{\partial x}\right) + p_9\left(m, \frac{C_B}{C_{B,max}(m)}\right) C_B \frac{n}{n+n_0} H\left(n-n_1\right) \\ &\quad - p_{10} C_B H\left(n_1 - n\right),\end{aligned} \tag{5.6}$$

where D_{C_B} is the osteoblast migration (diffusion) coefficient, p_9 is the osteoblast proliferation rate and p_{10} is the osteoblast death rate. We use similar expressions as in Eqs. (5.3,5.5) for the matrix-dependent osteoblast diffusion and proliferation ratio, given by:

$$\begin{aligned}
&\frac{1}{D_{C_B}(m)} = \left(\frac{m_C}{m}\right)^{\alpha} \frac{1}{D_{C_{B,C}}(m_C)} + \left(\frac{m_B}{m}\right)^{\alpha} \frac{1}{D_{C_{B,B}}(m_B)} + \left(\frac{m_{Ca}}{m}\right)^{\alpha} \frac{1}{D_{C_{B,Ca}}(m_{Ca})}, \quad \alpha \geq 2, \\
&D_{C_{B,C}}(m_C) = D_{C_{B,C_0}} \frac{m_C}{m_C^2 + m_{C,1}^2}, \quad D_{C_{B,B}}(m_B) = D_{C_{B,B_0}} \frac{m_B}{m_B^2 + m_{B,1}^2}, \\
&D_{C_{B,Ca}}(m_{Ca}) = D_{C_{B,Ca_0}} \frac{m_{Ca}}{m_{Ca}^2 + m_{Ca,1}^2}, \quad p_9\left(m, \frac{C_B}{C_{B,max}(m)}\right) = p_{9,m}\left(1 - \frac{C_B}{C_{B,max}(m)}\right), \\
&\frac{1}{p_{9,m}(m)} = \left(\frac{m_{C_{tot}}}{m}\right)^{\alpha} \frac{1}{p_{9,C}(m_{C_{tot}})} + \left(\frac{m_B}{m}\right)^{\alpha} \frac{1}{p_{9,B}(m_B)}, \quad \alpha \geq 2, \\
&p_{9,C}(m_{C_{tot}}) = p_{9,C_0} \frac{m_{C_{tot}}}{m_{C_{tot}}^2 + m_{C,2}^2}, \quad p_{9,B}(m_B) = p_{9,B_0} \frac{m_B}{m_B^2 + m_{B,2}^2}, \\
&C_{B,max}(m) = C_{B,max0}\left(1 - \frac{m}{m_{max}}\right),
\end{aligned} \tag{5.7}$$

where $D_{C_{B,C_0}}, D_{C_{B,B_0}}, D_{C_{B,Ca_0}}$ are reference osteoblast migration rates through cartilage, bone and calcified cartilage, respectively, and p_{9,C_0}, p_{9,B_0} are reference osteoblast proliferation rates in the presence of cartilage and bone, respectively. The maximum osteoblast

density, $C_{B,max}$, is assumed to decrease linearly with total matrix density, m. C_{B,max_0} is a reference maximum osteoblast density. We choose the reference maximum normal and mature chondrocyte and osteoblast densities, C_{C,max_0}, C_{H,max_0}, C_{B,max_0}, respectively, such that $C_{C,max_0} + C_{H,max_0} + C_{B,max_0} = C_{total,max_0}$, where C_{total,max_0} is a reference maximum total cell density. Hence, using the expressions for $C_{C,max}$ and $C_{B,max}$ in Eqs. (5.3,5.7) gives, $(C_{C,max} + C_{B,max})(m) = (C_{total,max_0} - C_{H,max_0})(1 - m/m_{max})$.

The rate of change of cartilage matrix density is

$$\frac{\partial m_C}{\partial t} = D_{m_C}\frac{\partial^2 m_C}{\partial x^2} + p_{11}(m_C)\frac{n}{n+n_0}C_C - p_{12}(m_C)C_H, \tag{5.8}$$

where D_{m_C} is the cartilage matrix diffusion coefficient (assumed constant), p_{11} is the cartilage matrix synthesis rate and p_{12} is the rate of localized cartilage matrix degradation. We choose

$$p_{11}(m_C) = p_{11_0} - p_{11_1}m_C, \tag{5.9}$$

where p_{11_0} is a cartilage matrix production rate and p_{11_1} is its degradation rate. This assumes that the cartilage matrix synthesis rate decreases linearly with increasing cartilage matrix density [7, 147].

As described in the beginning of this section, the conversion of cartilage to calcified matrix can occur at locations where m_C reaches $m_{C_{crit}}$, taken in our model to be 95% of $m_{C_{max}}$.

The last term in Eq. (5.8) models localized degradation of cartilage matrix to form calcified matrix and is assumed to be proportional to the hypertrophied chondrocyte density. We

choose

$$p_{12}(m_C) = p_{12_0} m_C, \tag{5.10}$$

where p_{12_0} is a cartilage matrix degradation rate. This assumes that the degradation is proportional to the cartilage matrix density. We allow cartilage degradation to occur once $\bar{m}_C$ has reached the critical density, $m_{C_{crit}}$, and to cease when m_{Ca} and m_B have reached maximum matrix density.

The rate of change of calcified cartilage matrix density is given by

$$\frac{\partial m_{Ca}}{\partial t} = p_{12}(m_C) C_H - p_{20} m_{Ca} C_B. \tag{5.11}$$

The first term on the right of Eq. (5.11) describes the formation of calcified cartilage as the cartilage matrix degrades in the presence of hypertrophic chondrocytes.The second term describes degradation of calcified cartilage matrix and is assumed to be proportional to its density and the osteoblast cell density and p_{20} the degradation rate. Here, we do not distinguish between osteoblasts and osteoclasts which are responsible for converting calcified cartilage into bone.

The rate of change of bone matrix density is

$$\frac{\partial m_B}{\partial t} = D_{m_B} \frac{\partial^2 m_B}{\partial x^2} + p_{13}(m_B) \frac{n}{n + n_0} C_B + p_{20} m_{Ca} C_B, \tag{5.12}$$

where D_{m_B} is the bone matrix diffusion coefficient (assumed constant) and p_{13} is the bone matrix synthesis rate. We choose

$$p_{13}(m_B) = p_{13_0} - p_{13_1} m_B, \tag{5.13}$$

where p_{13_0} is a bone matrix production rate and p_{13_1} is its degradation rate. The last term in Eq. (5.12) models bone matrix formation from calcified cartilage matrix.

The rate of change of hypertrophy-inducing growth factor concentration is modelled as

$$\frac{\partial g_{HI}}{\partial t} = D_{g_{HI}} \frac{\partial^2 g_{HI}}{\partial x^2} - p_{24} g_{HM} - p_{25} g_{HI}, \tag{5.14}$$

where $D_{g_{HI}}$ is the hypertrophy-inducing growth factor diffusion coefficient (assumed constant), p_{24} is rate of degradation via hypertrophy-modulating growth factor (second term in the right of Eq 5.14) and is assumed proportional to the hypertrophy-modulating growth factor concentration, and p_{25} is the rate of degradation (assumed constant).

The rate of change of hypertrophy-suppressing growth factor concentration is modelled as

$$\frac{\partial g_{HS}}{\partial t} = D_{g_{HS}} \frac{\partial^2 g_{HS}}{\partial x^2} + p_{15} g_{HM} - p_{22} g_{HS}, \tag{5.15}$$

where $D_{g_{HS}}$ is the hypertrophy-suppressing growth factor diffusion coefficient (assumed constant), p_{15} and p_{21} represents its production rate and p_{22} is the degradation rate (assumed constant). The second term in Eq. (5.15) models the production of hypertrophy-suppressing growth factor from chondrocytes and is hence assumed to be proportional to the chondrocyte density. We assume here that this growth factor is produced only by the chondrocytes at the top of the defect ($x = d$). The third term models the production of hypertrophy-suppressing growth factor by the hypertrophy-modulating growth factor. The fourth term represents the degradation of this growth factor (assumed to be proportional to the hypertrophy-modulating growth factor concentration).

The rate of change of hypertrophy-modulating growth factor concentration is modelled as

$$\frac{\partial g_{HM}}{\partial t} = D_{g_{HM}} \frac{\partial^2 g_{HM}}{\partial x^2} + C_H - p_{23} g_{HM}, \tag{5.16}$$

where $D_{g_{HM}}$ is the hypertrophy-modulating growth factor diffusion coefficient (assumed constant), and p_{23} represents the degradation rate (assumed constant). The production of hypertrophy-modulating growth factor is assumed to be proportional to the hypertrophied chondrocyte density.

Finally, the rate of change of nutrient concentration is modelled as

$$\frac{\partial n}{\partial t} = D_n \frac{\partial^2 n}{\partial x^2} - \frac{n}{n + n_0} \left(p_{17} C_C + p_{18} C_B + p_{19} C_H \right), \tag{5.17}$$

where D_n is the nutrient diffusion coefficient (assumed constant), p_{17}, p_{18} and p_{19} represent the nutrient uptake rate by chondrocytes, osteoblasts and mature chondrocytes, respectively (assumed constant).

5.2.1 Boundary conditions

We need to specify two boundary conditions for each species (except m_{Ca}, which does not require spatial boundary conditions). These are specified at either end of the defect domain. We choose $x = 0$ at the bottom (subchondral bone interface) and $x = d$ (normal cartilage interface) at its upper end. The boundary conditions chosen at $x = 0$ are:

$$-D_{C_C}(m) \frac{\partial C_C}{\partial x} = -D_{C_H}(m) \frac{\partial C_H}{\partial x} = -D_{m_C} \frac{\partial m_C}{\partial x} = -D_{m_B} \frac{\partial m_B}{\partial x} = 0,$$

$$C_B = C_{B_0}, \;\; n = N_0, \;\; g_{HI} = g_{HI_1}, \;\; g_{HS} = g_{HM} = 0.$$

The first four boundary conditions represent no flux of chondrocytes, hypertrophied chondrocytes, cartilage matrix and osteoblasts from the subchondral bone. We assume that a reservoir of osteoblasts, with uniform cell density, C_{B_0}, and nutrients, with uniform concentration, N_0, are always available at this end, represented by the fourth and fifth boundary conditions, respectively. The last three boundary conditions represent a constant supply of hypertrophy-inducing growth factor, with uniform concentration, g_{HI_1}, and no hypertrophy-suppressing or modulating growth factor, respectively, at this end.

At $x = d$, we impose:

$$
\begin{aligned}
&-D_{C_C}(m)\frac{\partial C_C}{\partial x} = -D_{C_B}(m)\frac{\partial C_B}{\partial x} = -D_{C_H}(m)\frac{\partial C_H}{\partial x} = -D_{m_C}\frac{\partial m_C}{\partial x} = -D_{m_B}\frac{\partial m_B}{\partial x} = 0,\\
&n = N_1,\ \ g_{HI} = g_{HI_2},\ \ -D_{g_{HS}}\frac{\partial g_{HS}}{\partial x} = \gamma g_{HS},\ \ g_{HM} = 0.
\end{aligned}
\tag{5.18}
$$

The first five boundary conditions represent no flux of chondrocytes, osteoblasts, hypertrophied chondrocytes and matrix, respectively, from the normal cartilage interface. We assume that a reservoir of nutrients with uniform concentration, N_1, is always available at this end. A constant supply of hypertrophy-inducing growth factor, with uniform concentration, g_{HI_2} is available at this boundary. We allow the hypertrophy-suppressing growth factor to permeate (or diffuse) in through this boundary, represented by the eighth boundary condition, with the diffusive flux proportional to the growth factor concentration, and constant of proportionality γ (assumed constant). There is no hypertrophy-modulating growth factor at the upper boundary.

5.2.2 Initial conditions

We need to prescribe profiles for each species at time $t = 0$. We are interested in the Autologous Chondrocyte Implantation (ACI) scenario. Initially, chondrocytes (and osteoblasts)

are seeded into a nutrient-filled defect with a small amount of matrix present. The initial conditions chosen for this case are:

$$C_C = C_C^{(0)} h(x),\ \ C_B = C_{B_0} h_1(x),\ \ C_H = 0,\ \ n = N_0 - (N_0 - N_1)\frac{x}{d},\ \ m_C = m_{C,3},\ \ m_B = m_{B,3},$$
$$m_{Ca} = 0,\ \ g_{HI} = g_{HI_1} - (g_{HI_1} - g_{HI_2})\frac{x}{d},\ \ g_{HS} = g_{HM} = 0. \tag{5.19}$$

Here, $C_C^{(0)}$, $C_B^{(0)}$, $h(x)$ and $h_1(x)$ are an initial chondrocyte and osteoblast density and their specified spatial profiles, respectively.

There are several parameters appearing in the model. Their estimated values and the references from which they are obtained are provided in Table 5.1. All approximated parameters are disclosed in the table and references are given where available.

dimensional parameters	**estimated value**, *source type*
defect thickness, d	3-5 mm (1-2 mm cartilage, 2-3 mm bone) (guess)
maximum chondrocyte migration (or diffusion) coefficient in cartilage, $D_{C_{C,C}}$	3.6×10^{-4} mm^2/hr [144], *in silico*
maximum chondrocyte migration (or diffusion) coefficient in bone, $D_{C_{C,B}}$	3.6×10^{-4} mm^2/hr (assumed same as $D_{C_{C,C}}$)
maximum chondrocyte migration (or diffusion) coefficient in calcified cartilage, $D_{C_{C,Ca}}$	3.6×10^{-4} mm^2/hr (assumed same as $D_{C_{C,C}}$)
maximum mature chondrocyte migration (or diffusion) coefficient in cartilage, $D_{C_{H,C}}$	10^{-5} mm^2/hr (guess)
maximum mature chondrocyte migration (or diffusion) coefficient in bone, $D_{C_{H,B}}$	10^{-5} mm^2/hr (assumed same as $D_{C_{H,C}}$)
maximum mature chondrocyte migration (or diffusion) coefficient in calcified cartilage, $D_{C_{H,Ca}}$	10^{-5} mm^2/hr (assumed same as $D_{C_{H,C}}$)
maximum osteoblast migration (or diffusion) coefficient in cartilage, $D_{C_{B,C}}$	10^{-6} - 10^{-5} mm^2/hr (guess)
maximum osteoblast migration (or diffusion) coefficient in bone, $D_{C_{B,B}}$	10^{-4} - 10^{-3} mm^2/hr (guess)

maximum osteoblast migration (or diffusion) coefficient in calcified cartilage, $D_{C_{B,Ca}}$	10^{-4} - 10^{-3} mm^2/hr (guess)
chondrocyte migration (or diffusion) coefficient, $D_{C_{C,C_0}} = 2m_{C,1}D_{C_{C,C}}$	7.2×10^{-9} (mm^2/hr) (g/mm^3) (assuming $m_{C,1} = 10^{-5}$ g/mm^3)
chondrocyte migration (or diffusion) coefficient, $D_{C_{C,B_0}} = 2m_{B,1}D_{C_{C,B}}$	7.2×10^{-9} (mm^2/hr) (g/mm^3) (assuming $m_{B,1} = 10^{-5}$ g/mm^3)
chondrocyte migration (or diffusion) coefficient, $D_{C_{C,Ca_0}} = 2m_{Ca,1}D_{C_{C,Ca}}$	7.2×10^{-9} (mm^2/hr) (g/mm^3) (assuming $m_{Ca,1} = 10^{-5}$ g/mm^3)
mature chondrocyte migration (or diffusion) coefficient, $D_{C_{H,C_0}} = 2m_{C,1}D_{C_{H,C}}$	10^{-10} (mm^2/hr) (g/mm^3) (assuming $m_{C,1} = 10^{-5}$ g/mm^3)
mature chondrocyte migration (or diffusion) coefficient, $D_{C_{H,B_0}} = 2m_{B,1}D_{C_{H,B}}$	10^{-10} (mm^2/hr) (g/mm^3) (assuming $m_{B,1} = 10^{-5}$ g/mm^3)
mature chondrocyte migration (or diffusion) coefficient, $D_{C_{H,Ca_0}} = 2m_{Ca,1}D_{C_{H,Ca}}$	10^{-10} (mm^2/hr) (g/mm^3) (assuming $m_{Ca,1} = 10^{-5}$ g/mm^3)
osteoblast migration (or diffusion) coefficient, $D_{C_{B,C_0}} = 2m_{C,1}D_{C_{B,C}}$	10^{-11} - 10^{-10} (mm^2/hr) (g/mm^3) (assuming $m_{C,1} = 10^{-5}$ g/mm^3)
osteoblast migration (or diffusion) coefficient, $D_{C_{B,B_0}} = 2m_{B,1}D_{C_{B,B}}$	10^{-9} (mm^2/hr) (g/mm^3) (assuming $m_{B,1} = 10^{-5}$ g/mm^3)
osteoblast migration (or diffusion) coefficient, $D_{C_{B,Ca_0}} = 2m_{Ca,1}D_{C_{B,Ca}}$	10^{-9} (mm^2/hr) (g/mm^3) (assuming $m_{Ca,1} = 10^{-5}$ g/mm^3)
nutrient diffusion coefficient, D_n	4.6 mm^2/hr [195], *mathematical model*
cartilage matrix diffusion coefficient, D_{m_C}	0 - 2.5×10^{-5} mm^2/hr [144], *in silico*

bone matrix diffusion coefficient, D_{m_B}	0 - 10^{-6} mm^2/hr (guess)
hypertrophy-inducing growth factor diffusion coefficient, $D_{g_{HI}}$	0.8 mm^2/hr [181], *in vitro, in vivo*
hypertrophy-suppressing growth factor diffusion coefficient, $D_{g_{HS}}$	0.18 mm^2/hr [54], *mathematical model, in vivo*
hypertrophy-modulating growth factor diffusion coefficient, $D_{g_{HM}}$	0.18 mm^2/hr [54], *mathematical model, in vivo*
maximum chondrocyte proliferation rate in cartilage, $p_{5,C}$	2×10^{-4}/hr (guess)
maximum chondrocyte proliferation rate in bone, $p_{5,B}$	2×10^{-4}/hr (assumed same as $p_{5,C}$)
chondrocyte proliferation rate, $p_{5_{C,0}} = 2m_{C,2}p_{5,C}$	4×10^{-9} g/mm^3/hr (assuming $m_{C,2} = 10^{-5}$ g/mm^3)
chondrocyte proliferation rate, $p_{5_{B,0}} = 2m_{B,2}p_{5,B}$	4×10^{-9} g/mm^3/hr (assuming $m_{B,2} = 10^{-5}$ g/mm^3)
chondrocyte hypertrophic differentiation rate, p_6	2×10^{-2}/hr [182], *in vivo*
chondrocyte death rate, p_7	3.75×10^{-3}/hr (guess)
mature chondrocyte death rate, p_8	6×10^{-3}/hr [182], *in vivo*
maximum osteoblast proliferation rate in cartilage, $p_{9,C}$	(10^{-3}-10^{-2})/hr (guess)
maximum osteoblast proliferation rate in bone, $p_{9,B}$	(10^{-3}-10^{-2})/hr (assumed same as $p_{9,C}$)

osteoblast proliferation rate, $p_{9,C_0} = 2m_{C,2}p_{9,C}$	$2 \times (10^{-8}$-$10^{-7})$ g/mm^3/hr (assuming $m_{C,2} = 10^{-5}$ g/mm^3)
osteoblast proliferation rate, $p_{9,B_0} = 2m_{B,2}p_{9,B}$	$2 \times (10^{-8}$-$10^{-7})$ g/mm^3/hr (assuming $m_{B,2} = 10^{-5}$ g/mm^3)
osteoblast death rate, p_{10}	10^{-3}/hr (guess)
cartilage matrix production rate, p_{11_0}	3.75×10^{-13}(g/mm^3)/((Nc/mm^3) hr)[144], *in silico*
cartilage matrix degradation rate, p_{11_1}	3.75×10^{-9}/((Nc/mm^3) hr) [144], *in silico*
cartilage matrix degradation rate, p_{12_0}	4×10^{-5} /((Nc/mm^3) hr) [182], *in vivo*
bone matrix production rate, p_{13_0}	5×10^{-12} (g/mm^3)/((Nc/mm^3) hr)
bone matrix degradation rate, p_{13_1}	10^{-12}/((Nc/mm^3) hr) (guess)
hypertrophy-suppressing growth factor production rate, p_{15}	10^{-24}Nm/(Nc hr) [64], *mathematical model*
nutrient uptake rate by chondrocytes, p_{17}	1.5×10^{-14}Nm/(Nc hr) [195], *mathematical model*
nutrient uptake rate by osteoblasts, p_{18}	1.5×10^{-14}Nm/(Nc hr) (assumed same as p_{16}, p_{17})
nutrient uptake rate by mature chondrocytes, p_{19}	1.5×10^{-14}Nm/(Nc hr) (assumed same as p_{16}, p_{17})
calcified cartilage matrix degradation rate, p_{20}	$8 \times (10^{-3}$-$10^{-2})$/((Nc/mm^3) hr) [7], *mathematical model*
hypertrophy-modulating growth factor degradation rate, p_{23}	$0 - 5.8 \times 10^{-2}$ (based on 0-12hr half-life)
hypertrophy-suppressing growth factor degradation rate, p_{22}	4/hr (assuming half-life 10 minutes) [7], *mathematical model*

hypertrophy-modulating growth factor degradation rate, p_{24}	4/hr (assuming half-life 10 minutes) [7], *mathematical model*
maximum total cell density, C_{total,max_0}	10^6 Nc/mm^3 (assuming $10\mu m$ cell diameter)
maximum chondrocyte density, C_{C,max_0}	$0 - 10^6$ Nc/mm^3
maximum mature chondrocyte density, C_{H,max_0}	$0 - 10^6$ Nc/mm^3
maximum osteoblast density, C_{B,max_0}	$0 - 10^6$ Nc/mm^3
maximum cartilage matrix density, $m_{C,max}$	10^{-4} g/mm^3 [7], *mathematical model*
maximum bone matrix density, $m_{B,max}$	$(1-2) \times 10^{-3}$ g/mm^3 (guess)
maximum calcified cartilage matrix density, $m_{Ca,max}$	$(1-2) \times 10^{-3}$ g/mm^3 (assumed same as $m_{B,max}$)
maximum matrix density, $m_{max} = m_{C,max} + m_{B,max} + m_{Ca,max}$	$(2.1-4.1) \times 10^{-3}$ g/mm^3
maximum total cartilage matrix density, $m_{C_{tot},max} = m_{C,max} + m_{Ca,max}$	$(1.1-2.1) \times 10^{-3}$ g/mm^3
critical cartilage matrix density, $m_{C,crit}$	0.95×10^{-4} g/mm^3 (assumed 95% of $m_{C,max}$)
initial chondrocyte cell density, $C_C^{(0)}$	2.5×10^5 Nc/mm^3 (based on 10^6 cells in 20mm x 20mm x 10μm volume)
matrix density, $m_{C,1}$	10^{-5} g/mm^3 (assumed $m_{max}/100$)
matrix density, $m_{C,2}$	10^{-5} g/mm^3 (assumed $m_{max}/100$)
matrix density, $m_{Ca,1}$	10^{-5} g/mm^3 (assumed $m_{max}/100$)
matrix density, $m_{B,1}$	10^{-5} g/mm^3 (assumed $m_{max}/100$)
matrix density, $m_{B,2}$	10^{-5} g/mm^3 (assumed $m_{max}/100$)

initial cartilage/bone matrix density, $m_{C,3}$,$m_{B,3}$	10^{-8} g/mm^3 (assumed $m_{max}/10^5$)
initial nutrient concentration, N_1	(2.85 - 9.5) $\times$ 10^{-11} Nm/mm^3 (3-10% oxygen tension - [195], *mathematical model*)
initial nutrient concentration, N_0	9.5 $\times$ 10^{-11} Nm/mm^3 [95], *human*
threshold nutrient concentration, n_0	2.3 $\times$ 10^{-11} Nm/mm^3 [195], *mathematical model*
critical nutrient concentration, n_1	9.5 $\times$ 10^{-12} Nm/mm^3 (assumed $N_0/10$)
threshold hypertrophy-inducing growth factor concentration, g_{HI_0}	$(0.5 - 1) \times 10^{-15}$ Nm/mm^3
threshold hypertrophy-suppressing growth factor concentration, g_{HS_0}	$(0.5 - 1) \times 10^{-15}$ Nm/mm^3
initial hypertrophy-inducing growth factor concentration, g_{HI_1}	2×10^{-15} Nm/mm^3
initial hypertrophy-inducing growth factor concentration, g_{HI_2}	2×10^{-15} Nm/mm^3
initial osteoblast cell density, $C_{B^{(0)}}$	9 $\times$ 10^3 Nc/mm^3 [126], *human*
rate of hypertrophy-suppressing growth factor leaving top boundary, γ	0 (no flux) - ∞ (zero concentration)

Table 5.1: Estimated values of dimensional parameters. In the above, N_C represents number of cells and N_m is number of moles.

5.2.3 Non-dimensionalisation

We nondimensionalise introducing the following dimensionless variables based on characteristic quantities for each variable:

$$\bar{x} = x/d,\ \bar{t} = t(p_{11_0}C_{total,max_0}/m_{C,max}),\ (\bar{C}_C, \bar{C}_H, \bar{C}_B) = (C_C, C_H, C_B)/C_{total,max_0},$$

$$(\bar{m}, \bar{m}_C, \bar{m}_{Ca}, \bar{m}_B, \bar{m}_{C_{tot}}) = (m/m_{max}, m_C/m_{C,max}, m_{Ca}/m_{Ca,max}, m_B/m_{B,max}, m_{C_{tot}}/m_{C_{total},max}),$$

$$\bar{n} = n/N_1,\ \bar{g}_{HI} = g_{HI}/g_{HI_1},\ \bar{g}_{HM} = g_{HM}\big(p_{11_0}/(p_{23}m_{C,max})\big),$$

$$\bar{g}_{HS} = g_{HS}\big(p_{11_0}^2 C_{total,max_0}/(p_{21}p_{23}m_{C,max}^2)\big), \tag{5.20}$$

where the overbars represent dimensionless quantities. The characteristic quantities used to measure the spatial variable, x, cell densities, matrix densities, nutrient concentration and the hypertrophy-inducing growth factor concentration are the defect thickness, d, the reference maximum total cell density, C_{total,max_0}, the maximum cartilage and bone matrix densities, $m_{C,max}$, $m_{Ca,max}$, $m_{B,max}$, respectively, the total matrix density, $m_{max} = m_{C,max} + m_{Ca,max} + m_{B,max}$, the total cartilage matrix density, $m_{C_{total},max} = m_{C,max} + m_{Ca,max}$, the initial nutrient concentration at $x = d$, N_1, and the initial hypertrophy-inducing growth factor concentration at $x = 0$, g_{HI_1}, respectively. We choose to measure time, t, based on the cartilage matrix production time scale, $m_{C,max}/(p_{11_0}C_{total,max_0})$. Using the parameter values in Table 5.1, we estimate this time scale to be approximately 11 days. Henceforth, a unit of time corresponds to approximately 11 days. We choose to measure the hypertrophy-modulating growth factor concentration based on it's production by hypertrophic chondrocytes, namely, $p_{22}m_{C,max}/p_{11_0}$ and the hypertrophy-suppressing growth factor concentration based on it's production by hypertrophy-modulating growth factor, namely, $p_{21}p_{23}m_{C,max}^2/(p_{11_0}^2 C_{total,max_0})$.

Using the above dimensionless variables, the non-dimensional equations can be written as

$$\frac{\partial \bar{C}_C}{\partial \bar{t}} = \frac{\partial}{\partial \bar{x}}\left(\bar{D}_{C_C}(\bar{m})\frac{\partial \bar{C}_C}{\partial \bar{x}}\right) + \bar{p}_5\left(\bar{m}, \frac{\bar{C}_C}{\bar{C}_{C,max}(\bar{m})}\right)\frac{\bar{n}}{\bar{n}+\bar{n}_0}\bar{C}_C H(\bar{n}-\bar{n}_1) \tag{5.21a}$$

$$- \bar{p}_6 \bar{C}_C H(\bar{g}_{HI} - \bar{g}_{HI_0}) H(\bar{g}_{HS_0} - \bar{g}_{HS}) - \bar{p}_7 \bar{C}_C H(\bar{n}_1 - \bar{n}), \tag{5.21b}$$

$$\frac{\partial \bar{C}_H}{\partial \bar{t}} = \frac{\partial}{\partial \bar{x}}\left(\bar{D}_{C_H}(\bar{m})\frac{\partial \bar{C}_H}{\partial \bar{x}}\right) + \bar{p}_6 \bar{C}_C H(\bar{g}_{HI} - \bar{g}_{HI_0}) H(\bar{g}_{HS_0} - \bar{g}_{HS}) - \bar{p}_8 \bar{C}_H, \tag{5.21c}$$

$$\frac{\partial \bar{C}_B}{\partial \bar{t}} = \frac{\partial}{\partial \bar{x}}\left(\bar{D}_{C_B}(\bar{m})\frac{\partial \bar{C}_B}{\partial \bar{x}}\right) + \bar{p}_9\left(\bar{m}, \frac{\bar{C}_B}{\bar{C}_{B,max}(\bar{m})}\right)\frac{\bar{n}}{\bar{n}+\bar{n}_0}\bar{C}_B H(\bar{n}-\bar{n}_1) \tag{5.21d}$$

$$- \bar{p}_{10} \bar{C}_B H(\bar{n}_1 - \bar{n}),$$

$$\frac{\partial \bar{m}_C}{\partial \bar{t}} = \bar{D}_{m_C}\frac{\partial^2 \bar{m}_C}{\partial \bar{x}^2} + \bar{p}_{11}(\bar{m})\frac{\bar{n}}{\bar{n}+\bar{n}_0}\bar{C}_C - \bar{p}_{12}(\bar{m}_C)\bar{C}_H, \tag{5.21e}$$

$$\frac{\partial \bar{m}_{Ca}}{\partial \bar{t}} = \frac{1}{\Gamma}\bar{p}_{12}(\bar{m}_C)\bar{C}_H - \bar{p}_{20}\bar{m}_{Ca}\bar{C}_B, \tag{5.21f}$$

$$\frac{\partial \bar{m}_B}{\partial \bar{t}} = \bar{D}_{m_B}\frac{\partial^2 \bar{m}_B}{\partial \bar{x}^2} + \bar{p}_{13}(\bar{m})\frac{\bar{n}}{\bar{n}+\bar{n}_0}\bar{C}_B + \bar{p}_{20}\frac{m_{Ca,max}}{m_{B,max}}\bar{m}_{Ca}\bar{C}_B, \tag{5.21g}$$

$$\frac{\partial \bar{g}_{HI}}{\partial \bar{t}} = \bar{D}_{g_{HI}}\frac{\partial^2 \bar{g}_{HI}}{\partial \bar{x}^2} - \bar{p}_{24}\bar{g}_{HM} - \bar{p}_{25}\bar{g}_{HI}, \tag{5.21h}$$

$$\frac{\partial \bar{g}_{HS}}{\partial \bar{t}} = \bar{D}_{g_{HS}}\frac{\partial^2 \bar{g}_{HS}}{\partial \bar{x}^2} + \bar{g}_{HM} - \bar{p}_{22}\bar{g}_{HS}, \tag{5.21i}$$

$$\frac{\partial \bar{g}_{HM}}{\partial \bar{t}} = \bar{D}_{g_{HM}}\frac{\partial^2 \bar{g}_{HM}}{\partial \bar{x}^2} + \bar{C}_H - \bar{p}_{23}\bar{g}_{HM}, \tag{5.21j}$$

$$\frac{\partial \bar{n}}{\partial \bar{t}} = \bar{D}_n\frac{\partial^2 \bar{n}}{\partial \bar{x}^2} - \frac{\bar{n}}{\bar{n}+\bar{n}_0}\left(\bar{p}_{16}\bar{C}_S + \bar{p}_{17}\bar{C}_C + \bar{p}_{18}\bar{C}_B + \bar{p}_{19}\bar{C}_H\right), \tag{5.21k}$$

where

$$\bar{p_5}\left(\bar{m}, \frac{\bar{C}_C}{\bar{C}_{C,max}(\bar{m})}\right) = \bar{p}_{5,m}(\bar{m})\left(1 - \frac{\bar{C}_C}{\bar{C}_{C,max}(\bar{m})}\right),\ \bar{C}_{C,max}(\bar{m}) = \bar{C}_{C,max_0}(1-\bar{m}),$$

$$\frac{1}{\bar{p}_{5,m}(\bar{m})} = (\beta+\epsilon)^\alpha \left(\frac{\bar{m}_{C_{total}}}{\bar{m}}\right)^\alpha \frac{1}{\bar{p}_{5,C}(\bar{m}_{C_{total}})} + \eta^\alpha \left(\frac{\bar{m}_B}{\bar{m}}\right)^\alpha \frac{1}{\bar{p}_{5,B}(\bar{m}_B)},\ \ \alpha \geq 2,$$

$$\bar{p}_{5,C}(\bar{m}_{C_{total}}) = \bar{p}_{5,C_0}\frac{\bar{m}_{C_{total}}}{\bar{m}^2_{C_{total}} + \bar{m}^2_{C,2}},\ \bar{p}_{5,B}(\bar{m}_B) = \bar{p}_{5,B_0}\frac{\bar{m}_B}{\bar{m}^2_B + \bar{m}^2_{B,2}},$$

$$\bar{p_9}\left(\bar{m}, \frac{\bar{C}_B}{\bar{C}_{B,max}(\bar{m})}\right) = \bar{p}_{9,m}(\bar{m})\left(1 - \frac{\bar{C}_B}{\bar{C}_{B,max}(\bar{m})}\right),\ \bar{C}_{B,max}(\bar{m}) = \bar{C}_{B,max_0}(1-\bar{m}),$$

$$\frac{1}{\bar{p}_{9,m}(\bar{m})} = (\beta+\epsilon)^\alpha \left(\frac{\bar{m}_{C_{total}}}{\bar{m}}\right)^\alpha \frac{1}{\bar{p}_{9,C}(\bar{m}_{C_{total}})} + \eta^\alpha \left(\frac{\bar{m}_B}{\bar{m}}\right)^\alpha \frac{1}{\bar{p}_{9,B}(\bar{m}_B)},\ \ \alpha \geq 2,$$

$$\bar{p}_{9,C}(\bar{m}_{C_{total}}) = \bar{p}_{9,C_0}\frac{\bar{m}_{C_{total}}}{\bar{m}^2_{C_{total}} + \bar{m}^2_{C,2}},\ \bar{p}_{9,B}(\bar{m}_B) = \bar{p}_{9,B_0}\frac{\bar{m}_B}{\bar{m}^2_B + \bar{m}^2_{B,2}},$$

$$\bar{p}_{11}(\bar{m}_C) = 1 - \bar{p}_{11_1}\bar{m}_C,\ \bar{p}_{12}(\bar{m}_C) = \bar{p}_{12_0}\bar{m}_C,\ \bar{p}_{13}(\bar{m}_B) = \bar{p}_{13_0} - \bar{p}_{13_1}\bar{m}_B,$$

$$\bar{D}_{C_{C,C}}(\bar{m}_C) = \bar{D}_{C_{C,C_0}}\frac{\bar{m}_C}{\bar{m}^2_C + \bar{m}^2_{C,1}},\ \bar{D}_{C_{C,B}}(\bar{m}_B) = \bar{D}_{C_{C,B_0}}\frac{\bar{m}_B}{\bar{m}^2_B + \bar{m}^2_{B,1}},$$

$$\bar{D}_{C_{C,Ca}}(\bar{m}_{Ca}) = \bar{D}_{C_{C,Ca_0}}\frac{\bar{m}_{Ca}}{\bar{m}^2_{Ca} + \bar{m}^2_{Ca,1}},$$

$$\frac{1}{\bar{D}_{C_H}(\bar{m})} = \beta^\alpha \left(\frac{\bar{m}_C}{\bar{m}}\right)^\alpha \frac{1}{\bar{D}_{C_{H,C}}(\bar{m}_C)} + \eta^\alpha \left(\frac{\bar{m}_B}{\bar{m}}\right)^\alpha \frac{1}{\bar{D}_{C_{H,B}}(\bar{m}_B)} + \epsilon^\alpha \left(\frac{\bar{m}_{Ca}}{\bar{m}}\right)^\alpha \frac{1}{\bar{D}_{C_{H,Ca}}(\bar{m}_{Ca})},$$

$$\bar{D}_{C_{H,C}}(\bar{m}_C) = \bar{D}_{C_{H,C_0}}\frac{\bar{m}_C}{\bar{m}^2_C + \bar{m}^2_{C,1}},\ \bar{D}_{C_{H,B}}(\bar{m}_B) = \bar{D}_{C_{H,B_0}}\frac{\bar{m}_B}{\bar{m}^2_B + \bar{m}^2_{B,1}},$$

$$\bar{D}_{C_{H,Ca}}(\bar{m}_{Ca}) = \bar{D}_{C_{H,Ca_0}}\frac{\bar{m}_{Ca}}{\bar{m}^2_{Ca} + \bar{m}^2_{Ca,1}},$$

$$\frac{1}{\bar{D}_{C_B}(\bar{m})} = \beta^\alpha \left(\frac{\bar{m}_C}{\bar{m}}\right)^\alpha \frac{1}{\bar{D}_{C_{B,C}}(\bar{m}_C)} + \eta^\alpha \left(\frac{\bar{m}_B}{\bar{m}}\right)^\alpha \frac{1}{\bar{D}_{C_{B,B}}(\bar{m}_B)} + \epsilon^\alpha \left(\frac{\bar{m}_{Ca}}{\bar{m}}\right)^\alpha \frac{1}{\bar{D}_{C_{B,Ca}}(\bar{m}_{Ca})},$$

$$\bar{D}_{C_{B,C}}(\bar{m}_C) = \bar{D}_{C_{B,C_0}}\frac{\bar{m}_C}{\bar{m}^2_C + \bar{m}^2_{C,1}},\ \bar{D}_{C_{B,B}}(\bar{m}_B) = \bar{D}_{C_{B,B_0}}\frac{\bar{m}_B}{\bar{m}^2_B + \bar{m}^2_{B,1}},$$

$$\bar{D}_{C_{B,Ca}}(\bar{m}_{Ca}) = \bar{D}_{C_{B,Ca_0}}\frac{\bar{m}_{Ca}}{\bar{m}^2_{Ca} + \bar{m}^2_{Ca,1}},$$

$$\bar{C}_{C,max_0} + \bar{C}_{B,max_0} = 1 - \bar{C}_{H,max_0}. \tag{5.22}$$

The non-dimensional boundary and initial conditions are

$$-\bar{D}_{C_C}(\bar{m})\frac{\partial \bar{C}_C}{\partial \bar{x}} = -\bar{D}_{C_H}(\bar{m})\frac{\partial \bar{C}_H}{\partial \bar{x}} = -\bar{D}_{m_C}\frac{\partial \bar{m}_C}{\partial \bar{x}} = -\bar{D}_{m_B}\frac{\partial \bar{m}_B}{\partial \bar{x}} = 0, \tag{5.23a}$$

$$\bar{C}_B = \bar{C}_{B_0},\ \ \bar{n} = \bar{N}_0,\ \ \bar{g}_{HI} = 1,\ \ \bar{g}_{HS} = 0,\ \ \bar{g}_{HM} = 0,\quad \text{at } \bar{x} = 0,$$

$$-\bar{D}_{C_C}(\bar{m})\frac{\partial \bar{C}_C}{\partial \bar{x}} = -\bar{D}_{C_H}(\bar{m})\frac{\partial \bar{C}_H}{\partial \bar{x}} = -\bar{D}_{C_B}(\bar{m})\frac{\partial \bar{C}_C}{\partial \bar{x}} = -\bar{D}_{m_C}\frac{\partial \bar{m}_C}{\partial \bar{x}} = -\bar{D}_{m_B}\frac{\partial \bar{m}_B}{\partial \bar{x}} = 0, \tag{5.23b}$$

$$\bar{n} = 1,\ \ \bar{g}_{HI} = \bar{g}_{HI_2},\ \ -\bar{D}_{g_{HS}}\frac{\partial \bar{g}_{HS}}{\partial \bar{x}} = \bar{\gamma}\bar{g}_{HS},\qquad \bar{g}_{HM} = 0, \text{at } \bar{x} = 1,$$

$$\bar{C}_C = \bar{C}_C^{(0)}\bar{h}(\bar{x}),\ \ \bar{C}_B = \bar{C}_{B_0}\bar{h}_1(\bar{x}),\ \ \bar{C}_H = 0, \tag{5.23c}$$

$$\bar{n} = \bar{N}_0 - (\bar{N}_0 - 1)\bar{x},\ \ \bar{m}_C = \bar{m}_{C,3},\ \ \bar{m}_B = \bar{m}_{B,3},\ \ \bar{m}_{Ca} = 0,$$

$$\bar{g}_{HI} = 1 - (1 - \bar{g}_{HI_2})\bar{x},\ \ \bar{g}_{HS} = \bar{g}_{HM} = 0,\ \ \text{at } \bar{t} = 0, \tag{5.23d}$$

dimensionless parameters	**estimated value**
chondrocyte migration (or diffusion) coefficient $\bar{D}_{C_{C,C_0}} = D_{C_{C,C_0}}/(p_{11_0} C_{total,max_0} d^2)$	10^{-3}
chondrocyte migration (or diffusion) coefficient $\bar{D}_{C_{C,B_0}} = D_{C_{C,B_0}}/(p_{11_0} C_{total,max_0} d^2 \gamma)$	10^{-3}
chondrocyte migration (or diffusion) coefficient $\bar{D}_{C_{C,Ca_0}} = D_{C_{C,Ca_0}}/(p_{11_0} C_{total,max_0} d^2 \Gamma)$	10^{-3}
hypertrophied chondrocyte migration (or diffusion) coefficient $\bar{D}_{C_{H,C_0}} = D_{C_{H,C_0}}/(p_{11_0} C_{total,max_0} d^2)$	10^{-5}
hypertrophied chondrocyte migration (or diffusion) coefficient $\bar{D}_{C_{H,B_0}} = D_{C_{H,B_0}}/(p_{11_0} C_{total,max_0} d^2 \gamma)$	10^{-5}
hypertrophied chondrocyte migration (or diffusion) coefficient $\bar{D}_{C_{H,Ca_0}} = D_{C_{H,Ca_0}}/(p_{11_0} C_{total,max_0} d^2 \Gamma)$	10^{-5}
osteoblast migration (or diffusion) coefficient $\bar{D}_{C_{B,C_0}} = D_{C_{B,C_0}}/(p_{11_0} C_{total,max_0} d^2)$	10^{-6}
osteoblast migration (or diffusion) coefficient $\bar{D}_{C_{B,B_0}} = D_{C_{B,B_0}}/(p_{11_0} C_{total,max_0} d^2 \gamma)$	10^{-4}
osteoblast migration (or diffusion) coefficient $\bar{D}_{C_{B,Ca_0}} = D_{C_{B,Ca_0}}/(p_{11_0} C_{total,max_0} d^2 \Gamma)$	10^{-4}
cartilage matrix diffusion coefficient $\bar{D}_{m_C} = D_{m_C} m_{C,max}/(p_{11_0} C_{total,max_0} d^2)$	0 - 10^{-3}
bone matrix diffusion coefficient $\bar{D}_{m_B} = D_{m_B} m_{C,max}/(p_{11_0} C_{total,max_0} d^2)$	0 - 10^{-5}

nutrient diffusion coefficient $\bar{D}_n = D_n m_{C,max}/(p_{11_0} C_{total,max_0} d^2)$	100
hypertrophy-inducing growth factor diffusion coefficient $\bar{D}_{g_{HI}} = D_{g_{HI}} m_{C,max}/(p_{11_0} C_{total,max_0} d^2)$	2
hypertrophy-suppressing growth factor diffusion coefficient $\bar{D}_{g_{HS}} = D_{g_{HS}} m_{C,max}/(p_{11_0} C_{total,max_0} d^2)$	0.5
hypertrophy-modulating growth factor diffusion coefficient $\bar{D}_{g_{HM}} = D_{g_{HM}} m_{C,max}/(p_{11_0} C_{total,max_0} d^2)$	0.5
chondrocyte proliferation rate $\bar{p}_{5,C_0} = p_{5,C_0}/(p_{11_0} C_{total,max_0}/\tau)$	10^-3
chondrocyte proliferation rate $\bar{p}_{5,B_0} = p_{5,B_0}/(p_{11_0} C_{total,max_0}\gamma)$	10^{-3}
chondrocyte hypertrophic differentiation rate $\bar{p}_6 = p_6 m_{C,max}/(p_{11_0} C_{total,max_0})$	0.1
chondrocyte death rate $\bar{p}_7 = p_7 m_{C,max}/(p_{11_0} C_{total,max_0})$	1
hypertrophied chondrocyte death rate $\bar{p}_8 = p_8 m_{C,max}/(p_{11_0} C_{total,max_0})$	3×10^-2
osteoblast proliferation rate $\bar{p}_{9,C_0} = p_{9,C_0}/(p_{11_0} C_{total,max_0}/\tau)$	10^-3
osteoblast proliferation rate $\bar{p}_{9,B_0} = p_{9,B_0}/(p_{11_0} C_{total,max_0}\gamma)$	10^-3
osteoblast death rate $\bar{p}_{10} = p_{10} m_{C,max}/(p_{11_0} C_{total,max_0})$	0.2
cartilage matrix degradation rate $\bar{p}_{11_1} = p_{11_1} m_{C,max}/p_{11_0}$	1

cartilage matrix degradation rate $\bar{p}_{12_0} = p_{12_0} m_{C,max}/p_{11_0}$	3×10^1
bone matrix production rate $\bar{p}_{13_0} = p_{13_0}/(p_{11_0}\gamma)$	3×10^-2
bone matrix degradation rate $\bar{p}_{13_1} = p_{13_1} m_{C,max}/p_{11_0}$	10^{-3}
nutrient uptake rate by chondrocytes $\bar{p}_{17} = p_{17} m_{C,max}/(p_{11_0} N_1)$	10^4
nutrient uptake rate by osteoblasts $\bar{p}_{18} = p_{18} m_{C,max}/(p_{11_0} N_1)$	10^4
nutrient uptake rate by hypertrophied chondrocytes $\bar{p}_{19} = p_{19} m_{C,max}/(p_{11_0} N_1)$	10^4
calcified cartilage matrix degradation rate $\bar{p}_{20} = p_{20} m_{C,max}/p_{11_0}$	10^{-1}
hypertrophy-suppressing growth factor production rate $\bar{p}_{15} = p_{15} p_{11_0} C_{total,max_0}/(p_{21} p_{23} m_{C,max})$	10
hypertrophy-suppressing growth factor degradation rate $\bar{p}_{22} = p_{22} m_{C,max})/(p_{11_0} C_{total,max_0})$	0
hypertrophy-modulating growth factor degradation rate $\bar{p}_{24} = p_{24} m_{C,max})/(p_{11_0} C_{total,max_0})$	1
hypertrophy-modulating growth factor degradation rate $\bar{p}_{23}$	0
hypertrophy-suppressing growth factor degradation rate $\bar{p}_{21}$	1
maximum mature chondrocyte density $\bar{C}_{H,max_0} = C_{H,max_0}/C_{total,max_0}$	0-1

maximum osteoblast density $\bar{C}_{B,max_0} = C_{B,max_0}/C_{total,max_0}$	0-1
initial chondrocyte density $\bar{C}_C^{(0)} = C_C^{(0)}/C_{total,max_0}$	0.25
initial nutrient concentration $\bar{N}_0 = N_0/N_1$	1-3
threshold nutrient concentration $\bar{n}_0 = n_0/N_1$	0.24-0.81
critical nutrient concentration $\bar{n}_1 = n_1/N_1$	0.1
critical matrix density $\bar{m}_{C,crit} = m_{C,crit}/m_{C,max}$	0.95
matrix density $\bar{m}_{C,1} = m_{C,1}/m_{C,max}$	0.1
matrix density $\bar{m}_{Ca,1} = m_{Ca,1}/m_{Ca,max}$	0.1
matrix density $\bar{m}_{C,2} = m_{C,2}/m_{C_{tot},max}$	0.1
matrix density $\bar{m}_{B,1} = m_{B,1}/m_{B,max}$	10^{-2}
matrix density $\bar{m}_{B,2} = m_{B,2}/m_{B,max}$	10^{-2}
initial cartilage matrix density $\bar{m}_{C,3} = m_{C,3}/m_{C,max}$	10^{-5}
initial bone matrix density $\bar{m}_{B,3} = m_{B,3}/m_{B,max}$	10^{-5}
threshold hypertrophy-inducing growth factor concentration $\bar{g}_{HI_0} = g_{HI_0}/g_{HI_1}$	0.5
threshold hypertrophy-suppressing growth factor concentration $\bar{g}_{HS_0} = g_{HS_0}p_{11_0}/(p_{15}m_{C,max})$	2-4
initial hypertrophy-inducing growth factor concentration $\bar{g}_{HI_2} = g_{HI_2}/g_{HI_1}$	1
initial osteoblast cell density $\bar{C}_{B_0} = C_{B_0}/C_{total,max_0}$	10^{-2}
maximum cartilage matrix density $\beta = m_{C,max}/m_{max}$	0.04
maximum bone matrix density $\eta = m_{B,max}/m_{max}$	0.48
exponent α	2

Table 5.2: Estimated values of dimensionless parameters.

5.3 Results and parameter sensitivity analysis

5.3.1 Methods

We use a second order accurate finite difference discretisation scheme to discretise the spatial variable x in Eqs. (5.21)-(5.23), keeping the time derivative t continuous. The resulting ordinary differential equations are solved in MATLAB (Release 2013a, The MathWorks, Inc., Natick, Massachusetts, United States) using the stiff ODE solver *ode15s*. The dimensionless parameters and their estimated values are provided in Table 5.2. The initial chondrocyte cell density spatial profile is $\bar{C}_C(x,0) = \bar{C}_C^{(0)}[1-\tanh(A(\bar{x}-\bar{x}_0))]/2$, with $A = 10^4$ and $\bar{x}_0 = 0.1$. Additionally, the initial bone cell density spatial profile is $\bar{C}_B(x,0) = \bar{C}_B^{(0)}[1-\tanh(A(\bar{x}-\bar{x}_1))]/2$, with $A = 10^4$ and $\bar{x}_1 = 10^{-3}$.

We simulate the evolution of chondrocytes, C_C, hypertrophied chondrocytes, C_H, bone cells, C_B, cartilage matrix, m_C, calcified matrix, m_{Ca}, bone matrix, m_B, and nutrients, n, along with growth factors (not shown here). Initially we have a population of chondrocytes, $\bar{C}_{C^{(0)}}$, implanted at the bottom of the defect at the subchondral bone interface ($x = 0$), corresponding to an ACI procedure [21, 22, 119]. We also include a small density of bone cells, $\bar{C}_{B^{(0)}}$, assumed already present in the defect.

5.3.2 Numerical results

Figs 5.3-5.5 show the evolution of osteochondral defect healing following an ACI procedure, for times ranging between 1 month and 36 months.

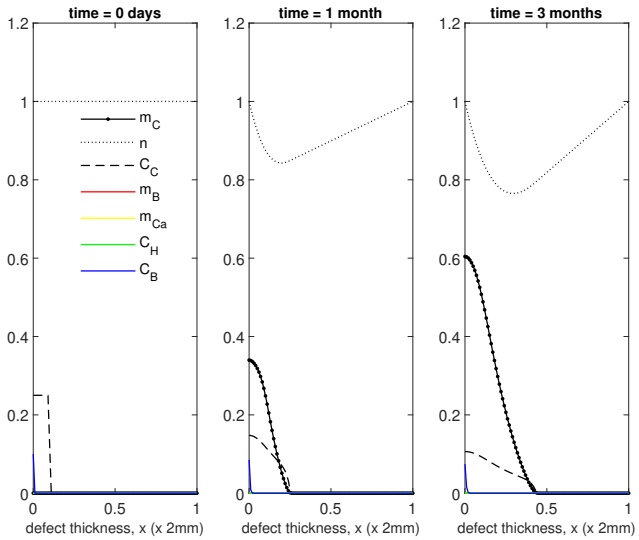

Figure 5.3: Evolution of cell and matrix densities, and nutrient concentration at times t =0 days, 1 month and 3 months following implantation of chondrocytes. $x = 0$ in the figure represents the location of the base of the defect, $x = 1$ represents the surface of articular cartilage.

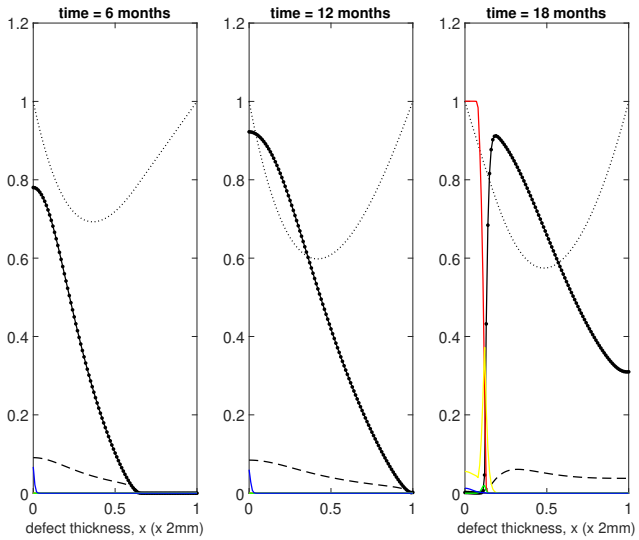

Figure 5.4: Evolution of cell and matrix densities, and nutrient concentration at times t =6, 12 and 18 months following implantation of chondrocytes. $x = 0$ in the figure represents the location of the base of the defect, $x = 1$ represents the surface of articular cartilage.

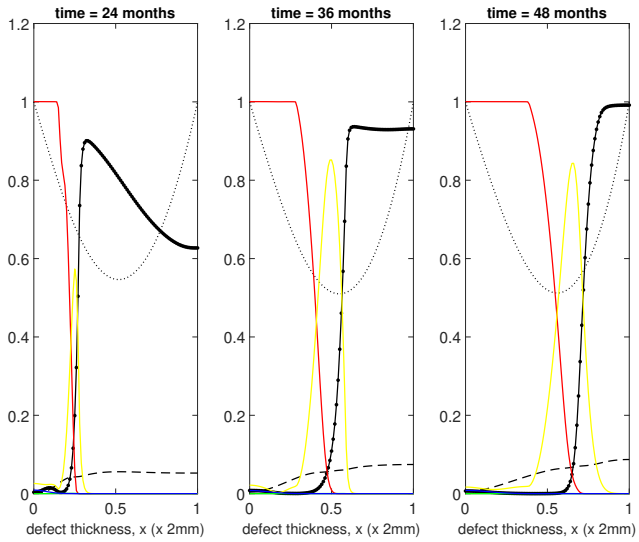

Figure 5.5: Evolution of cell and matrix densities, and nutrient concentration at times t =24, 36 and 48 months following implantation of chondrocytes. $x = 0$ in the figure represents the location of the base of the defect, $x = 1$ represents the surface of articular cartilage.

As early as 1 month chondrocytes produce cartilage matrix and migrate towards the top of the defect, limited by low diffusivity through the cartilage matrix and low chondrocyte proliferation ($\bar{p}_{5_{c0}} = 0.012$ [119]). By 3 months cartilage matrix continues to form towards the top, having covered over half of the defect depth. The results replicate those from our earlier chondral healing studies [119], except that cartilage is deposited at a much faster rate due to higher availability of nutrients [119].

At 6 months, cartilage matrix is steadily filling from the base of the defect. As time continues to 12 months, we can see that the defect continues to fill, with new cartilage matrix having now reached the top of the defect and a density close to the maximum at the bottom (Fig 5.4, Panel 2). The critical cartilage density is attained at the bottom of the defect at $t =$ 18 months, beyond which chondrocytes here start to hypertrophy enabling cartilage matrix to be converted into calcified matrix (Fig 5.4, Panel 3). We observe that cartilage matrix at the bottom of the defect has been converted entirely into calcified matrix (yellow), and bone

matrix (red).

At 24 months chondrocytes higher up in the defect are undergoing hypertrophy and converting cartilage matrix into calcified matrix. The bottom of the defect is now completely filled with bone, with a middle calcified zone and a top layer of cartilage that has not yet fully formed across the top of the defect. Now that bone matrix has been formed in the defect, osteoblast cells migrate within this matrix towards the top of the defect, further enhancing the production of bone. At 36 months we observe that the bottom half of the defect is completely filled with bone. In the mid-zone of the defect endochondral ossification continues to occur, with cartilage being remodelled into calcified matrix, to be converted into bone in the region where bone cells are present. At the top of the defect there is a section of cartilage that has not calcified due to a flux of hypertrophy-suppressing growth factor permeating in from the top of the defect. In this zone, chondrocyte hypertrophy is suppressed, and consequently endochondral ossification does not occur. At 36 months the defect is almost entirely full of matrix, whether bone, calcified or cartilage. As time progresses to 48 months the defect is now entirely filled with bone and cartilage matrix, with a thin calcified matrix layer in-between.

Convergence analysis

A convergence analysis has been performed in space, x, as within Chapter 3, with results showing the numerical scheme is reliable. For the simulations shown above the numerical scheme is performed over $n = 100$ grid points. Increasing n by a factor of 10 results in a slower runtime in the ODE15s solver, with the solution path unchanged. Convergence in time has also been explored, with a steady state obtained where the constituents of the regenerated defect remain full (at 1), with the cartilage layer remaining at the top and bone below.

5.3.3 Sensitivity of parameters and initial conditions

The model has several parameters, and its solution could be particularly sensitive to some changes, potentially indicating their biological significance. In addition, some parameter values were approximated because their exact value could not be found. If the solution is not sensitive to change in value of these parameters, then the approximate value is a good representation of that parameter. Here we will present a sensitivity analysis on parameters deemed to be significant to the model, based on extensive simulations varying each parameter while keeping the others fixed. This allows us to focus specifically on the sensitivity of any parameters related to growth factors, hypertrophied chondrocytes, and the critical cartilage density, $\bar{m}_{C_{crit}}$, triggering endochondral ossification. We focus on these parameters due to their significant role in the regulation of the stages associated with endochondral ossification and subsequent bone production, and overall defect healing.

Parameters	Sensitivity description
Hypertrophy-suppressing growth factor diffusion coefficient, $\bar{D}_{g_{HS}}$	See details in text.
Hypertrophy-suppressing growth factor degradation rate, $\bar{p}_{22}$	Increasing $\bar{p}_{22}$ by a factor or 10 at t=36 months results in increased $\bar{m}_B$ and also increased levels of $\bar{C}_H$, with a clear trade-off visible between $\bar{C}_C$ and $\bar{C}_H$. There appears to be lower levels of $\bar{m}_{Ca}$ due to increased conversion of $\bar{m}_{Ca}$ to $\bar{m}_B$. At t=48 months the entire defect is filled with bone and calcified matrix, indicating the defect will fill entirely with bone due to high suppressing growth factor degradation. Decreasing $\bar{p}_{22}$ by a factor of 100 significantly impacts chondrocyte hypertrophy, with no $\bar{C}_H$ visible in the defect and cartilage remaining full with no conversion to $\bar{m}_{Ca}$. This is due to extremely high levels of $\bar{g}_{HS}$ in the defect as there is no degradation, suppressing the entire endochondral ossification process.
Hypertrophy-inducing growth factor degradation rate, $\bar{p}_{25}$	Increasing or decreasing $\bar{p}_{25}$ resulted in no significant change in simulations, indicating our boundary condition of $\bar{g}_{HI} = 1$ at $x = 0$ is high enough to induce hypertrophy, as $\bar{g}_{HI_0}$ is smaller than 1 and $\bar{g}_{HI}$ is always high at the base of the defect, where calcification is initiated.

Hypertrophy-modulating growth factor degradation rate, $\bar{p}_{23}$	Increasing $\bar{p}_{23}$ to 0.1 and 1 from 0 resulted in marginally higher $\bar{m}_{Ca}$ levels at t=18 months and minimal differences in simulations thereafter. $\bar{p}_{23} = 1$ increases chondrocyte hypertrophy noticeably, with a clear conversion of $\bar{C}_C$ to $\bar{C}_H$ at the base of the defect. $\bar{p}_{23} = 0.1$ has a more subtle effect, with a small increase in $\bar{m}_{Ca}$ at the base of the defect at this time point.
Hypertrophied chondrocyte production rate, $\bar{p}_6$	Increasing $\bar{p}_6$, the hypertrophied chondrocyte production rate, by a factor of 100 resulted in little difference at t=2 years or thereafter, with a visible increase in $\bar{m}_{Ca}$ due to higher $\bar{C}_H$, but as healing evolution is primarily dictated by cell migration and matrix production, cartilage is not degraded sooner nor bone formed faster. Decreasing $\bar{p}_6$ by a factor of 100 results in slower endochondral ossification evident by less $\bar{m}_{Ca}$, less cartilage degradation and less bone at t=2 years. This effect slows down the progression of healing within the defect thereafter.

Hypertrophied chondrocyte degradation rate, $\bar{p}_8$	Increasing $\bar{p}_8$ by a factor of 10 results in slightly higher bone density at the base by t=24 months, with $\bar{m}_{Ca}$ produced towards the top of the defect faster. This will be due to $\bar{C}_H$ reducing faster, meaning $\bar{g}_{HM}$ and $\bar{g}_{HS}$ levels are lower, meaning $\bar{g}_{HI}$ is higher and able to induce hypertrophy in more chondrocytes towards the top of the defect, allowing conversion of calcified cartilage to occur here. At 3 years there is cartilage remaining in the defect where bone should be produced due to low $\bar{C}_H$ levels, resulting in less conversion of $\bar{m}_C$ to $\bar{m}_{Ca}$. Decreasing $\bar{p}_8$ results in lower $\bar{m}_B$ at the bottom of the defect and a higher localised concentration of $\bar{m}_{Ca}$, with a higher peak observed between bone and cartilage matrix populations. There is also a larger concentration of $\bar{m}_{Ca}$ at the bottom of the defect and a larger concentration of chondrocytes.
Bone cell proliferation rate, $\bar{p}_9$	Decreasing $\bar{p}_9$ results in marginally lower bone matrix at 24 months, though effects of direct bone production are minimal due to $\bar{p}_{130}$ & $\bar{p}_{131}$ having low values as the model primarily focuses on the endochondral ossification pathway. Increasing $\bar{p}_9$ significantly increases the bone cell population, though bone matrix does not increase as $\bar{m}_B$ is bounded by $\bar{m}_{B_{max}}$, meaning $\bar{m}_B$ cannot surpass 1.

Calcified matrix production rate (from cartilage), $\bar{p}_{12}$	Increasing $\bar{p}_{12}$ by a factor of 10 leads to a sharp increase in $\bar{m}_{Ca}$ production and $\bar{m}_C$ degradation at t=2 years, while bone production remains relatively unchanged, with only a minor increase observed at the base of the defect. Decreasing $\bar{p}_{12}$ leads to very low $\bar{m}_{Ca}$ levels, with less cartilage degradation. As the $\bar{m}_{Ca}$ conversion to $\bar{m}_B$ pathway is unaffected by varying $\bar{p}_{12}$, bone levels remain fairly consistent despite $\bar{m}_{Ca}$ levels varying greatly.
Bone matrix production rate (from calcified matrix), $\bar{p}_{20}$	Increasing $\bar{p}_{20}$ enhances bone production, resulting in lower $\bar{m}_{Ca}$, as bone remodelling is increased. Decreasing $\bar{p}_{20}$ resulted in higher $\bar{m}_{Ca}$ and lower bone matrix levels as remodelling is decreased as a result of lower bone matrix production.
Hypertrophy-inducing growth factor critical concentration, $\bar{g}_{HI_0}$	Increasing $\bar{g}_{HI_0}$ by a factor of 10 results in no $\bar{m}_{Ca}$ production at t=18 months. This indicates chondrocyte hypertrophy has been stopped due to $\bar{g}_{HI_0}$ being significantly greater than $\bar{g}_{HI}$. Increasing $\bar{g}_{HI_0}$ inhibits $\bar{C}_H$ production which is the expected effect. Decreasing $\bar{g}_{HI_0}$ does not alter simulations, which is expected as the threshold of unchanged $\bar{g}_{HI_0}$ is relatively low, so lowering it further will not have a significant impact on the outcome of the model.
Hypertrophy-suppressing growth factor critical concentration, $\bar{g}_{HS_0}$	See details in text.

Critical cartilage density, $\bar{m}_{C_{crit}}$	See details in text.

Table 5.3: Sensitivity of parameters. Those highlighted in bold are further described in the text.

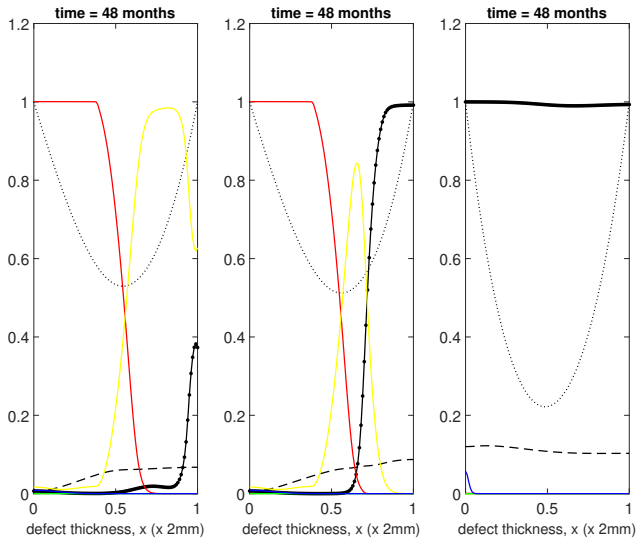

Figure 5.6: Sensitivity of hypertrophy-suppressing growth factor diffusion coefficient, $D_{g_{HS}}$ at t=48 months, following implantation of chondrocytes, with Panel 1 decreased $D_{g_{HS}}$, Panel 2 normal $D_{g_{HS}}$ and Panel 3 increased $D_{g_{HS}}$. $x = 0$ in the figure represents the location of the base of the defect, $x = 1$ represents the surface of articular cartilage.

Decreasing $\bar{D}_{g_{HS}}$ by a factor of 100 decreases the layer of cartilage remaining at the top of the defect. At 4 years the defect is almost entirely either bone or calcified matrix, with calcified matrix having reached the top of the defect. This suggests that the hypertrophy-suppressing growth factor is no longer inhibiting endochondral ossification due to not being able to diffuse further into the defect (Fig. 5.6, Panel 1). Conversely, the defect is entirely cartilage when $\bar{D}_{g_{HS}}$ is increased by a factor of 100, suppressing the entire endochondral ossification process, resulting in purely chondral healing (Fig. 5.6, Panel 3).

Decreasing the suppressing growth factor threshold concentration, $\bar{g}_{HS_0}$, to 10^{-4} slowed cartilage degradation at 3 years, and hence decreased $\bar{m}_{Ca}$ and $\bar{m}_B$ production (Fig. 5.7, Panel 1). Decreasing $\bar{g}_{HS_0}$ is expected to suppress chondrocyte hypertrophy, hence slowing down cartilage degradation to calcified cartilage and bone production.

Increasing $\bar{g}_{HS_0}$ activates hypertrophy much sooner, explaining the sudden jump in $\bar{m}_{Ca}$ pro-

duction and increase in $\bar{C}_H$ (Fig. 5.7, Panel 3). The increase of $\bar{g}_{HS_0}$ to 1 leads to triggering this pathway much sooner, meaning there is no suppression, resulting in chondrocyte hypertrophy occurring sooner.

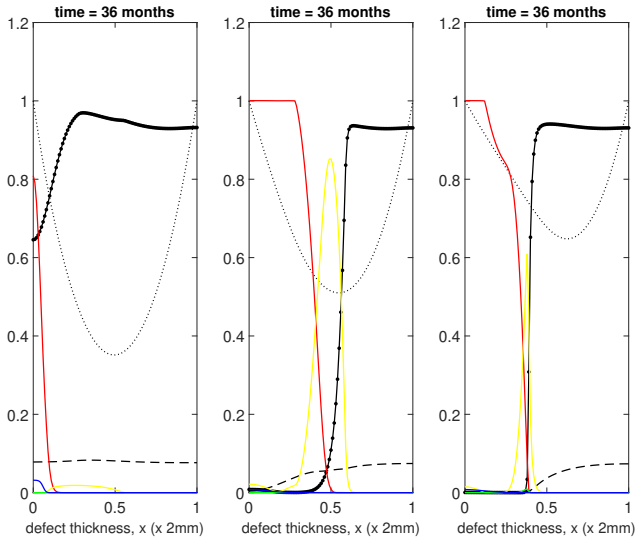

Figure 5.7: Sensitivity of hypertrophy-suppressing growth factor critical concentration, $\bar{g}_{HS_0}$ at t=3 years, following implantation of chondrocytes, with Panel 1 decreased $\bar{g}_{HS_0}$, Panel 2 normal $\bar{g}_{HS_0}$ and Panel 3 increased $\bar{g}_{HS_0}$. $x = 0$ in the figure represents the location of the base of the defect, $x = 1$ represents the surface of articular cartilage.

Increasing $\bar{g}_{HS_0}$ to 1 increased $\bar{m}_{Ca}$ production, with higher levels of chondrocyte hypertrophy at the bottom of the defect with a visible replacement of $\bar{C}_C$ with $\bar{C}_H$ observable (Fig. 5.7, Panel 3).

Decreasing the critical cartilage density, $m_{C_{crit}}$, from 95% to 80% to activate chondrocyte hypertrophy results in early calcified matrix and bone formation, but does not significantly impact healing time.

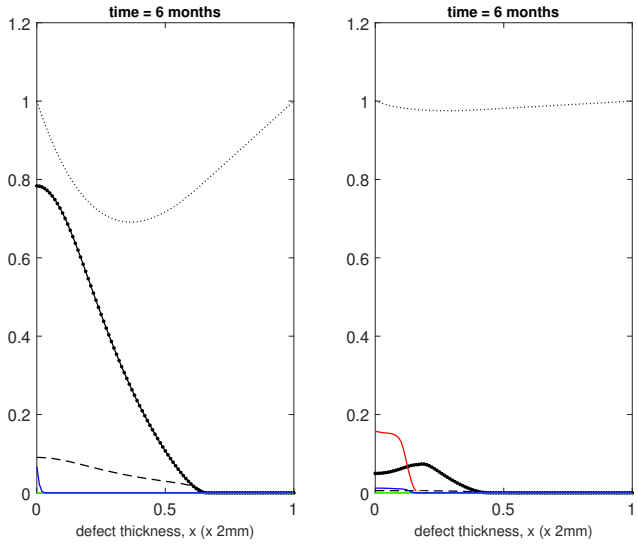

Figure 5.8: Sensitivity of the critical cartilage density at t=6 months, following implantation of chondrocytes, with Panel 1 normal critical cartilage density (95%) and Panel 2 decreased critical cartilage density (10%). $x = 0$ in the figure represents the location of the base of the defect, $x = 1$ represents the surface of articular cartilage.

Decreasing the critical density $m_{C_{crit}}$ to 10%, however, results in no initial cartilage fill of the defect as expected to occur from description in the literature, with chondrocytes undergoing hypertrophy as soon as $\bar{g}_{HI}$ levels are high enough and $\bar{g}_{HS}$ levels are low enough (Fig. 5.8 Panel 2, shown at 6 months). Bone formation begins almost immediately and chondrocyte proliferation is suppressed as C_C proliferation in bone matrix, $\bar{p}_{5_{b0}}$, is lower than in cartilage matrix, $\bar{p}_{5_{c0}}$. Additionally, chondrocyte migration in bone matrix, $\bar{D}_{C_{B0}}$ is lower than in cartilage matrix. This significantly decreases healing evolution, indicating the initial cartilage formation stage we have included in our model is required to achieve the sequential type of healing process described by [120].

5.4 Summary & conclusions

We have constructed a one-dimensional mathematical model to depict the various processes occurring during osteochondral defect healing after autologous chondrocyte implantation (ACI). Our model has successfully simulated healing via endochondral ossification, the process of an initial fill of cartilage remodelling into bone, whilst also successfully achieving the layer of cartilage remaining at the top of the defect.

The model reproduces several healing characteristics seen in animal models and clinical studies. Lydon *et al.* [120] first observe cartilage formation to occur along the edges of the defect, with cartilage then filling the defect inwards and upwards from the base. Endochondral ossification is also observed to first occur at the base of the defect, with bone formation continuing upwards towards the top of the defect, which our model achieves. Our results indicate the osteochondral defect fills with regenerative tissue, comprised of bone, calcified matrix and cartilage matrix, by 2 years, which other treatment strategies of osteochondral defects indicates to be a reasonable time-scale [18].

Chapter 6

Discussion

The main achievements of the work undertaken in this thesis have been the formulation of mathematical models of cartilage and bone defect regeneration after cell implantation. Specifically, the inclusion of growth factors and a co-implantation procedure for chondral defect regeneration, and a novel mathematical model for osteochondral defect regeneration under the assumption these defects heal via endochondral ossification. These models have successfully simulated chondral and osteochondral defect regeneration characteristics as described in the literature. Here we discuss the findings of chapters 3, 4 and 5, detailing the implications of the models and how the work undertaken in this thesis can be continued with.

6.1 Summary and conclusions

6.1.1 Chapter 3

The primary aim of this chapter was to formulate a mathematical model of cartilage regeneration following cell implantation, focusing on the effects of growth factors to see if a

trophic effect on the system can be replicated as shown *in vitro* [184]. Chondrocytes and mesenchymal stem cells are implanted into chondral defects in the hope to promote cartilage regeneration. MSCs are inserted to differentiate into chondrocytes, leading to a cell implantation scenario where we have 2 populations of cells (chondrocytes and MSCs) in the defect at any one time. The interaction between MSCs and chondrocytes is well documented in the literature, with studies hypothesising a trophic effect observed as a result of their co-implantation into chondral defects, thought to be due to the release of growth factors such as FGF-1 and BMP-2 [184]. The aim of this chapter was to include the effects of these growth factors on a pre-existing mathematical model of cartilage regeneration, where an articular stem cell implantation (ASI) procedure is undertaken, where MSCs are inserted into a chondral defect [119]. The inclusion of these growth factors was to recreate the hypothesised trophic effect observed at early times *in vitro* [184].

The model considered two cell types, mesenchymal stem cells and chondrocytes, and as a result studied the actions of the two growth factors within these bounds. However, it is important to acknowledge that these growth factors probably also play a role within cartilage defect regeneration beyond these two cell types. Aside from promoting chondrogenic differentiation of MSCs, BMP-2 can also cause chondrocytes to undergo hypertrophy and lead to endochondral bone formation. FGF-1, along with other members of the fibroblast growth factor family, is thought to enhance collagen I expression resulting in fibro-cartilage formation during the chondral healing process. It is thought that when FGF-1 and BMP-2 are both present during the regeneration process, chondrocyte hypertrophy and fibro-cartilage formation is not observed in the defect, indicating that FGF-1 suppresses chondrocyte hypertrophy and BMP-2 inhibits the formation of fibro-cartilage [184]. These functions indicate that both growth factors are involved in adverse aspects of the healing process that we did not consider

in this model, specifically chondrocyte hypertrophy and endochondral ossification. In further work, we could extend our model to study these effects. However, chondrocyte hypertrophy and endochondral bone formation have not been flagged as adverse effects after autologous stem cell or chondrocyte implantation to treat chondral defects, suggesting that with respect to the clinical application of these therapies our model may be considered representative [141].

Our model allowed us to investigate the influence of either growth factor, independent of the other. This allowed us to determine the sensitivity of the MSC-chondrocyte interaction to either FGF-1, BMP-2 or both. The results obtained when including only BMP-2 were very similar to those including both FGF-1 and BMP-2, with cases both showing clearly increased matrix production at early time points. On the other hand, for the case where only FGF-1 was included the matrix density levels at early times were increased only marginally when compared to the baseline case of no growth factors. This suggests that BMP-2 dominates the interaction and that the main positive effect of a co-implantation of the two cell types is due to enhanced chondrogenesis.

Our model found that the influence of chondrocytes on stem cell differentiation through the release of BMP-2 affected the result more than the influence of stem cells on chondrocyte proliferation via FGF-1. This may be related to the effects of nutrient concentration in our model, which did influence chondrocyte proliferation but did not directly influence stem cell differentiation, though a knock on effect would be expected from nutrient's limiting effect on stem cell proliferation, but we would not expect this effect to be significant in our simulations due to a 100% MSC cell seeding. The lack of influence of FGF-1 could potentially indicate the initial growth factor concentration and rates we have obtained from the literature are con-

tentious, but our sensitivity analysis indicates these parameters are not sensitive to change. This allows us to make the assumption our parameters are within a realistic biological range of which FGF-1 is effective. In our model, low nutrient concentration (hypoxia) reduced or, if below the threshold nutrient concentration, completely stopped chondrocyte proliferation. We think this may explain why the effects of FGF-1 were relatively small, as in all of our simulations the nutrient concentration seems to be the main limiting factor of cartilage regeneration. The nutrient concentration in our model influences chondrocyte proliferation and has been demonstrated experimentally [196]. In contrast, stem cell differentiation was not affected by nutrient concentration in our model, and as a result a low nutrient concentration did not constrain the effects of BMP-2. We are not aware of experimental studies addressing adverse effects of nutrition on mesenchymal stem cell *differentiation* into chondrocytes, but one study extensively addressed this issue related to osteoblast differentiation [65]. This study concluded that during 3D micromass culture, a scenario comparable to the one in our model, osteoblast differentiation was not affected by nutrition but was a function of cell-cell contacts and cell-cell communication, exactly the mechanism we included in our model.

The influence of BMP-2 on stem cell differentiation was implemented through a lowering of the threshold stem cell density C_{S_0} as a function of BMP-2 concentration. An alternative implementation would be through the stem cell differentiation rate, in a manner similar to our implementation of the influence of FGF-1 on chondrocyte proliferation. We compared both approaches in a sensitivity study and found no clear differences between them. In our sensitivity analysis we found $p_{12}, p_{13}, C_{S0_{min}}$, and α to be the most sensitive parameters in our model, which is discussed in detail in the section on 3.3.2 *Sensitivity of parameters and initial conditions*. Despite a handful of our variables being approximated, our sensitivity indicates these parameters are not significantly sensitive to change, indicating our values are

a good representation of the parameter values we needed for the model but could not find data for.

Our model used two specific growth factors, BMP-2 and FGF-1, to investigate the interactions between mesenchymal stem cells and chondrocytes during cartilage repair following a cell implantation procedure. However, we should stress that our results are not limited to these two. We see these two growth factors as examples of how such interactions could occur. For instance, some experiments have found evidence that the influence from chondrocytes on stem cell differentiation acts via direct cell-cell contact instead of through soluble factors, or that other growth factors might be involved [184]. A similar situation exists in relation to the influence of stem cells on chondrocyte proliferation. Nevertheless, whatever the precise mechanism through which the interaction occurs, the main aspect will always be that chondrocytes influence stem cell differentiation and stem cells influence chondrocyte proliferation. Although our model may therefore not capture all details of this mechanism, it captures the essence of the interaction between the two cell types and we believe its broad conclusions are still relevant if specific details of the growth factors involved may be fallacious.

The model proposed in this chapter enables us to better understand the underlying mechanisms taking place during chondral healing when we consider the effects of growth factors. This model can be used as an informative tool for clinicians and experimentalists alike, giving insight into the effects of the growth factors FGF-1 and BMP-2 on chondrocyte proliferation and mesenchymal stem cell differentiation. This work provides insight regarding the clinical significance of the mechanisms involved in the FGF-1-BMP-2 feedback loop without requiring experimentation, also enabling us to identify with ease the most effective growth factor in our

model. Our sensitivity analysis demonstrates increasing FGF-1 and BMP-2 will have minor effect due to limiting factors such as nutrient concentration and growth factor degradation. Our results also provide verification for experimental work already undertaken [184].

6.1.2 Chapter 4

In this chapter we continue with the model formulated in Chapter 3, and alter the implantation ratio to simulate a co-implantation procedure, where MSCs and chondrocytes are implanted into a chondral defect after they have been cultured together *in vitro*. The aims of this procedure is to alleviate the need for chondrocyte harvest when a cell implantation procedure is undertaken to heal a chondral defect, which is often problematic due to low volumes of chondrocytes in the human body and tendency for site morbidity. Culturing with MSCs means less chondrocytes are required for implantation, with the implanted MSCs intended to differentiate into chondrocytes to make-up cell numbers. Additionally, this approach is hypothesised to regenerate cartilage on a better time-scale due to high cell-to-cell interaction releasing growth factors, with the aim of this chapter to replicate this effect specifically [184].

Our model enabled us to compare matrix densities following co-implantation of MSCs and chondrocytes at various ratios, visualising not only the cartilage matrix density distribution at any time point, but also investigating how the concentrations of MSCs, chondrocytes and nutrients change within the defect in response to different co-implantation ratios. The five ratios we focused on were 90% MCSs plus 10% chondrocytes, 70% MSCs plus 30% chondrocytes, 50% MSCs plus 50% chondrocytes, 30% MSCs plus 70% chondrocytes and 10% MSCs plus 90% chondrocytes, with 90:10 and 50:50 having been or are being investigated clinically [44, 154]. We compared these to autologous chondrocyte implantation (ACI, 100%

chondrocytes) and articular stem cell implantation (ASI, 100% MSCs). When comparing co-implantation scenarios with the ACI and ASI results from previous work and Chapter 3 [119, 21], it is clear that a mixture of MSCs and chondrocytes delivers the desired effect of increased matrix deposition, as hypothesised in the literature [78] and in previous experiments [184]. This effect is especially significant during the first few months following cell implantation, but from around six months onwards the differences, especially with ASI, become small. As time progresses, the 0:100 case continues to produce matrix at a steady rate, but the 100:0 and co-implantation cases soon surpass these levels. Figure 4.18(a) shows how total matrix levels of 100:0 (ASI), 90:10, 10:90 and 0:100 (ACI) simulations compare at over a period of 2 years. At early time there is a monotonic increase in the total matrix density with the 0:100 case having the highest density, 100:0 having produced almost no matrix at all, and the co-implantation cases having almost similar intermediate levels of matrix. This indicates that at early time chondrocyte proliferation balanced with adequate nutrient availability is the main identifiable mechanism responsible for the formation of new cartilage in our model. As time progresses, 0:100 continues to produce matrix at a steady rate, but 100:0 and co-implantation cases soon surpass these levels. Beyond 6 months there is a non-monotonic increase in the total matrix density with a peak in matrix levels in the co-implantation cases, and the 100:0 case still producing the lowest level of matrix. Although we cannot say with any certainty that the maximum matrix density is obtained precisely for the 10:90 or 90:10 case, there is a definite optimal ratio of stem cells and chondrocytes that can produce maximum matrix at intermediate times. This indicates that at these times cell differentiation and diffusion are the dominant mechanisms driving new cartilage formation. From six months onwards, we found little difference in the distribution of cell types and cartilage matrix between the five co-implantation cases and implanting only stem cells. This suggests that implanting a cell population that includes stem cells will lead to a stable solution path, regardless of the

exact proportion of stem cells. Although co-implantation of chondrocytes and stem cells led to more matrix deposition at earlier time points, this difference was not maintained and by 12 months the difference in matrix production between the five cases was very small. Similar small differences have been found between 1-year biopsies obtained in human trials of co-implanted cells, stem cells or chondrocytes [44, 141]. Nevertheless, the larger matrix deposition at earlier time may give advantages with respect to the rehabilitation, which could be faster if matrix is formed earlier. This alone could be an important clinical advance in the treatment of articular cartilage damage.

Figure 4.18 shows the overall cell and matrix densities for Articular Stem Cell Implantation (ASI, 100:0), Autologous Chondrocyte Implantation (ACI, 0:100) and 10:90 and 90:10 mesenchymal stem cell and chondrocyte co-implantation cell therapy. It is clear from these results that a co-implantation of mesenchymal stem cells and chondrocytes enhances healing, most notably within the first 12 months, due to the effects of growth factors and the more efficient utilisation of nutrients between the 2 cell types. We find that ASI initiates healing at a slower rate due to no implanted chondrocytes, meaning cells must first uptake large concentrations of nutrients before healing can be initiated [21]. ACI typically starts well, with good levels of matrix in the defect within the first few months, but the rate of matrix deposition is extremely steady and achieves the slowest healing time [119]. Our co-implantation cases begin matrix deposition almost immediately, initiated by the implanted chondrocytes, leaving the remaining MSC population to proliferate and differentiate. This leads to the highest chondrocyte, MSC and matrix densities at 3 months, despite our other 2 therapies having higher densities of each cell type implanted into the defect.

These results indicate that nutrient availability within the defect and cell motility is highly important. When nutrients fall below the critical condition in our model, cells must diffuse to areas of higher nutrient concentrations to continue proliferation and differentiation. Despite ACI never having low nutrient levels (Lutianov *et al.* [119]), it does not achieve fast healing, typically taking 24 months to fill the defect with new cartilage. This is due to chondrocytes diffusing slower than MSCs, meaning the ASI procedure, despite having a very slow start, can achieve a good rate of healing as time continues as cells are able to diffuse to higher concentrations of nutrients at a faster rate, and also are able to proliferate quicker. Our co-implantation cases are able to deposit matrix well at early times, due to implanted chondrocytes, and at late times, due to MSCs, meaning a co-implantation cell therapy embodies the good qualities of both procedures, and even results in enhanced matrix deposition due to FGF-1 and BMP-2 being released via cell-to-cell interaction [21].

A mixture of stem cells and chondrocytes produces more consistent levels of matrix due to the balance of nutrient used between the two cell types and the release of important growth factors that influence chondrocyte proliferation and stem cell differentiation. In our model, this effect is partly due to the cell-cell interactions between MSCs and chondrocytes, releasing growth factors such as FGF-1 and BMP-2 that cause an increase in matrix deposition from increased chondrocyte proliferation and enhanced chondrogenesis (see also Wu *et al.* [184]). Additionally, the increase of matrix deposition and chondrocyte density at early times for our co-implantation cases is in part due to the lower proliferation rate of chondrocytes, allowing more nutrients to be available in the defect for MSC proliferation and differentiation.

An important assumption in our model concerns the role of chondrogenesis, the differentia-

tion of stem cells into chondrocytes. Our results suggest that stem cell differentiation plays an important part in increasing the number of chondrocytes, and eventually the extracellular matrix, due to large quantities of chondrocytes, comparable to our 50:50 case, being present in the defect when 90% MSCs are implanted. Most *in vitro* co-culture studies suggest that the more important contribution from the stem cells is their positive effect on chondrocyte proliferation whereas their differentiation into chondrocytes is less important [41].

6.1.3 Chapter 5

In this chapter we formulate a mathematical model of osteochondral defect regeneration after chondrocyte implantation that simulates key processes occurring during the repair of an osteochondral defect after autologous chondrocyte implantation (ACI). Our model achieved this by simulating the key stages of natural cartilage healing as observed in a large animal experiment [120], namely the process of an initial fill of the defect by cartilage, followed by a process of endochondral ossification starting at the bottom of the defect that resulted in bone formation at this location, eventually leaving a layer of articular cartilage remaining at the top of the defect separated from the bone by a thin layer of calcified cartilage. Our model thus gives an answer to the question how an osteochondral defect, which is treated by injecting a solution containing chondrocytes under a patch covering the defect, can heal such that both bone and cartilage are reconstituted.

In formulating our mathematical model, we made extensive use of the insights from a series of experiments based around an ovine model of natural osteochondral defect healing in skeletally mature animals [120]. We did so for two main reasons. Firstly, a sheep is a relatively large animal with a knee anatomy comparable to that of humans, which makes the animal model

closer to the clinical situation than for instance murine or laprine models [1] [30]. Secondly, Lydon *et al.* [120] analysed 5 separate time points (1-2 weeks, 4-8 weeks, 8-12 weeks, 18 weeks and 26 weeks). Such a detailed study of a healing process over time is not uncommon when conducted using small animals (see Shapiro *et al.* 1993 [161] or Anraku *et al.* 2008 [4]) but is unique when conducted in large animals. Of course, we realise that the process by which a freshly created osteochondral defect heals naturally is not necessarily the same as that by which a clinical osteochondral defect in humans, treated using autologous chondrocytes, heals. Nevertheless, key stages observed during the natural healing process of osteochondral defects are also seen following chondrocyte implantation. Filling of the complete defect by cartilage or cartilage-like tissue before bone starts to form at the bottom of the defect has been observed in large-animal experiments (i.e. Munirah *et al.* 2007 [136] and Jurgens *et al.* 2013 [87]). After one year, osteochondral defects up to 1 cm deep in humans and treated with ACI demonstrate new bone formation at the bottom and a layer of mature (hyaline) or immature cartilage at the top [10].

Our chondral defect healing models (Chapters 3 and 4) simulate the filling of a defect with cartilage, but do not simulate the conversion of cartilage into bone at the bottom of the defect. Lydon *et al.* [120] observed that this process occurs via endochondral ossification, similar to the process observed during bone formation in the growth plate or during fracture healing. The objective of this work was therefore to primarily focus on the endochondral ossification process. In this process, cartilage converts into bone via chondrocyte hypertrophy, where the hypertrophic chondrocytes form a primary spongiosa which is then invaded and remodelled by osteoblasts and osteoclasts [120]. Crucially, not all chondrocytes hypertrophy and form primary spongiosa; a layer of hyaline cartilage is left in the top section of the defect, forming articular cartilage.

In our mathematical model we approached this by concentrating on key regulatory pathways that control chondrocyte hypertrophy during growth. Specifically, we concentrated on factors that initiate the process and other factors that suppress the process. The process is known to be initiated by systemic factors (hormones) and locally produced growth factors [121]. The hypertrophy-inducing factor in our model represents the systemic factors, a potent example of which is PTHrP [121]. We modelled these systemic factors as a flux coming in from the top and bottom of the defect. We assumed that this hypertrophy-inducing systemic factor would have to reach a threshold value before initiating hypertrophy. The local factors were represented in our model as a critical or threshold cartilage density, below which hypertrophy is not initiated. This implementation of local factors is similar to that used in models of endochondral ossification during fracture healing [24, 66]. We chose the critical density to be around 95% fill, but also investigated other values in our sensitivity analysis. Both critical values would need to be reached before chondrocyte hypertrophy was initiated. In our model, the process was dominated by the local factor (critical cartilage density): once this density was reached, chondrocytes started to hypertrophy and produce calcified matrix from the cartilage model. This would also halt local chondrocyte proliferation and cartilage matrix formation.

Further regulation of hypertrophy, once initiated, was represented in our model to replicate the Ihh-PTHrP pathway [103]. The Ihh-PTHrP pathway is not only a key regulator of chondrocyte hypertrophy, but also important in relation to the question why bone forms in the bottom section but not the top section of an osteochondral defect. PTHrP, a suppressor of hypertrophy, is produced only by chondrocytes in the superficial zone of cartilage, possibly

related to local mechanical loading [28, 84, 103]. Its production is stimulated by Ihh, which is produced by pre-hypertrophic chondrocytes. In our model, we called Ihh a hypertrophy-modulating growth factor and assumed it would be produced by hypertrophic chondrocytes. To simulate the production of PTHrP by superficial chondrocytes, we modelled a flux of hypertrophy-suppressing growth factor that permeated from the upper layer of the defect. Due to its low diffusion coefficient, this growth factor only penetrated the top few grid points of the simulated defect. The effects of PTHrP at the top of the defect regulated the remaining cartilage layer. The hypertrophic chondrocytes would produce calcified matrix, which then was converted to bone by osteoblasts and osteoclasts, simply referred to as 'bone cells' in our model. Finally, we assumed the underlying bone at the base of the defect and the surrounding synovial fluid at the top of the defect to provide nutrients within the model. This was unlike our previous chondral healing model, where subchondral bone is left intact during debridement of a chondral defect and no flux of nutrient from the base was allowed. In combination, this relatively simplistic approach captivates the key mechanisms driving osteochondral healing after ACI via an endochondral ossification-like process. It is noteworthy to mention our model would not be valid for deep osteochondral defects where a bone-plug may be a more appropriate treatment strategy, as opposed to cell therapy alone as we have modelled here [43]. However, bone defects up to 1 cm in depth can be treated using cell therapy alone [10]. Data from the German Cartilage Registry suggest that using cell therapy alone for osteochondral defects is indeed common practice; over 60% of defects in this registry are osteochondral defects, but only 1 in 9 ACI cases use bone graft augmentation [142].

During the initial phase of regeneration, a purely chondral healing mechanism took place. The results corresponded to our chondral defect healing model (Chapters 3 and 4), with slightly improved matrix formation due to a higher concentration of nutrients available from

the base of the defect. In our models of chondral defect healing a lack of nutrients constrained cell proliferation and matrix deposition. By 1-year cartilage half-filled the defect, with low-density cartilage matrix at the top of the defect and a high-density matrix covering the base. By 18 months the critical cartilage density required for initiation of chondrocyte hypertrophy was reached at the defect base, initiating the conversion of cartilage to calcified matrix by hypertrophic chondrocytes and formation of bone. As time continued, cartilage continued to be converted into calcified matrix with bone subsequently being produced, progressing upwards to the top. This simulated pattern of conversion followed the formation of bone and cartilage as found by Lydon et al. *et al* [120]. By 2 years the layer of cartilage that would remain at the top of the defect became more evident, with bone entirely covering the base of the defect and cartilage degradation to calcified matrix occurring in the midsection. This trend continued until at 48 months the defect was entirely filled with new bone, aside from a section of calcified matrix and a thin layer of cartilage remaining along the top of the defect. The thickness of this layer was regulated by the hypertrophy-suppressing growth factor which was produced by the chondrocytes at the top of the defect. This was based off observations by Jiang *et al.* 2008 [84], that shows PTHrP suppresses hypertrophy and is produced by chondrocytes in the superficial zone. Mechanical loading is also thought to be important in the regulation of PTHrP expression, and is something we do not consider here [28].

The assumptions we made in this model do simplify the biological process occurring during osteochondral healing, potentially limiting conclusions we can draw from this work. Important factors we do not consider in our model include biochemical and biomechanical influences (as detailed in Chapter 2), which play a key role in cell differentiation, matrix synthesis and cell proliferation, among other important mechanisms within osteochondral defect regeneration

[106]. Mechanical loading is also thought to influence the patterns of endochondral ossification, specifically in the formation of long bones [183]. We also excluded the effects of other local growth factors, with FGFs and BMPs thought to play an important role in the endochondral ossification process [103]. Additionally, we considered our critical cartilage density, $m_{C_{crit}}$, as the local hypertrophy-initiating factor, following earlier work [24, 66]. However, a biologically more appropriate method of modelling the local factor might be through a locally produced growth factor. A specific candidate would be C-type natriuretic peptide (CNP), which is produced by chondrocytes and is thought to have a critical concentration above which hypertrophy is initiated [100]. Effectively, our model used cartilage density as a proxy for CNP concentration and although modelling CNP separately might affect the results, the change is most likely minor.

Lydon *et al* describes initial cartilage formation occurring at the top edges of the defect adjacent to damaged cartilage [120]. The reason cartilage first forms here is unknown, but this could possibly be due to chondrocytes attaching preferentially to damaged cartilage rather than bone. In our 1-dimensional model we had to omit this preferential attachment to top edges of the defect because these edges were not represented. This simplification meant we also did not include the invasion of cells from the defect walls. In addition, when an osteochondral defect is created, damaged blood vessels nested within bone at the site of the defect are damaged. These damaged vessels produce blood which coagulates and forms a fibrous clot within the defect. This fibrous clot will act as a nutrient source at the beginning of regeneration, as well as acting as a scaffold for cells to travel along. These functions of a clot were not explicitly modelled in our work, and neither was clot formation.

Finally, we did not consider mesenchymal stem cells to be present in this model, despite their well-documented role in osteochondral defect healing [122, 53, 68]. Lutianov *et al.* [119] explore the effects of autologous chondrocyte implantation (ACI) and articular stem cell implantation (ASI) in chondral defects, which are surgical procedures where either chondrocytes or MSCs are inserted into a defect with the hope to promote healing. In this work, despite MSCs achieving higher cartilage formation at early time, overall healing time did not significantly change [119]. In Chapters 3 & 4 of this thesis we explored the effects of growth factors on the chondral healing process, and also how a co-implantation of MSCs and chondrocytes could promote an earlier healing time [21, 22]. Our work demonstrated that within the first year an enhanced rate of healing was observed when a co-implantation procedure was carried out, with an increase of up to 136% at 3 months when compared with ACI cartilage healing alone, but despite this, an earlier healing time was not achieved; the conclusion of this work was that a co-implantation procedure could have benefits by allowing a patient to become mobile sooner after surgery. The consideration of MSCs in our model could lead to MSC differentiation into chondrocytes or osteoblasts and having trophic effects, requiring extra assumptions around the control of their differentiation into osteoblasts and the mutual effect of osteoblasts and MSCs. However, based on our models of co-implanting MSCs and chondrocytes, it is doubtful whether the effects on the amount of cartilage formation would be large. Alternatively, MSCs may influence the healing environment via an alternative mechanism by their production of paracrine factors, such as transforming growth factor$-\beta$ (TGF$-\beta$), insulin-like growth factor-1 (IGF-1), and vascular endothelial growth factor (VEGF), among others. Depending on the physiological conditions they are exposed to, MSCs may secrete biologically active molecules that influence tissue and cell regeneration and survival, and gene expression [59, 113]. It is thought MSCs may be most effective within tissue regeneration via their paracrine signalling, not their direct contribution to extracellular

matrix production via differentiation to osteoblasts and chondrocytes. Based on the findings in Chapters 3 and 4, and the paracrine effect MSCs may contribute to the healing environment we have not currently considered, we think it is instructive to start the modelling process by including only chondrocytes and osteoblasts.

In future work, the inclusion of the modulatory effects of MSCs via their paracrine signalling would more accurately simulate the cell environment. Other growth factors could also be considered, such as FGF-1 and BMP-2, produced by the chondrocyte-MSC interaction as shown in Chapters 3 &4.

6.2 Future work

The work undertaken in this thesis can be refined to give even more realistic regeneration scenarios. Specifically, by combining the principles behind the refinements made to the cartilage healing model in chapters 3 and 4 with the osteochondral defect regeneration model formulated in Chapter 5, a model of osteochondral defect regeneration that includes the mediatory and direct effects of the inclusion of MSCs, the effects of important factors, along with the regulatory effects of mechanics by the inclusion of the critical cartilage density that initiates chondrocyte hypertrophy, leading to endochondral ossification, could be formulated. More refinements such as the inclusion of other important growth factors not yet considered, other treatment strategies such as the implantation of collagen/glycosaminoglycan scaffolds, and the effects of the mechanical environment can also be considered.

The work in Chapter 3 is refined further in Chapter 4, so we will treat these chapters as

a singular model that can be extended in unison. The inclusion of BMP-2 and FGF-1 are thought to also potentially induce undesirable healing mechanisms such as endochondral ossification and chondrocyte hypertrophy; these are effects we do not consider these growth factors to contribute to in our chondral healing model. Including these potentially occurring mechanisms would result in a more refined healing scenario, where these adverse effects on chondral healing could be explored, but it is suggested in the literature these effects are rarely reported, as explained in 6.1.1, indicating the mechanism we currently consider for chondral regeneration is a sufficient representation [141, 184]. Other mixtures of MSCs and chondrocytes could be investigated to find an 'optimal' MSC/chondrocyte ratio, where nutrient constraints are minimised and matrix deposition maximised. Our criterion for suggesting an optimal co-implantation ratio is based on mean matrix densities. However, other criteria could also be used to determine an optimal ratio. Some justification of our current criteria are clinical data comparing MRI imaging and clinical outcome (McCarthy *et al.*[127]). The signal intensity is a measure of mean matrix density, and thus our chosen measure will give a clinically relevant comparison. However, other parameters such as the required time for cartilage matrix to fill the defect and the required time to achieve a threshold density at the surface might also be appropriate. The spatial distribution of matrix might also be relevant, as seen in Figs 4.16 and 4.17. However, our results suggest that this may be difficult to translate in a criterion. The comparison between MRI and clinical outcome suggests that the articular surface of the repair tissue may be most important [127], which would suggest that the repairs including stem cells, which form denser matrix at the defect surface, might be better. However, the distribution of matrix density is less homogeneous for these cases, and poor matrix homogeneity is associated with poorer clinical outcome [127]. The limitations of our model dictate that all simulations are subject to nutrient concentration constraints, typically meaning an optimal split of MSCs and chondrocytes is not at all obvious; this

would require further investigation. This effect of nutrient concentration impacting the overall healing process has been hypothesised in our previous model as well as similar work [196], with this co-implantation model now corroborating this hypothesis further. Availability of cell types, overall cost and efficacy of the procedure are factors that would also have to be considered when considering an optimal MSC-chondrocyte co-implantation ratio.

In chapter 5, the model proposed for osteochondral defect regeneration is 1-dimensional, i.e. spatial variation is assumed to occur along the thickness of the defect alone. This is a stringent assumption, as many osteochondral defects are deep as well as thick; a 2-dimensional modelling approach here would be more refined. Disregarding other dimensions could result in healing evolution occurring in other directions that the current model would struggle to capture. In addition to this, the effects of the mechanical environment on osteochondral defect regeneration is likely to be significant, with various studies demonstrating this [49, 125]. The mechanical effect on endochondral ossification is also well-established, which is the underlying healing mechanism we assume to be occurring during osteochondral defect regeneration. It is likely the mechanical environment stimulates the release of various growth factors, enhances cell proliferation, initiates cell differentiation, and influences many other important mechanisms in the healing process. We do, however, consider a critical cartilage density for the initiation of chondrocyte hypertrophy and cartilage calcification, which is likely to be regulated by the mechanical environment [24], along with the expression of endochondral-suppressing growth factors located at the top of the defect, thought to be released by the chondrocytes adjacent to damaged cartilage. Additionally, we do not consider an initial population of MSCs, which would be present in the defect within the fibrous clot [49]. It is assumed MSCs would differentiate into chondrocytes, where a chondral healing mechanism would then continue to take place before chondrocytes exit their proliferative state and

undergo hypertrophy, regulated by a critical cartilage density. We neglect their inclusion initially to give a simpler initial modelling scenario. Furthermore, the works in Chapters 3 & 4 demonstrate little difference between the consideration of either chondrocytes or MSCs for cartilage regeneration, indicating any differences observed based on the inclusion of MSCs would be at early times before calcification and endochondral ossification has been initiated, which is the main area of interest in Chapter 5. To refine this model further, an initial population of MSCs should be considered, along with the implantation of chondrocytes we consider, and with the effects of FGF-1 and BMP-2 we consider in Chapters 3 & 4. This would likely lead to a slightly quicker initial cartilage fill time, and would be a better representation of the osteochondral healing process after chondrocyte implantation. The higher density of implanted cells would not likely have a significant impact on healing time though, as demonstrated in Lutianov *et al.* [119], where doubling the implantation of chondrocytes in an ACI procedure or MSCs in an ASI procedure did not impact overall healing time; increased cell levels utilise more nutrients which in-turn constrains the cell environment by decreasing cell proliferation. However, in the osteochondral defect healing scenario the reported effects could differ as nutrient concentration is typically less constrained, so is something that could be explored in more detail. Additionally, the consideration of other growth factors involved in the PTHrP-Ihh feedback loop would lead to a more refined growth factor inclusion; it is thought FGF-18 and CNP (C-type natriuretic peptide), which form an antagonistic signalling pathway, are involved in the regulation of proliferative and pre-hypertrophic chondrocyte cell numbers, ensuring Ihh production and chondrocyte hypertrophy when PTHrP is distant enough [100]. Furthermore, the inclusion of a biphasic collagen/glycosaminoglycan scaffold containing FGF-18, specifically recombinant human FGF-18, in osteochondral defect repair in ovine models is reported to result in improved chondrogenesis, reduced fibrocartilage production and a better quality of the regenerated cartilage tissue when compared with empty

defects, empty scaffolds and scaffolds containing BMP-7 [67]. rhFGF-18 is also reported to improve microfracture treated chondral defects, again resulting in more hyaline-like and less fibrocartilage regenerated tissue, demonstrating increased FGF-18 expression enhances chondral regeneration [151], a stage of healing our model has demonstrated is highly important to successful osteochondral defect regeneration. Collagen/GAG scaffolds containing FGF-18, along with other treatment strategies using collagen scaffolds seeded with various cell types and growth factors [68, 153, 158, 159], could be the topic of further work with this model of osteochondral defect regeneration.

6.3 Final thoughts

The work undertaken in this thesis replicates chondral or osteochondral regeneration under the same assumptions; relevant cell types are implanted or pre-exist in the defect, proliferate to appropriate cell numbers, potentially differentiate, undergo hypertrophy, or begin depositing ECM for repair. Cartilage regeneration is the main mechanism behind both chondral and osteochondral defect healing, with the sensitivity analysis in Chapter 5 successfully showing osteochondral defect regeneration is unsuccessful unless an initial cartilage healing phase takes place, where chondrocytes are purely proliferative and do not undergo hypertrophy until a critical cartilage density has been achieved. The regenerated cartilage then acts as a model for calcification and bone deposition to take place via endochondral ossification.

The ideas explored within this thesis demonstrate the importance of understanding the underlying mechanisms behind healing of the bone-cartilage unit, the effect growth factors have on this healing process, and how better treatment strategies can be formulated to treat defects

of cartilage and bone. It has been demonstrated in this chapter how future work combining the principles explored in Chapters 3, 4 & 5 could result in a refined mathematical model of osteochondral defect regeneration, where an initial population of MSCs is considered and their mediatory or direct healing effects could be explored. Additionally, this refined model could be used to explore other popular treatment strategies of osteochondral defect regeneration, such as those that utilise collagen scaffolds [25, 35, 137, 153].

Chapter 7

Glossary

- **Autologous**: Where tissues or cells are taken from the same individual.
- **Apoptosis**: Programmed cell death occurring during an organism's development.
- **Angiogenesis**: The production of new blood vessels.
- **Avascular**: Indicating lack of blood vessels/supply.
- **Chondrocyte**: A cartilage cell that produces cartilage matrix.
- **Chondroclast**: A large cell that drives calcified cartilage resorption.
- **Chondrogenesis**: The process of cartilage formation from mesenchyme tissue.

- **Differentiation**: The process of one cell type changing to another, typically from a less specialised cell type (i.e. mesenchymal stem cell) to a more specialised cell type (i.e. chondrocyte, osteoblast).

- **Endochondral**: Situated within cartilage.

- **Extracellular matrix**: The structural support where cells are embedded, comprised of various collagens and proteins. It is found in connective tissues such as cartilage and bone.

- **Hypertrophy**: Enlargement of cells resulting in an increase in tissue size.

- **Mesenchymal stem cell**: A cell that is able to differentiate into a variety of cell types, such as chondrocytes and osteoblasts.

- **Mesenchyme**: An embryonic tissue that is a precursor of connective and skeletal tissues.

- **Osteoblast**: A cell that produces bone.

- **Osteoclast**: A large bone cell that assists bone growth and healing by absorbing bone.

- **Osteocyte**: An osteoblast that has become embedded in bone matrix.

- **Perichondrium**: An irregular dense connective tissue found surrounding cartilage in bones of the developing skeleton. This material is not found in cartilage in the joints.

- **Proliferation**: Rapid reproduction of a cell.

- **Substrate**: A material upon which an organism, such as a cell population, lives and proliferates.

Bibliography

[1] B. J. Ahern, J. Parvizi, R. Boston, and T. P. Schaer. Preclinical animal models in single site cartilage defect testing: a systematic review. *Osteoarthritis and Cartilage*, 17(6):705–713, 2009.

[2] K. D. Allen and Y. M. Golightly. Epidemiology of osteoarthritis: state of the evidence. *Current Opinion in Rheumatology*, 27(3):276–283, 2015.

[3] S. Amini, D. Veilleux, and I. Villemure. Three-dimensional in situ zonal morphology of viable growth plate chondrocytes: A confocal microscopy study. *Journal of Orthopaedic Research*, 29(5):710–717, 2011.

[4] Y. Anraku, H. Mizuta, A. Sei, S. Kudo, E. Nakamura, K. Senba, K. Takagi, and Y. Hiraki. The chondrogenic repair response of undifferentiated mesenchymal cells in rat full-thickness articular cartilage defects. *Osteoarthritis and Cartilage*, 16(8):961–964, 2008.

[5] U. K. Arthritis Research. *Osteoarthritis in general practice: Data and perspectives.* 2013.

[6] H. D. E. Atkinson. The negatives of knee replacement surgery: complications and the dissatisfied patient. *Orthopaedics and Trauma*, 31(1):25–33, 2017.

[7] A. Bailón-Plaza and M. C. Vander Meulen. A Mathematical Framework to Study the Effects of Growth Factor Influences on Fracture Healing. *Journal of Theoretical Biology*, 212(2):191–209, 2001.

[8] E. Basad, B. Ishaque, G. Bachmann, H. Stürz, and J. Steinmeyer. Matrix-induced autologous chondrocyte implantation versus microfracture in the treatment of cartilage defects of the knee: A 2-year randomised study. *Knee Surgery, Sports Traumatology, Arthroscopy*, 18(4):519–527, 2010.

[9] J. E. J. Bekkers, a. I. Tsuchida, M. H. P. van Rijen, L. a. Vonk, W. J. a. Dhert, L. B. Creemers, and D. B. F. Saris. Single-Stage Cell-Based Cartilage Regeneration Using a Combination of Chondrons and Mesenchymal Stromal Cells: Comparison With Microfracture. *The American Journal of Sports Medicine*, 41(9):2158–2166, 2013.

[10] G. Bentley, L. C. Biant, R. W. J. Carrington, M. Akmal, A. Goldberg, A. M. Williams, J. A. Skinner, and J. Pringle. A prospective, randomised comparison of autologous chondrocyte implantation versus mosaicplasty for osteochondral defects in the knee. *J Bone Joint Surg Br*, 85(2):223–230, 2003.

[11] A. M. Bhosale and J. B. Richardson. Articular cartilage: Structure, injuries and review of management. *British Medical Bulletin*, 87(1):77–95, 2008.

[12] L. C. Biant, G. Bentley, S. Vijayan, J. a. Skinner, and R. W. J. Carrington. Long-term Results of Autologous Chondrocyte Implantation in the Knee for Chronic Chrondral and Osteochondral Defects. *The American journal of sports medicine*, pages 2178–2183, 2014.

[13] F. Birrell, N. Howells, and M. Porcheret. Osteoarthritis: pathogenesis and prospects for treatment. *Reports on the Rheumatic Diseases, Series*, 6:1–12, 2011.

[14] D. S. Bramono, S. Murali, B. Rai, L. Ling, W. T. Poh, Z. X. Lim, G. S. Stein, V. Nurcombe, A. J. Van Wijnen, and S. M. Cool. Bone marrow-derived heparan sulfate potentiates the osteogenic activity of bone morphogenetic protein-2 (bmp-2). *Bone*, 50(4):954–964, 2012.

[15] M. Brittberg. Articular Cartilage Repair in the Knee Joint with Autologous Chondrocytes and Periosteal Graft. *Orthopedics and Traumatology*, (3):185–194, 2001.

[16] M. Brittberg. Autologous chondrocyte implantation-Technique and long-term follow-up. *Injury*, 39(1 SUPPL.):40–49, 2008.

[17] M. Brittberg, A. Lindahl, A. Nilsson, C. Ohlsson, O. Isaksson, and L. Peterson. Treatment of deep cartilage defects in the knee with autologous chondrocyte transplantation. *New England Journal of Medicine*, 331(14):889–895, 1994.

[18] P. Brun, S. C. Dickinson, B. Zavan, R. Cortivo, A. P. Hollander, and G. Abatangelo. Characteristics of repair tissue in second-look and third-look biopsies from patients treated with engineered cartilage: Relationship to symptomatology and time after implantation. *Arthritis Research and Therapy*, 10(6):1–8, 2008.

[19] J. A. Buckwalter and H. J. Mankin. Articular cartilage repair and transplantation. *Arthritis and Rheumatism*, 41(8):1331–1342, 1998.

[20] H. Byrne and D. Drasdo. Individual-based and continuum models of growing cell populations: A comparison. *Journal of Mathematical Biology*, 58(4-5):657–687, 2009.

[21] K. Campbell, S. Naire, and J. H. Kuiper. A mathematical model of cartilage regeneration after chondrocyte and stem cell implantation – I: the effects of growth factors. *Journal of Tissue Engineering*, 10:204173141982779, Jan 2019.

[22] K. Campbell, S. Naire, and J. H. Kuiper. A mathematical model of cartilage regeneration after chondrocyte and stem cell implantation – II: the effects of co-implantation. *Journal of Tissue Engineering*, 10:204173141982779, Jan 2019.

[23] A. I. Caplan and J. E. Dennis. Mesenchymal stem cells as trophic mediators. *Journal of cellular biochemistry*, 98(5):1076–1084, 2006.

[24] A. Carlier, H. Brems, J. M. A. Ashbourn, I. Nica, E. Legius, and L. Geris. Capturing the wide variety of impaired fracture healing phenotypes in Neurofibromatosis Type 1 with eight key factors : a computational study. *Nature Publishing Group*, (November 2015):1–15, 2016.

[25] C. H. Chang, T. F. Kuo, C. C. Lin, C. H. Chou, K. H. Chen, F. H. Lin, and H. C. Liu. Tissue engineering-based cartilage repair with allogenous chondrocytes and gelatin-chondroitin-hyaluronan tri-copolymer scaffold: A porcine model assessed at 18, 24, and 36 weeks. *Biomaterials*, 27(9):1876–1888, 2006.

[26] J. L. Chen, L. Duan, W. Zhu, J. Xiong, and D. Wang. Extracellular matrix production in vitro in cartilage tissue engineering. *Journal of Translational Medicine*, 12(1):1–9, 2014.

[27] M. J. Chen, J. P. Whiteley, C. P. Please, A. Schwab, F. Ehlicke, S. L. Waters, and H. M. Byrne. Inducing chondrogenesis in MSC/chondrocyte co-cultures using exogenous TGF- β : a mathematical model. *Journal of Theoretical Biology*, 439:1–13, 2018.

[28] X. Chen, C. M. Macica, A. Nasiri, and A. E. Broadus. Regulation of articular chondrocyte proliferation and differentiation by Indian hedgehog and parathyroid hormone-related protein in mice. *Arthritis and Rheumatism*, 58(12):3788–3797, 2008.

[29] H. Chiang and C.-c. Jiang. Repair of articular cartilage defects: review and perspectives. *Journal of the Formosan Medical Association*, 108(2):87–101, 2009.

[30] C. R. Chu, M. Szczodry, and S. Bruno. Animal models for cartilage regeneration and repair. *Tissue Engineering Part B: Reviews*, 16(1):105–115, feb 2010.

[31] F. Cicuttini, C. Ding, A. Wluka, S. Davis, P. R. Ebeling, and G. Jones. Association of cartilage defects with loss of knee cartilage in healthy, middle-age adults: A prospective study. *Arthritis & Rheumatology*, 52(7):2033–2039, 2005.

[32] S. Cowin and D. Hegedus. Bone remodeling I: theory of adaptive elasticity. *Journal of Elasticity*, 6(3):313–326, 1976.

[33] S. C. Cowin and L. Cardoso. Mixture theory-based poroelasticity as a model of interstitial tissue growth. *Mechanics of Materials*, 44:47–57, 2012.

[34] E. J. Crampin, W. W. Hackborn, M. S. Division, and P. K. Maini. Pattern Formation in Reaction – Diffusion Models with Nonuniform Domain Growth. *Bulletin of Mathematical Biology*, 64(4):747–769, 2002.

[35] R. L. Dahlin, L. A. Kinard, J. Lam, C. J. Needham, S. Lu, F. K. Kasper, and A. G. Mikos. Articular chondrocytes and mesenchymal stem cells seeded on biodegradable scaffolds for the repair of cartilage in a rat osteochondral defect model. *Biomaterials*, 35(26):7460–7469, 2014.

[36] J. Dahmen, K. T. Lambers, M. L. Reilingh, C. J. van Bergen, S. A. Stufkens, and G. M. Kerkhoffs. No superior treatment for primary osteochondral defects of the talus. *Knee Surgery, Sports Traumatology, Arthroscopy*, 26(7):2142–2157, 2018.

[37] S. L. Dallas and L. F. Bonewald. Dynamics of the transition from osteoblast to osteocyte. *Annals of the New York Academy of Sciences*, 1192(816):437–443, 2010.

[38] D. H. Damon, R. R. Lobb, P. A. D'Amore, and J. A. Wagner. Heparin potentiates the action of acidic fibroblast growth factor by prolonging its biological half-life. *Journal of cellular physiology*, 138(2):221–226, 1989.

[39] M. L. Davies-Tuck, A. E. Wluka, Y. Wang, A. J. Teichtahl, G. Jones, C. Ding, and F. M. Cicuttini. The natural history of cartilage defects in people with knee osteoarthritis. *Osteoarthritis and Cartilage*, 16(3):337–342, 2008.

[40] C. De Bari and A. J. Roelofs. Stem cell-based therapeutic strategies for cartilage defects and osteoarthritis. *Current Opinion in Pharmacology*, 40(Figure 1):74–80, 2018.

[41] T. S. de Windt, J. A. Hendriks, X. Zhao, L. A. Vonk, L. B. Creemers, W. J. Dhert, M. A. Randolph, and D. B. Saris. Concise review: unraveling stem cell cocultures in regenerative medicine: which cell interactions steer cartilage regeneration and how? *Stem cells translational medicine*, 3(6):723–733, 2014.

[42] T. S. de Windt, J. A. A. Hendriks, X. Zhao, L. A. Vonk, L. B. Creemers, W. J. A. Dhert, M. A. Randolph, and D. B. F. Saris. Concise Review: Unraveling Stem Cell Cocultures in Regenerative Medicine: Which Cell Interactions Steer Cartilage Regeneration and How? *Stem Cells Translational Medicine*, 3(6):723–733, 2014.

[43] T. S. de Windt and D. B. F. Saris. Treatment algorithm for articular cartilage repair of the knee: Towards patient profiling using evidence-based tools. In A. A. Shetty, S.-J. Kim, N. Nakamura, and M. Brittberg, editors, *Techniques in Cartilage Repair Surgery*, pages 23–31. Springer Berlin Heidelberg, Berlin, Heidelberg, 2014.

[44] T. S. de Windt, L. A. Vonk, I. C. Slaper-Cortenbach, R. Nizak, M. H. van Rijen, and D. B. Saris. Allogeneic MSCs and recycled autologous chondrons mixed in a one-stage

cartilage cell transplantion: a first-in-man trial in 35 patients. *Stem cells*, 35(8):1984–1993, 2017.

[45] M. L. Delco, J. G. Kennedy, L. J. Bonassar, and L. A. Fortier. Post-traumatic osteoarthritis of the ankle: A distinct clinical entity requiring new research approaches. *Journal of Orthopaedic Research*, 35(3):440–453, mar 2017.

[46] C. Ding, F. Cicuttini, F. Scott, C. Boon, and G. Jones. Association of prevalent and incident knee cartilage defects with loss of tibial and patellar cartilage: A longitudinal study. *Arthritis and Rheumatism*, 52(12):3918–3927, 2005.

[47] M. Doherty. Articular Cartilage and Osteoarthritis. *Annals of the Rheumatic Diseases*, 51(9):1028–1028, Sep 1992.

[48] J. E. Dowd and D. S. Riggs. A comparison of estimates of Michaelis-Menten kinetic constants. *The Journal of biological chemistry*, 240(2):863–869, 1965.

[49] G. N. Duda, Z. M. Maldonado, P. Klein, M. O. Heller, J. Burns, and H. Bail. On the influence of mechanical conditions in osteochondral defect healing. *Journal of Biomechanics*, 38(4):843–851, 2005.

[50] T. A. Einhorn. The cell and molecular biology of fracture healing. *Clinical orthopaedics and related research®*, 355:S7–S21, 1998.

[51] D. Eyre. Collagen of articular cartilage. *Arthritis Research*, 4(1):30–35, 2002.

[52] M. Falah, G. Nierenberg, M. Soudry, M. Hayden, and G. Volpin. Treatment of articular cartilage lesions of the knee. *International Orthopaedics*, 34(5):621–630, 2010.

[53] J. M. Farmer, D. F. Martin, C. A. Boles, and W. W. Curl. Chondral and Osteochondral Injuries. *Clinics in Sports Medicine*, 20(2):299–320, 2001.

[54] A. Fasano, M. A. Herrero, J. M. López, and E. Medina. On the dynamics of the growth plate in primary ossification. *Journal of Theoretical Biology*, 265(4):543–553, 2010.

[55] X. Feng. Chemical and Biochemical Basis of Bone Cell. *NIH Public Access*, 3(2):975–990, 2010.

[56] H. P. Fischer. Mathematical modeling of complex biological systems: From parts lists to understanding systems behavior. *Alcohol Research and Health*, 31(1):49–59, 2008.

[57] R. Florencio-Silva, G. R. D. S. Sasso, E. Sasso-Cerri, M. J. Simões, and P. S. Cerri. Biology of Bone Tissue: Structure, Function, and Factors That Influence Bone Cells. *BioMed Research International*, 2015, 2015.

[58] C. B. Foldager, A. H. Gomoll, M. Lind, and M. Spector. Cell seeding densities in autologous chondrocyte implantation techniques for cartilage repair. *Cartilage*, 3(2):108–117, 2012.

[59] M. J. Fontaine, H. Shih, R. Schäfer, and M. F. Pittenger. Unraveling the Mesenchymal Stromal Cells' Paracrine Immunomodulatory Effects. *Transfusion Medicine Reviews*, 30(1):37–43, 2016.

[60] N. I. for Health and C. Excellence. Autologous chondrocyte implantation for repairing symptomatic articular cartilage defects of the knee. (October):1–5, 2014.

[61] A. Franz-Odendaal, Tamara. Induction and patterning of intramembranous bone. *Frontiers in Bioscience*, 16(1):2734, 2011.

[62] I. Gadjanski and G. Vunjak-Novakovic. Challenges in engineering osteochondral tissue grafts with hierarchical structures. *Expert Opinion on Biological Therapy*, 15(11):1583–1599, 2015.

[63] P. Garnero, J. C. Rousseau, and P. D. Delmas. Molecular basis and clinical use of biochemical markers of bone, cartilage, and synovium in joint diseases. *Arthritis and Rheumatism*, 43(5):953–968, 2000.

[64] D. A. Garzón-Alvarado, J. M. García-Aznar, and M. Doblaré. A reaction-diffusion model for long bones growth. *Biomechanics and Modeling in Mechanobiology*, 8(5):381–395, 2009.

[65] I. Gerber and I. Ap Gwynn. Influence of cell isolation, cell culture density, and cell nutrition on differentiation of rat calvarial osteoblast-like cells in vitro. *Eur Cell Mater*, 2:10–20, 2001.

[66] L. Geris, A. Gerisch, J. Vander, and H. V. Oosterwyck. Angiogenesis in bone fracture healing : A bioregulatory model. 251:137–158, 2008.

[67] A. Getgood, F. Henson, C. Skelton, R. Brooks, H. Guehring, L. A. Fortier, and N. Rushton. Osteochondral tissue engineering using a biphasic collagen/GAG scaffold containing rhFGF18 or BMP-7 in an ovine model. *Journal of Experimental Orthopaedics*, 1(1):1–11, 2014.

[68] A. M. J. Getgood, S. J. Kew, R. Brooks, H. Aberman, T. Simon, A. K. Lynn, and N. Rushton. Evaluation of early-stage osteochondral defect repair using a biphasic scaffold based on a collagen-glycosaminoglycan biopolymer in a caprine model. *Knee*, 19(4):422–430, 2012.

[69] M. B. Goldring. Chondrogenesis, chondrocyte differentiation, and articular cartilage metabolism in health and osteoarthritis. *Therapeutic advances in musculoskeletal disease*, 4(4):269–85, 2012.

[70] A. H. Gomoll, G. Filardo, F. K. Almqvist, W. D. Bugbee, M. Jelic, J. C. Monllau,

G. Puddu, W. G. Rodkey, P. Verdonk, R. Verdonk, S. Zaffagnini, and M. Marcacci. Surgical treatment for early osteoarthritis. Part II: Allografts and concurrent procedures. *Knee Surgery, Sports Traumatology, Arthroscopy*, 20(3):468–486, 2012.

[71] C. R. Gooding, W. Bartlett, G. Bentley, J. A. Skinner, R. Carrington, and A. Flanagan. A prospective, ranomised study comparing two techniques of autologous chondrocyte implantation for osteochondral defects in the knee: Periosteum covered versus type I/III collagen covered. *Knee*, 13(3):203–210, 2006.

[72] M. C. Googe. Deep–vein thrombosis following total knee replacement. *Orthopaedic Nursing*, 3(5):48, 1984.

[73] T. Gotterbarm, S. J. Breusch, U. Schneider, and M. Jung. The minipig model for experimental chondral and osteochondral defect repair in tissue engineering: retrospective analysis of 180 defects. *Laboratory Animals*, 42(71), 2008.

[74] X. Guo, C. Wang, C. Duan, M. Descamps, Q. Zhao, L. Dong, S. Lü, K. Anselme, J. Lu, and Y. Q. Song. Repair of Osteochondral Defects with Autologous Chondrocytes Seeded onto Bioceramic Scaffold in Sheep. *Tissue Engineering*, 10(11-12):1830–1840, 2004.

[75] J. D. Harris, R. A. Siston, X. Pan, and D. C. Flanigan. Autologous Chondrocyte Implantation: A Systematic Review. *The Journal of Bone and Joint Surgery (American)*, 92(12):2220–2233, 2010.

[76] J. D. Hayes, R. L. Brower, and K. J. John. Articular cartilage. anatomy, injury, and repair. *Clinics in podiatric medicine and surgery*, 18(1):35–53, 2001.

[77] D. Hegedus and S. Cowin. Bone remodeling ii: small strain adaptive elasticity. *Journal of elasticity*, 6(4):337–352, 1976.

[78] J. Hendriks, J. Riesle, and C. A. van Blitterswijk. Co-culture in cartilage tissue engineering. *Journal of tissue engineering and regenerative medicine*, 1(3):170–178, 2007.

[79] P. Hiltmann and P. Lory. On oxygen diffusion in a spherical cell with Michaelis-Menten oxygen uptake kinetics. *Bulletin of Mathematical Biology*, 45(5):661–664, 1983.

[80] R. Hishimura, T. Onodera, and K. Hontani. Osteochondral Autograft Transplantation Technique Augmented by an Ultrapurified Alginate Gel Enhances Osteochondral Repair in a Rabbit Model. pages 468–478, 2019.

[81] M. E. Hubbard and H. M. Byrne. Multiphase modelling of vascular tumour growth in two spatial dimensions. *Journal of Theoretical Biology*, 316:70–89, 2013.

[82] B. Ingalls. Mathematical Modeling in Systems Biology: An Introduction. pages 1–396, 2013.

[83] D. W. Jackson, P. A. Lalor, H. M. Aberman, and T. M. Simon. Spontaneous Repair of Full- Thickness Defects of Articular Cartilage in a Goat Model. *The Journal of Bone & Joint Surgery*, 83-A(1), 2001.

[84] J. Jiang, N. L. Leong, J. C. Mung, C. Hidaka, and H. H. Lu. Interaction between zonal populations of articular chondrocytes suppresses chondrocyte mineralization and this process is mediated by PTHrP. *Osteoarthritis and Cartilage*, 16(1):70–82, 2008.

[85] D. D. Joseph, T. S. Lundgren, R. Jackson, and D. A. Saville. Ensemble averaged and mixture theory equations for incompressible fluid-particle suspensions. *International Journal of Multiphase Flow*, 16(1):35–42, 1990.

[86] M. Jung, S. Breusch, W. Daecke, and T. Gotterbarm. The effect of defect localization on spontaneous repair of osteochondral defects in a Göttingen minipig model: a

retrospective analysis of the medial patellar groove versus the medial femoral condyle. *Laboratory Animals*, 43:191–197, 2009.

[87] W. J. Jurgens, R. J. Kroeze, B. Zandieh-Doulabi, A. van Dijk, G. A. Renders, T. H. Smit, F. J. van Milligen, M. J. Ritt, and M. N. Helder. One-step surgical procedure for the treatment of Osteochondral defects with Adipose-derived stem cells in a Caprine knee defect: A pilot study. *BioResearch Open Access*, 2(4):315–325, 2013.

[88] C. A. Kahlenberg, B. U. Nwachukwu, A. S. McLawhorn, M. B. Cross, C. N. Cornell, and D. E. Padgett. Patient satisfaction after Total Knee Replacement: A systematic review. *HSS Journal*, 14(2):192–201, 2018.

[89] H. S. Kan, P. K. Chan, K. Y. Chiu, C. H. Yan, S. S. Yeung, Y. L. Ng, K. W. Shiu, and T. Ho. Non-surgical treatment of knee osteoarthritis. *Hong Kong Medical Journal*, 25(2):127–133, 2011.

[90] D. Karataglis, M. A. Green, and D. J. A. Learmonth. Autologous osteochondral transplantation for the treatment of chondral defects of the knee. *Knee*, 13(1):32–35, 2006.

[91] D. J. Kelly and P. J. Prendergast. Mechano-regulation of stem cell differentiation and tissue regeneration in osteochondral defects. *Journal of Biomechanics*, 38(7):1413–1422, 2005.

[92] D. J. Kelly and P. J. Prendergast. Prediction of the optimal mechanical properties for a scaffold used in osteochondral defect repair. *Tissue Engineering*, 12(9):2509–2519, 2006.

[93] H. P. Kelly. Many-body perturbation theory applied to atoms. *Physical Review*, 136(3B):B896, 1964.

[94] J. Kerkhofs, S. J. Roberts, F. P. Luyten, H. van Oosterwyck, and L. Geris. Relating the chondrocyte gene network to growth plate morphology: From genes to phenotype. *PLoS ONE*, 7(4):1–11, 2012.

[95] T. Kiaer, J. Grønlund, and K. Sørensen. Intraosseous pressure and partial pressures of oxygen and carbon dioxide in osteoarthritis. In *Seminars in arthritis and rheumatism*, volume 18, pages 57–60. Elsevier, 1989.

[96] L. S. Kimpton, A. Schwab, F. Ehlicke, S. L. Waters, C. P. Please, J. P. Whiteley, and H. M. Byrne. A mathematical model for cell infiltration and proliferation in a chondral defect. *Mathematical Biosciences*, 292:46–56, 2017.

[97] J. Klein-Nulend, R. G. Bacabac, and A. D. Bakker. Mechanical loading and how it affects bone cells: The role of the osteocyte cytoskeleton in maintaining our skeleton. *European Cells and Materials*, 24:278–291, 2012.

[98] G. Knutsen, V. Isaksen, O. Johansen, L. Engebretsen, T. C. Ludvigsen, J. O. Drogset, T. Grøntvedt, E. Solheim, T. Strand, and S. Roberts. Autologous chondrocyte implantation compared with microfracture in the knee: A randomized trial. *Journal of Bone and Joint Surgery - Series A*, 86(3):455–464, 2004.

[99] S. Kondo and T. Miura. Reaction-diffusion model as a framework for understanding biological pattern formation. *Science*, 329(5999):1616–1620, 2010.

[100] E. Kozhemyakina, A. B. Lassar, and E. Zelzer. A pathway to bone: signaling molecules and transcription factors involved in chondrocyte development and maturation. *Development*, 142(5):817–831, 2015.

[101] M. J. Kraeutler, T. Kaenkumchorn, C. Pascual-Garrido, M. A. Wimmer, and S. Chubinskaya. Peculiarities in ankle cartilage. *Cartilage*, 8(1):12–18, 2017.

[102] P. C. Kreuz, M. R. Steinwachs, C. Erggelet, S. J. Krause, G. Konrad, M. Uhl, and N. Südkamp. Results after microfracture of full-thickness chondral defects in different compartments in the knee. *Osteoarthritis and Cartilage*, 14(11):1119–1125, 2006.

[103] H. M. Kronenberg. Developmental regulation of the growth plate. *Nature*, 423(6937):332–6, 2003.

[104] J. H. Kuiper. Personal communication, 2020.

[105] C. Kuttler. Reaction-diffusion equations with applications. In *Internet Seminar*, 2011.

[106] D. Lacroix and P. J. Prendergast. A mechano-regulation model for tissue differentiation during fracture healing: Analysis of gap size and loading. *Journal of Biomechanics*, 35(9):1163–1171, 2002.

[107] J. C. Leijten, N. Georgi, L. Wu, C. A. Van Blitterswijk, and M. Karperien. Cell sources for articular cartilage repair strategies: Shifting from monocultures to cocultures. *Tissue Engineering - Part B: Reviews*, 19(1):31–40, 2013.

[108] G. Lemon and J. R. King. Multiphase modelling of cell behaviour on artificial scaffolds: Effects of nutrient depletion and spatially nonuniform porosity. *Mathematical Medicine and Biology*, 24(1):57–83, 2007.

[109] G. Lemon, J. R. King, H. M. Byrne, O. E. Jensen, and K. M. Shakesheff. Mathematical modelling of engineered tissue growth using a multiphase porous flow mixture theory. *Journal of Mathematical Biology*, 52(5):571–594, 2006.

[110] G. Lemon, S. Sjöqvist, M. L. Lim, N. Feliu, A. B. Firsova, R. Amin, Y. Gustafsson, A. Stuewer, E. Gubareva, J. Haag, P. Jungebluth, and P. Macchiarini. The use of mathematical modelling for improving the tissue engineering of organs and stem cell therapy. *Current stem cell research & therapy*, 0(0):1–12, 2015.

[111] G. Li, J. Yin, J. Gao, T. S. Cheng, N. J. Pavlos, C. Zhang, and M. H. Zheng. Subchondral bone in osteoarthritis: Insight into risk factors and microstructural changes. *Arthritis Research and Therapy*, 15(6), 2013.

[112] M. A. Liebschner. Biomechanical considerations of animal models used in tissue engineering of bone. *Biomaterials*, 25(9):1697–1714, 2004.

[113] I. Linero and O. Chaparro. Paracrine effect of mesenchymal stem cells derived from human adipose tissue in bone regeneration. *PLoS ONE*, 9(9), sep 2014.

[114] L. A. Liotta, G. M. Saidel, and J. Kleinerman. Diffusion model of tumor vascularization and growth. *Bulletin of mathematical biology*, 39(1):117–128, 1977.

[115] X. Liu, H. Sun, D. Yan, L. Zhang, X. Lv, T. Liu, W. Zhang, W. Liu, Y. Cao, and G. Zhou. In vivo ectopic chondrogenesis of BMSCs directed by mature chondrocytes. *Biomaterials*, 31(36):9406–9414, dec 2010.

[116] S. Løken, S. Heir, I. Holme, L. Engebretsen, and A. Årøen. 6-year follow-up of 84 patients with cartilage defects in the knee. *Acta Orthopaedica*, 81(5):611–618, 2010.

[117] R. J. Lories and F. P. Luyten. The bone-cartilage unit in osteoarthritis. *Nature Reviews Rheumatology*, 7(1):43–49, 2011.

[118] X. L. Lu and V. C. Mow. Biomechanics of Articular Cartilage and Determination of Material Properties. *Medicine & Science in Sports & Exercise*, 40(2):193–199, Feb 2008.

[119] M. Lutianov, S. Naire, S. Roberts, and J.-H. Kuiper. A mathematical model of cartilage regeneration after cell therapy. *Journal of Theoretical Biology*, 289:136–150, 2011.

[120] H. Lydon, A. Getgood, and F. M. D. Henson. Healing of Osteochondral Defects via Endochondral Ossification in an Ovine Model. *CARTILAGE*, 10(1):94–101, Jan 2019.

[121] E. J. Mackie, L. Tatarczuch, and M. Mirams. The skeleton: a multi-functional complex organ. The growth plate chondrocyte and endochondral ossification. *Journal of Endocrinology*, 211(2):109–121, Nov 2011.

[122] H. Madry and M. Cucchiarini. Signalling Pathways in Osteochondral Defect Regeneration. Number June in Mechanical Engineering Series, pages 219–228. Springer International Publishing, Cham, 2015.

[123] H. Madry, U. W. Grün, and G. Knutsen. Cartilage repair and joint preservation: medical and surgical treatment options. *Deutsches Ärzteblatt international*, 108(40):669–77, 2011.

[124] H. Madry, C. N. van Dijk, and M. Mueller-Gerbl. The basic science of the subchondral bone. *Knee Surgery, Sports Traumatology, Arthroscopy*, 18(4):419–433, 2010.

[125] I. Martin, S. Miot, A. Barbero, M. Jakob, and D. Wendt. Osteochondral tissue engineering. *Journal of Biomechanics*, 40(4):750–765, Jan 2007.

[126] R. B. Martin and D. B. Burr. Non-invasive measurement of long bone cross-sectional moment of inertia by photon absorptiometry. *Journal of biomechanics*, 17(3):195–201, 1984.

[127] H. S. McCarthy, I. W. McCall, J. M. Williams, C. Mennan, M. N. Dugard, J. B. Richardson, and S. Roberts. Magnetic Resonance Imaging Parameters at 1 Year Correlate With Clinical Outcomes Up to 17 Years After Autologous Chondrocyte Implantation. *Orthopaedic Journal of Sports Medicine*, 6(8):1–10, 2018.

[128] A. M. McCoy. Animal models of osteoarthritis: comparisons and key considerations. *Veterinary pathology*, 52(5):803–818, 2015.

[129] W. M. Mikkelsen, T. W. Bunch, and J. J. Calabro. Spontaneous osteonecrosis of the knee. *Arthritis and Rheumatism*, 24(2):111–455, 1981.

[130] H. Mistry, M. Connock, J. Pink, D. Shyangdan, C. Clar, P. Royle, R. Court, L. C. Biant, A. Metcalfe, and N. Waugh. Autologous chondrocyte implantation in the knee: Systematic review and economic evaluation. *Health Technology Assessment*, 21(6):V–160, 2017.

[131] K. Mithoefer, R. J. Williams, R. F. Warren, H. G. Potter, C. R. Spock, E. C. Jones, T. L. Wickiewicz, and R. G. Marx. The microfracture technique for the treatment of articular cartilage lesions in the knee: A prospective cohort study. *Journal of Bone and Joint Surgery - Series A*, 87(9 I):1911–1920, 2005.

[132] C. G. Moran and T. C. Horton. Total knee replacement: The joint of the decade. *British Medical Journal*, 320(7238):820, 2000.

[133] V. C. Mow, S. C. Kuei, W. M. Lai, and C. G. Armstrong. Biphasic creep and stress relaxation of articular cartilage in compression? Theory and experiments. *Journal of biomechanical engineering*, 102(1):73–84, 1980.

[134] T. F. Moyad. Cartilage injuries in the adult knee: Evaluation and management. *Cartilage*, 2(3):226–236, 2011.

[135] M. Müller-Gerbl, E. Schulte, and R. Putz. The thickness of the calcified layer of articular cartilage: a function of the load supported? *Journal of anatomy*, 154:103–11, 1987.

[136] S. Munirah, O. C. Samsudin, H. C. Chen, S. H. Sharifah Salmah, B. S. Aminuddin, and B. H. Ruszymah. Articular cartilage restoration in load-bearing osteochondral defects by implantation of autologous chondrocyte-fibrin constructs: An experimental study in sheep. *Journal of Bone and Joint Surgery - Series B*, 89(8):1099–1109, 2007.

[137] D. Murata, S. Tokunaga, T. Tamura, H. Kawaguchi, N. Miyoshi, M. Fujiki, K. Nakayama, and K. Misumi. A preliminary study of osteochondral regeneration using a scaffold-free three-dimensional construct of porcine adipose tissue-derived mesenchymal stem cells. *Journal of Orthopaedic Surgery and Research*, 10(1):1–12, 2015.

[138] J. D. Murray. Mathematical biology. second corrected edition. 1993.

[139] P. J. Murray, C. M. Edwards, M. J. Tindall, and P. K. Maini. From a discrete to a continuum model of cell dynamics in one dimension. *Physical Review E - Statistical, Nonlinear, and Soft Matter Physics*, 80(3):24–29, 2009.

[140] A. Nazempour and B. J. Van Wie. Chondrocytes, mesenchymal stem sells, and their combination in articular cartilage regenerative medicine. *Annals of Biomedical Engineering*, 44(5):1325–1354, 2016.

[141] H. Nejadnik, J. H. Hui, E. P. Feng Choong, B.-C. Tai, and E. H. Lee. Autologous bone marrow–derived mesenchymal stem cells versus autologous chondrocyte implantation: an observational cohort study. *The American journal of sports medicine*, 38(6):1110–1116, 2010.

[142] P. Niemeyer, D. Albrecht, S. Andereya, P. Angele, A. Ateschrang, M. Aurich, M. Baumann, U. Bosch, C. Erggelet, S. Fickert, H. Gebhard, K. Gelse, D. Günther, A. Hoburg, P. Kasten, T. Kolombe, H. Madry, S. Marlovits, N. M. Meenen, P. E. Müller, U. Nöth, J. P. Petersen, M. Pietschmann, W. Richter, B. Rolauffs, K. Rhunau, B. Schewe,

A. Steinert, M. R. Steinwachs, G. H. Welsch, W. Zinser, and J. Fritz. Autologous chondrocyte implantation (ACI) for cartilage defects of the knee: A guideline by the working group "Clinical Tissue Regeneration" of the German Society of Orthopaedics and Trauma (DGOU). *Knee*, 23(3):426–435, 2016.

[143] A. J. Nixon, L. Begum, H. O. Mohammed, B. Huibregtse, M. M. O'Callaghan, and G. L. Matthews. Autologous chondrocyte implantation drives early chondrogenesis and organized repair in extensive full- and partial-thickness cartilage defects in an equine model. *Journal of Orthopaedic Research*, 29(7):1121–1130, 2011.

[144] B. Obradovic, J. H. Meldon, L. E. Freed, and G. Vunjak-Novakovic. Glycosaminoglycan deposition in engineered cartilage: Experiments and mathematical model. *AIChE Journal*, 46(9):1860–1871, 2000.

[145] R. O'Dea, H. Byrne, and S. Waters. Continuum Modelling of In Vitro Tissue Engineering: A Review. pages 229–266. 2012.

[146] L. Olsen, J. A. Sherratt, and P. K. Maini. A mathematical model for fibro-proliferative wound healing disorders. *Bulletin of Mathematical Biology*, 58(4):787–808, 1996.

[147] L. Olsen, J. A. Sherratt, P. K. Maini, and F. Arnold. A mathematical model for the capillary endothelial cell-extracellular matrix interactions in wound-healing angiogenesis. *IMA Journal of Mathematics Applied in Medicine and Biology*, 14:261–281, 1997.

[148] M. Orme and M. Chaplain. A mathematical model of vascular tumour growth and invasion. *Mathematical and Computer Modelling*, 23(10):43–60, 1996.

[149] G. F. Oster, J. D. Murray, and P. K. Maini. A model for chondrogenic condensations in the developing limb: the role of extracellular matrix and cell tractions. *Journal of embryology and experimental morphology*, 89:93–112, 1985.

[150] E. Peña, B. Calvo, M. A. Martínez, and M. Doblaré. Effect of the size and location of osteochondral defects in degenerative arthritis. A finite element simulation. *Computers in Biology and Medicine*, 37(3):376–387, mar 2007.

[151] J. Power, P. Hernandez, H. Guehring, A. Getgood, and F. Henson. Intra-articular injection of rhFGF-18 improves the healing in microfracture treated chondral defects in an ovine model. *Journal of Orthopaedic Research*, 32(5):669–676, 2014.

[152] P. J. Prendergast, R. Huiskes, and K. Søballe. Biophysical stimuli on cells during tissue differentiation at implant interfaces. *Journal of Biomechanics*, 30(6):539–548, 1997.

[153] H. J. Pulkkinen, V. Tiitu, P. Valonen, J. S. Jurvelin, L. Rieppo, J. Töyräs, T. S. Silvast, M. J. Lammi, and I. Kiviranta. Repair of osteochondral defects with recombinant human type II collagen gel and autologous chondrocytes in rabbit. *Osteoarthritis and Cartilage*, 21(3):481–490, 2013.

[154] J. B. Richardson, K. T. Wright, J. Wales, J. H. Kuiper, H. S. McCarthy, P. Gallacher, P. E. Harrison, and S. Roberts. Efficacy and safety of autologous cell therapies for knee cartilage defects (autologous stem cells, chondrocytes or the two): randomized controlled trial design. *Regenerative medicine*, 12(5):493–501, 2017.

[155] S. Roberts, P. Genever, A. McCaskie, and C. De Bari. Prospects of stem cell therapy in osteoarthritis. *Regenerative medicine*, 6(3):351–366, 2011.

[156] J. a. Sanz-Herrera, J. M. García-Aznar, M. Doblaré, J. Garcia-Aznar, M. Doblare, J. M. García-Aznar, and M. Doblaré. A mathematical approach to bone tissue engineering. *Philosophical transactions. Series A, Mathematical, physical, and engineering sciences*, 367(1895):2055–2078, 2009.

[157] M. F. Schinsky, W. Macaulay, M. L. Parks, H. Kiernan, and O. A. Nercessian. Nerve

injury after primary total knee arthroplasty. *Journal of Arthroplasty*, 16(8):1048–1054, 2001.

[158] I. Schleicher, K. S. Lips, U. Sommer, I. Schappat, A. P. Martin, G. Szalay, S. Hartmann, and R. Schnettler. Biphasic scaffolds for repair of deep osteochondral defects in a sheep model. *Journal of Surgical Research*, 183(1):184–192, 2013.

[159] I. Schleicher, K. S. Lips, U. Sommer, I. Schappat, A. P. Martin, G. Szalay, and R. Schnettler. Allogenous bone with collagen for repair of deep osteochondral defects. *Journal of Surgical Research*, 185(2):667–675, 2013.

[160] K. Schlichting, H. Schell, R. U. Kleemann, A. Schill, A. Weiler, G. N. Duda, and D. R. Epari. Influence of scaffold stiffness on subchondral bone and subsequent cartilage regeneration in an ovine model of osteochondral defect healing. *American Journal of Sports Medicine*, 36(12):2379–2391, 2008.

[161] F. Shapiro, S. Koide, and M. Glimcher. Cell origin and differentiation in the repair of full thickness defects of articular cartilage. *The Journal of Bone and Joint Surgery*, 75A(4):532–553, 1993.

[162] G. Shen, J. F. Zhang, and F. Z. Fang. In vitro evaluation of artificial joints: a comprehensive review. *Advances in Manufacturing*, 7(1):1–14, 2019.

[163] K. Slynarski, W. Widuchowski, M. Snow, W. Weiss, J. Kruczynski, J. Hendriks, J. Guidoux, and P. Verdonk. Primary chondrocytes and bone marrow cells on a 3d co-polymer scaffold: 2-year results of a prospective, multicenter, single-arm clinical trial in patients with cartilage defects of the knee. *Revue de Chirurgie Orthopédique et Traumatologique*, 101(8):e17–e18, 2015.

[164] A. J. Sophia Fox, A. Bedi, and S. A. Rodeo. The basic science of articular cartilage: Structure, composition, and function. *Sports Health*, 1(6):461–468, 2009.

[165] M. Stephens. *Replacing Animal Experiments*, pages 144–168. Macmillan Education UK, London, 1989.

[166] J.-F. Stoltz, J. Magdalou, D. George, Y. Chen, Y. Li, N. De Isla, X. He, and Y. Remond. Influence of mechanical forces on bone: Introduction to mechanobiology and mechanical adaptation concept. *Journal of Cellular Immunotherapy*, 4(1):10–12, sep 2018.

[167] D. Studer, C. Millan, E. Öztürk, K. Maniura-Weber, and M. Zenobi-Wong. Molecular and biophysical mechanisms regulating hypertrophic differentiation in chondrocytes and mesenchymal stem cells. *European Cells and Materials*, 24:118–135, 2012.

[168] A. N. Suciu, T. Iwatsubo, M. Matsuda, and T. Nishino. A Study upon Durability of the Artificial Knee Joint with PVA Hydrogel Cartilage. *JSME International Journal Series C*, 47(1):199–208, 2004.

[169] W. Swieszkowski, B. H. S. Tuan, K. J. Kurzydlowski, and D. W. Hutmacher. Repair and regeneration of osteochondral defects in the articular joints. *Biomolecular Engineering*, 24(5):489–495, 2007.

[170] C. Truesdell and R. Toupin. The classical field theories. In *Principles of classical mechanics and field theory/Prinzipien der Klassischen Mechanik und Feldtheorie*, pages 226–858. Springer, 1960.

[171] A. M. Turing. The chemical basis of morphogenesis. *Bulletin of Mathematical Biology*, 52(1-2):153–197, 1990.

[172] C. N. van Dijk, M. L. Reilingh, M. Zengerink, and C. J. A. van Bergen. Osteochondral

defects in the ankle: Why painful? *Knee Surgery, Sports Traumatology, Arthroscopy*, 18(5):570–580, 2010.

[173] C. C. Van Donkelaar and R. Huiskes. The PTHrP-Ihh feedback loop in the embryonic growth plate allows PTHrP to control hypertrophy and Ihh to regulate proliferation. *Biomechanics and Modeling in Mechanobiology*, 6(1-2):55–62, 2007.

[174] P. Vavken and D. Samartzis. Effectiveness of autologous chondrocyte implantation in cartilage repair of the knee: a systematic review of controlled trials. *Osteoarthritis Cartilage*, 18(6):857–863, 2010.

[175] L. A. Vonk, T. S. De Windt, I. C. Slaper-Cortenbach, and D. B. Saris. Autologous, allogeneic, induced pluripotent stem cell or a combination stem cell therapy? where are we headed in cartilage repair and why: a concise review. *Stem cell research & therapy*, 6(1):94, 2015.

[176] G. D. Vries, T. Hillen, and M. Lewis. A Course in Mathematical Biology Reaction-Diffusion Equations. 2005.

[177] S. Wakitani, T. Goto, S. J. Pineda, R. G. Young, J. M. Mansour, A. I. Caplan, and V. M. Goldberg. Mesenchymal cell-based repair of large, full-thickness defects of articular cartilage. *The Journal of bone and joint surgery. American volume*, 76(4):579–92, 1994.

[178] J. P. Ward and J. R. King. Mathematical modelling of avascular-tumour growth. *IMA journal of mathematics applied in medicine and biology*, 14(1):39–69, 1997.

[179] M. M. Wilke, D. V. Nydam, and A. J. Nixon. Enhanced early chondrogenesis in articular defects following arthroscopic mesenchymal stem cell implantation in an equine model. *Journal of Orthopaedic Research*, 25(7):913–925, 2007.

[180] J. J. Williams, C. A. Bush-Joseph, and J. B. Bach. Osteochondritis dissecans of the knee. *The American journal of knee surgery*, 11(4):221–232, 1998.

[181] R. M. Williams, W. R. Zipfel, M. L. Tinsley, and C. E. Farnum. Solute transport in growth plate cartilage: In vitro and in vivo. *Biophysical Journal*, 93(3):1039–1050, 2007.

[182] N. J. Wilsman, C. E. Farnum, E. M. Green, E. M. Lieferman, and M. K. Clayton. Cell cycle analysis of proliferative zone chondrocytes in growth plates elongating at different rates. *Journal of Orthopaedic Research*, 14(4):562–572, 1996.

[183] M. Wong and D. R. Carter. A theoretical model of endochondral ossification and bone architectural construction in long bone ontogeny. *Anatomy and Embryology*, 181(6):523–532, 1990.

[184] L. Wu. *Mesenchymal stem cells as trophic mediators in cartilage regeneration.* PhD thesis, University of Twente, 2013.

[185] L. Wu, X. Cai, S. Zhang, M. Karperien, and Y. Lin. Regeneration of articular cartilage by adipose tissue derived mesenchymal stem cells: Perspectives from stem cell biology and molecular medicine. *Journal of Cellular Physiology*, 228(5):938–944, 2013.

[186] L. Wu, J. Leijten, C. A. Van Blitterswijk, and M. Karperien. Fibroblast growth factor-1 is a mesenchymal stromal cell-secreted factor stimulating proliferation of osteoarthritic chondrocytes in co-culture. *Stem Cells and Development*, 22(17):2356–2367, 2013.

[187] L. Wu, J. C. Leijten, N. Georgi, J. N. Post, C. A. Van Blitterswijk, and M. Karperien. Trophic effects of mesenchymal stem cells increase chondrocyte proliferation and matrix formation. *Tissue Engineering - Part A*, 17(9-10):1425–1436, 2011.

[188] L. Wu, H. J. Prins, M. N. Helder, C. A. Van Blitterswijk, and M. Karperien. Trophic effects of mesenchymal stem cells in chondrocyte Co-Cultures are independent of culture conditions and cell sources. *Tissue Engineering - Part A*, 18(15-16):1542–1551, 2012.

[189] X. L. Yuan, H. Y. Meng, Y. C. Wang, J. Peng, Q. Y. Guo, A. Y. Wang, and S. B. Lu. Bone-cartilage interface crosstalk in osteoarthritis: Potential pathways and future therapeutic strategies. *Osteoarthritis and Cartilage*, 22(8):1077–1089, 2014.

[190] C. Zhang, Y. zhi Cai, and X. jin Lin. Autologous chondrocyte implantation: Is it likely to become a saviour of large-sized and full-thickness cartilage defect in young adult knee? *Knee Surgery, Sports Traumatology, Arthroscopy*, 24(5):1643–1650, 2016.

[191] L. Zhang, J. Hu, and K. A. Athanasiou. The role of tissue engineering in articular cartilage repair and regeneration. *Critical reviews in biomedical engineering*, 37(1-2):1–57, 2009.

[192] Y. Zhang, F. Wang, H. Tan, G. Chen, L. Guo, and L. Yang. Analysis of the mineral composition of the human calcified cartilage zone. *International Journal of Medical Sciences*, 9(5):353–360, 2012.

[193] Y. Zhang, F. Wang, H. Tan, G. Chen, L. Guo, and L. Yang. Analysis of the mineral composition of the human calcified cartilage zone. *International Journal of Medical Sciences*, 9(5):353–360, 2012.

[194] Z. Zhao, X. Zhou, J. Guan, M. Wu, and J. Zhou. Co-implantation of bone marrow mesenchymal stem cells and chondrocytes increase the viability of chondrocytes in rat osteo-chondral defects. *Oncology Letters*, 15(5):7021–7027, 2018.

[195] S. Zhou, Z. Cui, and J. P. Urban. Factors influencing the oxygen concentration gra-

dient from the synovial surface of articular cartilage to the cartilage–bone interface: a modeling study. *Arthritis & Rheumatism*, 50(12):3915–3924, 2004.

[196] S. Zhou, Z. Cui, and J. P. Urban. Nutrient gradients in engineered cartilage: metabolic kinetics measurement and mass transfer modeling. *Biotechnology and bioengineering*, 101(2):408–421, 2008.